

R.T.
YILDIZ TECHNICAL UNIVERSITY
GRADUATE SCHOOL OF NATURAL AND APPLIED SCIENCES

**MONITORING OF LAND SURFACE SUBSIDENCE IN ZONGULDAK COAL
MINING FIELD IN THE NORTHERN TURKEY USING MULTI TEMPORAL SAR
INTERFEROMETRY**

SAYGIN ABDİKAN

PHD. THESIS
DEPARTMENT OF GEOMATIC ENGINEERING
PROGRAMME OF REMOTE SENSING AND GIS

SUPERVISOR
ASSIST. PROF. DR. FÜSUN BALIK ŞANLI

İSTANBUL, 2012

R.T.
YILDIZ TECHNICAL UNIVERSITY
GRADUATE SCHOOL OF NATURAL AND APPLIED SCIENCES

**MONITORING OF LAND SURFACE SUBSIDENCE IN ZONGULDAK COAL
MINING FIELD AT NORTHERN TURKEY USING MULTI TEMPORAL SAR
INTERFEROMETRY**

A thesis submitted by Saygın ABDİKAN in partial fulfillment of the requirements for the degree of **DOCTOR OF PHILOSOPHY** is approved by the committee on 26.12.2012 in Geomatics Engineering Department, Remote Sensing and GIS Programme.

Thesis Supervisor

Assist. Prof. Dr. Füsün BALIK ŞANLI
Yıldız Technical University

Co- supervisor

Assoc. Prof. Dr. Ziyadin ÇAKIR
İstanbul Technical University

Examining Committee Members

Assist. Prof. Dr. Füsün BALIK ŞANLI
Yıldız Technical University

Prof. Dr. Fatmagül KILIÇ
Yıldız Technical University

Prof. Dr. Filiz SUNAR
İstanbul Technical University

Prof. Dr. Zübeyde ALKIŞ
Yıldız Technical University

Prof. Dr. Cem GAZİOĞLU
İstanbul University

The study is supported by Yıldız Technical University in the frame of the Scientific Research Project Coordination with project 28-05-03-02.

FORWORD

This thesis is written in the context of the scientific research project which is supported by Yıldız Technical University to complete the Remote Sensing and GIS PhD program at Geomatics Engineering Department of Yıldız Technical University.

During my research there are many people who have contributed in various ways over the past six years to go further. First and foremost I offer my deepest gratitude to my supervisor Dr. Füsün Balık Şanlı for her valuable comments, perceptive advices and belief during all of the stages. I owe a lot to her being supportive and responsible. Her constant enthusiasm, encouragement and unrequited trust improved me to be a self-confident scientist.

I express my thankfulness to Dr. Ziyadin Çakır for accepting to become my co-supervisor, for the guidance and providing valuable feedback during my research.

I wish to thank my colleagues who worked with me at the period of my study at Geomatics Engineering Department of Yıldız Technical University. I also thank to Prof. Dr. Fatmagül Kılıç and Prof. Dr. Filiz Sunar for their advices and encouragement during my study.

I would like to thank Dr. Ramon Hanssen for supervising me and giving me opportunity to make research at the radar group in Delft University of Technology. I am also thankful to Dr. Andy Hooper and the friends from the radar group who gave me thoughtful suggestions during the period of my study at TUDelft.

My special thanks go to Mahmut Arıkan for his supportive advices, sharing his individual experience and giving his time for my unending questions. He always kept me up during my research. I would like to thank NUFFIC Huygens scholarship for supporting me for my research in TUDelft in the Netherlands. I extend thanks to Dr. Hüseyin Kemaldere from Bülent Ecevit University, who shared much information about the study area.

A special thank goes to Asude Arslan Sorensen for her friendship, endless support and presence. She always gave constructive criticism and suggestions to my all complain which kept my motivation up.

I am very grateful to my friends Mustafa Yaşar, Bilgiseven Vurdu, Merve Elma, Gökhan Özen, Mesut Kondu, Duygu Pınar Marçalı Doğru and Petek Tatlı for their friendship,

sharing and presence. I wish to thank Smiljan Grubešić for his understanding, sharing and support.

Last but not least, many thanks to my parents and my sister Saydam who gave me great support, help and understanding during my study.

September, 2012

Saygın ABDİKAN

TABLE OF CONTENTS

	Page
LIST OF SYMBOLS	ix
ABBREVIATIONS	xi
LIST OF FIGURES	xiii
LIST OF TABLES	xvii
ABSTRACT	xviii
ÖZET	xxi
CHAPTER 1	1
INTRODUCTION	1
1.1 Literature Review	1
1.2 Aim of the Thesis	5
1.3 Hypothesis	6
CHAPTER 2	9
RADAR INTERFEROMETRY: BACKGROUND	9
2.1 Synthetic Aperture Radar	9
2.1.1 Properties of SAR Image	13
2.1.2 Distortions in SAR Images	16
2.1.3 Satellite Acquisitions	17
2.2 InSAR Principles	21
2.2.1 InSAR Geometry	22
2.3 Deformation Monitoring by DInSAR	23
2.3.1 Topographic Phase Contribution	24
2.3.2 Atmospheric Delay	24

2.3.3	Orbit	25
2.3.4	Surface Deformation.....	25
2.3.5	Sources of Decorrelation in InSAR	26
CHAPTER 3	29
METHODOLOGY OF INSAR PROCESSING		29
3.1	Multi Temporal Time Series with InsAR Analysis	29
3.1.1	Persistent Scatterer Interferometry of StaMPS.....	30
3.1.2	Small Baseline Interferometry of StaMPS	32
CHAPTER 4	34
SUBSIDENCE IN ZONGULDAK COAL MINE AREA.....		34
4.1	Study area	34
4.1.1	Geological Background	37
4.2	Coal Mining Activities in Zonguldak.....	40
4.2.1	Definition of Problem	46
4.2.2	Formation of Mining Subsidence.....	52
4.2.3	Prior Subsidence Studies at Zonguldak Mine	54
CHAPTER 5	55
MULTI TEMPORAL INSAR OBSERVATIONS RESULTS.....		55
5.1	Available SAR Dataset	55
5.1.1	ERS Data Acquisitions	57
5.1.2	ENVISAT/ASAR Data Acquisitions	57
5.1.3	ALOS/PALSAR Data Acquisitions.....	58
5.2	ERS Multi Temporal InSAR Results.....	59
5.2.1	ERS PSI Processing	59
5.2.2	ERS SB Processing	60
5.2.3	ERS PSI-SB Comparison	61
5.3	ENVISAT Multi Temporal InSAR Results.....	66
5.3.1	ENVISAT Descending PSI	66
5.3.2	ENVISAT Descending SB.....	67
5.3.3	ENVISAT Descending PSI-SB Comparison	67
5.3.4	ENVISAT Ascending PSI	72
5.3.5	ENVISAT Ascending SB	72

5.3.6	ENVISAT Ascending PSI-SB Comparison	73
5.4	PALSAR Multi Temporal InSAR Results	78
5.4.1	PALSAR PSI Processing	78
5.4.2	PALSAR SB Processing	79
5.4.3	PALSAR PSI-SB Comparison.....	79
5.5	PSI Results Versus SB Results.....	84
CHAPTER 6	98
RESULTS AND DISCUSSION	98
REFERENCES	103
APPENDIX-A	111
FLOWCHART OF RESEARCH STUDY	111
APPENDIX-B	112
INSAR PAIRS GENERATED WITH SB APPROACH	112
APPENDIX-C	120
STANDARD DEVIATIONS OF RESULTS	120
APPENDIX-D	122
INTERSECTION OF RESULTS	122
APPENDIX-E	124
CONTRIBUTION PHASES	124
CURRICULUM VITAE	129

LIST OF SYMBOLS

A_1, A_2	Amplitudes of two epochs for the same pixel
A_{12}	Interferometric amplitude
B	Baseline
B_{crit}	Critical baseline
B_d	Bandwidth
B_{Dop}	Doppler bandwidth
B_w	Beam width
B_{\perp}	Perpendicular baseline
B_{\parallel}	Parallel baseline
c	Speed of light
C_p	Complex pixel
D	Antenna width
D_A	Amplitude dispersion index
$D_{\Delta A}$	Amplitude difference dispersion index
f_D	Doppler frequency
f_{DC}	Doppler centroid frequency
h	Mean height of surface roughness feature
h_A	Altitude of ambiguity
H	Altitude of satellite
H_p	Height of target P
L	RADAR antenna length
p, p'	Target points on the ground
P_D	slant range deformation
P_N	Power of the noise
P_S	Power of received signal
R	Range
R_1	Range of first acquisition
R_2	Range of second acquisition
R_f	Far slant range
R_m	Middle slant range
R_n	Near slant range
S_1	Complex master image
S_2	Complex slave image
S_w	Swath width

v_s	Platform velocity
α	Orientation angle of the baseline
β_a	Width of azimuth beam of the radar antenna
γ	Coherence
γ_{DC}	Doppler centroid decorrelation
γ_T	Thermal decorrelation
ΔA_g	Ground azimuth resolution
Δf_{DC}	Doppler centroids between master and slave images
ΔR	Range difference of two SAR acquisitions
ΔR_g	Ground range resolution
η	Incidence angle
θ	Look angle
λ	Wavelength
μ_A	Mean of SAR amplitude images
ζ	Topographic slope
σ_A	Standard deviation of the amplitude image
$\sigma_{\Delta A}$	Standard deviation of master and slave difference in amplitude
τ_p	Pulse duration
Φ	Phase difference
Φ_1, Φ_2	Phase components of two epochs for the same pixel
Φ_{atm}	Phase delay due to atmosphere
Φ_{def}	Phase change due to surface deformation
Φ_{orb}	Orbital errors
Φ_n	Phase noise
Φ_{topo}	Phase contribution of topography
ψ	Depression angle
ω_s	Squint angle

ABBREVIATIONS

ALOS	Advanced Land Observing Satellite
ASAR	Advanced SAR
ASI	Agenzia Spaciale Italiana (Italian Space Agency)
AVNIR	Advanced Visible and Near Infrared Radiometer
COSMO-SkyMed	Constellation of small Satellites for Mediterranean basin Observation
CDTI	Centro para el Desarrollo Tecnologico Industrial
CONAE	Comision Nacional de Actividades Espaciales
CSA	Canada Space Agency
DEM	Digital Elevation Modeling
DInSAR	Differential SAR Interferometry
DLR	Deutschen Zentrums für Luft- und Raumfahrt
DORIS	Delft Object-Oriented Radar Interferometric Software
ENVISAT	Environmental Satellite
ERS	European Remote Sensing
ESA	European Space Agency
FDB	Fine Dual Beam
FSB	Fine Single Beam
GMES	Global Monitoring for Environment and Security
GPS	Global Positioning System
INSAR	Interferometric Synthetic Aperture Radar
JERS	Japanese Earth Resources Satellite
JAXA	Japan Aerospace Exploration Agency
LOS	Line of Sight
MAPSAR	Multi Application Purpose SAR
MDA	MacDonald, Dettwiler and Associates
MTA	Maden Tetkik ve Arama (Mineral Research and Exploration)
NASA	National Aeronautics and Space Administration
PALSAR	Advanced Land Observing Satellite
PSI	Persistent Scatterers Interferometry
RADAR	Spaceborne Radio Detecting and Ranging
RAR	Real Aperture Radar
ROI_PAC	Repeat Orbit Interferometry Package
SAR	Synthetic Aperture Radar

SB	Small Baseline
SBAS	Small Baseline Subset
SEOSAR	Satélite Español de Observación SAR
SLR	Side Looking Radar
SLAR	Side Looking Airborne Radar
SLC	Single Look Complex
SIR	Shuttle Imaging Radar
SRTM	Shuttle Radar Topography Mission
StaMPS	Stanford Method for Persistent Scatterers
TCBMA	Turkey Coal Basin Management Agency
TCE	Turkish Coal Enterprises (Türkiye Taşkömürü Kurumu-TTK)
WGS84	World Geodetic System 1984

LIST OF FIGURES

		Page
Figure 2. 1	Electromagnetic spectrum (ESA, [39])	9
Figure 2. 2	Geometry of RAR (adapted from Cakir [40] and Wright [41])	10
Figure 2. 3	a)Range resolution, b)Azimuth resolution (adapted from Cakir [40] and Wright [41])	11
Figure 2. 4	SAR geometry (adapted from Cakir [40])	12
Figure 2. 5	Influence of wavelengths on objects (ESA, [45]).....	15
Figure 2. 6	Geometrical distortions in SAR images where F: Foreshortening, L: Layover, S: Shadow (adapted from Sousa [48])	16
Figure 2. 7	InSAR Geometry	22
Figure 2. 8	Repeat-pass DInSAR geometry (adapted from Sousa [48])	25
Figure 3. 1	a) Distributed scatterers that contribute to the phase in one pixel b) dominant PS in one pixel (Hooper [65]).....	31
Figure 3. 2	a) Flowchart of StaMPS steps (adapted from Sousa [48] and Hooper [66]).	31
Figure 4. 1	Study area [73]	35
Figure 4. 2	Weather conditions of Zonguldak (adapted from Turkish State Meteorological Service [75]).....	35
Figure 4. 3	DEM of Zonguldak city center	36
Figure 4. 4	Slope of the study area.....	36
Figure 4. 5	Aspect of the study area	37
Figure 4. 6	Stratigraphic section of the study area (adapted from [36], [79], [80]) ..	38
Figure 4. 7	The geological map of the Zonguldak city (adapted from [36]).....	38
Figure 4. 8	Caves of Zonguldak (Bülent Ecevit University, [83])	39
Figure 4. 9	Zonguldak coal basin (TCE, [73])	40
Figure 4. 10	Coal production of TTK in Zonguldak Province between 1941 and 2011 (TCE,[85]).....	41
Figure 4. 11	Coal productions of TTK in 5 regions a) Raw b) Processed (TCE,[85]).....	42

Figure 4. 12	Location of mining tunnels at the study area of Zonguldak showed on 20070724 dated panchromatic Landsat-ETM image (15 m ground resolution).....	44
Figure 4. 13	Mine galleries in Kozlu (Background optical image is GoogleEarth).....	45
Figure 4. 14	Mine galleries in Karadon (Background optical image is GoogleEarth)	45
Figure 4. 15	Mine galleries in Üzülmöz (Background optical image is GoogleEarth)	46
Figure 4. 16	a-Deformations on building (Turer et al. [78]) and b-Deformations on ground (Can et al. [34]).....	47
Figure 4. 17	Reserves in Zonguldak center.....	48
Figure 4. 18	a) No of dead per year and coal production, b) No of injures per year and coal production (TCE,[86]).....	49
Figure 4. 19	Landslide map of Zonguldak province (Turer et al. [78])	50
Figure 4. 20	Relationship between width of coal seam and the surface subsidence (Bauer [93]).....	52
Figure 4. 21	Subsidence at flat coal seam (adapted from Kutođlu et al [91], Can et al. [94])	53
Figure 4. 22	Subsidence at slopped coal seam (τ_1 and τ_2 are the slopes of the coal seam, τ_0 is the slope where subsidence is maximum) (Adapted from Can et al. [94])	53
Figure 5. 1	Available SAR data frames which cover the study area Zonguldak	56
Figure 5. 2	ERS descending orbit track 21	57
Figure 5. 3	ENVISAT-ASAR descending orbit track 21	58
Figure 5. 4	ENVISAT-ASAR ascending orbit track 343	58
Figure 5. 5	ALOS-PALSAR ascending orbit track 604	59
Figure 5. 6	Perpendicular baselines relative to 19970730 of ERS dataset a) PS baselines b) SB baselines.....	61
Figure 5. 7	ERS PSI and SB subsidence results along LOS from 1993 to 2001.....	62
Figure 5. 8	Profile at Kozlu on ERS a) PS result, b) SB result; at Karadon c) PS result, d) SB result; at Üzülmöz e) PS result, f) SB result	64
Figure 5. 9	Time series analysis from descending ERS for the regions Kozlu a) PSI results, b) SB results; Karadon c) PSI results, d) SB results; Üzülmöz e) PSI results, f) SB results	65
Figure 5. 10	Perpendicular baselines relative to 20050817 of ENVISAT descending dataset a) PSI baselines b) SB baselines.....	68
Figure 5. 11	ENVISAT descending track PSI and SB subsidence results along LOS from 2003 to 2010	69

Figure 5. 12	Profile at Kozlu on descending ENVISAT a) PS result, b) SB result; at Karadon c) PS result, d) SB result; at Üzülmöz e) PS result, f) SB result	70
Figure 5. 13	Time series analysis from descending ENVISAT for the regions Kozlu a) PSI results, b) SB results; Karadon c) PSI results, d) SB results	71
Figure 5. 14	Time series analysis from descending ENVISAT for the regions Üzülmöz a) PSI results, b) SB results; c) Area-1; d) Area-2	72
Figure 5. 15	Perpendicular baselines relative to 20050804 of ENVISAT ascending dataset a) PSI baselines b) SB baselines	73
Figure 5. 16	ENVISAT ascending track PSI and SB subsidence results along LOS from 2004 to 2010	75
Figure 5. 17	Profile at Kozlu on ascending ENVISAT a) PS result, b) SB result	75
Figure 5. 18	a) Profile at Karadon on ascending ENVISAT a) PS result, b) SB result; at Üzülmöz c) PS result, d) SB result	76
Figure 5. 19	Time series analysis from ascending ENVISAT for the regions Kozlu a) PSI results, b) SB results; Karadon c) PSI results, d) SB results; Üzülmöz e) PSI results, f) results ; g) Area-3; h) Area-4	77
Figure 5. 20	Perpendicular baselines relative to 20080723 of PALSAR ascending dataset a) PSI baselines b) SB baselines	79
Figure 5. 21	PALSAR ascending track PSI and SB subsidence results along LOS from 2007 to 2010	81
Figure 5. 22	Profile at Kozlu on ascending PALSAR a) PS result, b) SB result; at Karadon c) PS result, d) SB result; at Üzülmöz e) PS result, f) SB result	82
Figure 5. 23	Time series analysis from ascending PALSAR for the regions Kozlu a) PSI results, b) SB results; Karadon c) PSI results, d) SB results; Üzülmöz e) PSI results; f) SB results; g) Cave ; h) Üzülmöz maksimum	83
Figure 5. 24	Effects of baselines on ascending PALSAR coherence images	85
Figure 5. 25	Relationship between width of coal seam and surface subsidence (Bauer [93])	85
Figure 5. 26	Saturated PSI results shows the velocity along LOS direction with mining galleries on the city of Kozlu: a- Desc. ERS 1-2, b- Desc. ENVISAT, c-Asc. ENVISAT, d- Asc. PALSAR	87
Figure 5. 27	Saturated SB results shows the velocity along LOS direction with mining galleries on the city of Kozlu: a- Desc. ERS 1-2, b- Desc. ENVISAT, c-Asc. ENVISAT, d- Asc. PALSAR	88
Figure 5. 28	Saturated results shows the velocity along LOS direction with mining galleries on the Karadon: a) PSI of Asc. PALSAR, b) SB of Asc. PALSAR	89
Figure 5. 29	Saturated results shows the velocity along LOS direction with mining galleries on the Karadon: a) PSI of Desc. ERS 1-2, b) SB of Desc. ERS 1-2,	

	c) PSI of Desc. ENVISAT, d) SB of Desc. ENVISAT, e) PSI of Asc. ENVISAT, f) SB of Asc. ENVISAT	90
Figure 5. 30	Relationship between width of coal seam and surface subsidence (Bauer [93]).....	91
Figure 5. 31	Saturated results show the velocity along LOS direction with mining galleries on the Üzülmez : a) PSI of Asc. PALSAR, b) SB of Asc. PALSAR	22
Figure 5. 32	Saturated results shows the velocity along LOS direction on Catalagzi which is located in potential subsidence area: a) PS of Asc. ERS, b) SB of Desc. ERS, c) PSI of Desc. ENVISAT, d) SB of Desc. ENVISAT, e) PSI of Asc. ENVISAT, f) SB of Asc. ENVISAT	93
Figure 5. 33	Saturated results shows the velocity along LOS direction on Catalagzi which is located in potential subsidence area: a) PSI of Asc. PALSAR, b) SB of Asc. PALSAR	94
Figure 5. 34	Landslide regions acquired from MTA	95
Figure 5. 35	Landslide area at Zonguldak city overlaped with C-band results.....	96
Figure 5. 36	Landslide area at Zonguldak city overlaped with L-band results.....	97
Figure 5. 37	Profiles over landslide area from A to B; a) PSI results, b) SB results ...	98
Figure A. 1	Flowchart of research study	111
Figure A. 2	Standard deviations; a)ERS PSI result, b) ERS SB result, c) Desc. ENVISAT PSI result, d) Desc. ENVISAT SB result	120
Figure A. 3	Standard deviations; a)Asc. ENVISAT PSI result, b) Asc. ENVISAT SB result, c) PALSAR PSI result, d) PALSAR SB result	121
Figure A. 4	Common points of PSI and SB results: a) ERS, b) ENVISAT t-343.....	122
Figure A. 5	Common points of PSI and SB results: a) ENVISAT t-21, b) PALSAR....	123
Figure A. 6	DEM error removed from phase; a)ERS PSI result, b) ERS SB result, c) Desc. ENVISAT PSI result, d) Desc. ENVISAT SB result.....	124
Figure A. 7	DEM error removed from phase; a)Asc. ENVISAT PSI result, b) Asc. ENVISAT SB result, c) PALSAR PSI result, d) PALSAR SB result	125
Figure A. 8	Atmosphere and orbital error of master image (20080723) which is included in all interferograms in PSI process.	125
Figure A. 9	Unwrapped phase of PALSAR images in PSI application.....	126
Figure A. 10	Orbit errors of PALSAR images in PSI application	126
Figure A. 11	Atmospheric phase of PALSAR images in PSI application	127
Figure A. 12	DEM error and orbit phase removed unwrapped phase of PALSAR images in PSI application.....	127
Figure A. 13	DEM error, atmospheric and orbit phase of slave images and master image removed unwrapped phase of PALSAR images in PSI application	128

LIST OF TABLES

	Page
Table 1. 1	Summarized studies on deformation monitoring at coal mining using multi temporal InSAR.....4
Table 2. 1	SAR bands with frequency and wavelength [46]..... 15
Table 2. 2	Characteristics of SAR missions (adapted from [43], [44], [49], [50], [51], [52], [53])..... 19
Table 4. 1	Population growth of Zonguldak and Turkey [76]..... 37
Table 4. 2	Reserves of Zonguldak coal basin (tonnes) (TCE, [73])..... 43
Table 4. 3	Discharged waste water amounts of mining operations (TCE, [73])..... 50
Table 4. 4	Previous subsidence monitoring studies on Zonguldak.....54
Table 5. 1	Specifications of available dataset.....56
Table 5. 2	Specifications of ASAR image swaths (ESA, [98])..... 57
Table 5. 3	Specifications of PALSAR image modes..... 59
Table 5. 4	ERS data used in PSI approach.....60
Table 5. 5	ENVISAT descending data used in PSI approach.....66
Table 5. 6	ENVISAT ascending data used in PSI approach.....73
Table 5. 7	PALSAR ascending data used in PSI approach..... 78
Table 5. 8	Summary of results..... 84
Table 5. 9	Maksimum velocities estimated over study area..... 86
Table 5. 10	Extracted points in Kozlu..... 87
Table 5. 11	Common point list in the processes..... 95
Table A. 1	ERS Pairs used in SB approach.....109
Table A. 2	ENVISAT descending pairs used in SB approach.....111
Table A. 3	ENVISAT ascending pairs used in SB approach..... 113
Table A. 4	PALSAR pairs used in SB approach..... 114

**MONITORING OF LAND SURFACE SUBSIDENCE IN ZONGULDAK COAL
MINING FIELD IN THE NORTHERN TURKEY USING MULTI TEMPORAL SAR
INTERFEROMETRY**

Saygın ABDİKAN

Department of Geomatics Engineering

PhD. Thesis

Supervisor: Assist. Prof. Dr. Füsün BALIK SANLI

Co- supervisor: Assoc. Prof. Dr. Ziyadin ÇAKIR

This thesis examines the availability of finding out the ground surface deformation which occur in long time period with slow displacements by using multi temporal satellite SAR images. A case study is applied on Zonguldak underground coal mine areas using two techniques as Persistent Scatterers Interferometry (PSI) and Small Baseline (SB). The results of these techniques are compared and discussed.

In Turkey Zonguldak and Bartın provinces are the only mining area that underground hardcoal mine is produced. This mine has a national economy valuable especially for iron-steel industry and energy production. Mining activities have been started in the mid-19th. Century and is still active at five regions under Turkish Coal Enterprises (Türkiye Taşkömürü Kurumu - TTK) auditing. These mining are namely Kozlu, Karadon, Üzülmöz and Armutçuk which are located in Zonguldak province, and Amasra mine region which is located in Bartın province.

In this region mining has been continued more than 150 years and during this period approximately 400 million ton hardcoal is produced. Constant and dense production of coal mine caused subsidence at the surface of mine region. However, settlements and environment are suffered due to mining where urbanization is located on. This

situation effected negatively human life as life losses. It also effected people economically as many buildings became useless and people lost their properties.

Furthermore, in this region many landslide hazard is happening and also sinkholes occur resulting from having karstic properties at the geological structure. Additionally these mining activities trigger the natural hazards and increase the vulnerability. In last years the amount of coal mine production has been decreased and due to this fact government aimed to increase the production. New reserve survey was completed up to -1200 m from the surface by TTK. An amount of 1.3 billion tone reserve of coal was disclosed by the end of 2011.

In this study coal mines in Zonguldak city as Kozlu, Karadon and Üzülmöz regions are chosen as study area to investigate the deformation which occurred in long time period. Kozlu mining is the first mining area and also is the only mine where production is continued under sea. Coal production is processed at different levels under the surface in these three mines. Production is continued under surface level as -630 m, -540 m and -250 m deep in Kozlu, Karadon and Üzülmöz respectively.

The investigation is concerned on the behalf of to address these facts:

- a) Residential areas are under a significant danger because of constant surface subsidence
- b) Long term subsidence phenomena has not been monitored before. Previous techniques are used for short terms and have not been used for all mining areas. It is aimed to find out the deformation which occur both in urban and rural areas.
- c) InSAR technique gives a golden opportunity to monitor deformation which happen in long time period and also provide analysis of evolution of displacement in time.

For these purposes 33 C-band satellite SAR images of ERS-1 and ERS-2 are acquired between 1993 and 2001 years. Also C-band 29 descending ENVISAT images are acquired between 2003 and 2010, and 17 ascending ENVISAT images are gathered between 2004 and 2010. Moreover, 23 L-band ALOS/PALSAR SAR images are acquired for the long term InSAR analyses between 2007 and 2010. PSI and SB approaches are applied for all these four dataset.

PSI and SB approaches are applied for all these four dataset. For the PSI approach in each data set one image is chosen as master and interferograms are computed with this master image. For the SB processes all images are matched each other to compute interferograms. In SB applications InSAR pairs are computed with a threshold of temporal and geometrical baselines. Deformations are determined as mm/year. As a result it is found out that subsidence pattern at Kozlu is monitored with all ERS, ENVISAT and PALSAR processes. Results have consistency with previous DInSAR results. In the results of ERS and ENVISAT deformation is more clear at urbanized part of Kozlu city over the mine. Also at Karadon and Üzülmöz deformation is identified with less dense pattern. PALSAR results gave dense deformation pattern both at urbanized Kozlu and at rural Karadon and Üzülmöz. PSI results identified more points than SB results in all applications. Higher deformation is monitored in SB results at rural areas.

In this study surface subsidence caused by underground hardcoal mining at Zonguldak region is investigated. For this intention multi-temporal and multi-track satellite SAR

images are acquired. The evolution of subsidence phenomena for 17 years is revealed with InSAR method. Beside subsidence and potential subsidence areas which were identified by TTK new areas where deformation is monitored are found out. It is obvious that this region requires continuous monitoring. In conclusion, a footer information was prepared which can be useful for further risk analyses researches.

Key words: InSAR, surface subsidence, multi temporal SAR, time series, coal mining

**ZONGULDAK MADEN ALANLARINDA MEYDANA GELEN YÜZEY
HAREKETLERİNİN ÇOK ZAMANLI SAR İNTERFEROMETRİ YÖNTEMİ İLE
İZLENMESİ**

Saygın ABDİKAN

Harita Mühendisliği Anabilim Dalı

Doktora Tezi

Tez Danışmanı: Yrd. Doç. Dr. Füsün BALIK SANLI

Eş Danışman: Doç. Dr. Ziyadın ÇAKIR

Bu çalışmada uzun zaman aralığında yavaş hareketlerle oluşan yüzey deformasyonun belirlenmesi amacıyla çok zamanlı uydu SAR görüntülerinin kullanılabilirliği iki farklı yöntem ile karşılaştırmalı olarak Zonguldak maden alanları üzerinde incelenmiştir. Uygulamada sabit saçıcı (Persistent Scatterers Interferometry: PSI) ve kısa baz (Small Baseline: SB) yöntemleri incelenmiştir.

Zonguldak ve Bartın illerini kapsayan maden alanı Türkiye’ de ki tek yer altı taşkömürü madeninin çıkarıldığı alandır. Bu maden özellikle demir-çelik sanayisinde ve enerji üretiminde kullanıldığı için ulusal ekonomik değere sahiptir. Bölgede ki madencilik aktiviteleri 19 yy. ortalarında başlamış olup şu an Türkiye Taşkömürü Kurumu (TTK) tarafından beş alanda aktif bir şekilde taşkömürü üretilmektedir. Bunlardan Kozlu, Karadon, Üzülmüş ve Armutçuk müesseseleri Zonguldak ili içinde, Amasra müessesesi Bartın ili içerisinde kalmaktadır.

150 yıldan fazla bir süredir yapılan madencilik faaliyetleri sonucu yaklaşık olarak 400 milyon ton taşkömürü üretilmiştir. Sürekli ve büyük miktarlarda çıkarılan kömür sonucu maden yüzeyinde çökmeler olduğu gözlenmiştir. Ancak şehirleşmenin de kömür maden alanı üzerinde ve çevresinde olması burada bulunan yapılara zarar vererek insan

hayatını olumsuz yönde etkilemiştir. Pek çok can kaybı yanında binalar oturulamaz hale geldiği için binalar boşaltılmış ve mal kayıpları yaşanmıştır.

Ayrıca bölgede sürekli toprak kayması yaşanmakta bununla birlikte jeolojik yapısında karstik öğelerin bulunması obrukların oluşmasına neden olmaktadır. Bunlara ek olarak madencilik aktiviteleri doğal afetleri tetikleyerek zarar görebilirliğini artırmaktadır. Son yıllarda çıkarılan maden miktarının azalması nedeniyle daha çok maden çıkarılması planlanmış, bu amaçla -1200 m kota kadar kömür rezerv araştırmaları sürdürülmüştür. Bu inceleme sonucunda tüm alanda TTK tarafından 2011 yılı itibarı ile 1.3 milyar ton kömür rezervi olduğu belirtilmiştir.

Uzun süreli yüzey deformasyonunun belirlenmesi amacıyla Zonguldak şehir merkezinde bulunan üç alan olan Kozlu, Karadon ve Üzülmaz maden alanları çalışma alanı olarak seçilmiştir. Kozlu müessesesi Türkiye’de madencilik faaliyetlerinin başladığı ilk ve deniz altında sürdürülen tek işletmedir. Her işletmede farklı kotlarda üretim yapılmaktadır. Kozlu, Karadon ve Üzülmaz’de sırasıyla maksimum -630 m, -540 m ve -250 m de üretim gerçekleştirilmektedir.

Bu çalışmanın gerçekleşmesinde şu etkenler öncü olmuştur:

- a) Bölgedeki sürekli çökmeler nedeniyle yerleşim varlığı büyük bir tehlike altındadır
- b) Çökmeler sürekli olarak herhangi bir yöntem ile izlenmemektedir. İzlenen yöntemler kısa zaman aralıklı çalışmalardır ve her maden alanı için uygulanmamıştır. Hem şehir alanları hem de kırsal alanlarda meydana gelen deformasyonun belirlenmesi amaçlanmıştır.
- c) InSAR yöntemi ile uzun zaman aralığında meydana gelen deformasyonun zamansal gelişiminin detaylı bir şekilde incelenebilirliği.

Bu çalışmada C-band ERS-1 ve ERS-2 uydularına ait 1993-2001 yılları arasında elde edilmiş 33 SAR görüntüsü, yine C-band ENVISAT uydusuna ait 2003-2010 yılları arasında alçalan yönde alınmış 29 ve 2004-2010 yılları arasında yükselen yönde alınmış 17 SAR görüntüleri kullanılmıştır. Ayrıca 2007-2010 yılları arasında alınmış 23 L-band ALOS/PALSAR SAR uydu görüntüleri analiz edilmiştir.

Dört veri seti için hem PSI hem de SB uygulaması gerçekleştirilmiştir. PSI uygulamasında seçilen ana (master) görüntüye diğer görüntüler eşleştirilerek interferogramlar oluşturulmuştur. SB uygulamasında ise zamansal ve dik baz uzunluklarının kısa tutulması göz önüne alınarak her görüntü birbiriyle eşleştirilerek interferogramlar üretilmiştir. Deformasyon hızları mm/yıl olarak belirlenmiştir. Araştırma sonucunda Kozlu’da ki çökme şekli ERS, ENVISAT ve PALSAR sonuçlarının hepsinde gözlenmiştir. Daha önce yapılan kısa süreli DInSAR çalışmaları ile örtüşmektedir. ERS ve ENVISAT sonuçlarında deformasyon yerleşimin yoğun olduğu Kozlu bölgesinde daha belirginken Karadon ve Üzülmaz bölgelerinde daha seyrektiler. PALSAR sonuçlarında ise hem yerleşim yeri olan Kozlu’da hem de kırsal alan olan ve çevrenin ormanlık alanla kaplı olduğu Karadon ve Üzülmaz bölgelerinde yoğun bir şekilde ortaya çıktığı gözlenmiştir. PSI sonuçlarında daha fazla nokta olmasına rağmen deformasyon hızı SB sonuçlarına göre düşüktür. Ayrıca SB sonuçlarında kırsal alanda daha yüksek yüzey hareketi olduğu gözlenmiştir.

Bu alıřmada ok zamanlı ve ok izde alınmiř SAR uydu grntleri Zonguldak yeraltı tařkmr maden alanında meydana gelen yzey hareketlerinin arařtırılması iin izlenmiřtir. kmelerin 17 yıllık geliřimi ok zamanlı InSAR sonuları ile ortaya ıkarılmıřtır. TTK tarafından belirlenen kme ve potansiyel kme alanları dıřında da yzey hareketi gzlenmiřtir. Bu nedenle blgenin srekli izlenmesinin gereklilięi aıktır. Sonraki arařtırmalarda risk analizleri iin kullanılabilir bir alıřma gerekleřtirilmiřtir.

Anahtar Kelimeler: InSAR, yzey hareketi, ok zamanlı SAR, zamansal analiz, kmr madencilięi

INTRODUCTION

1.1 Literature Review

Since the launch of the first satellite for earth observation, remote sensing data became an essential source of geospatial information. Remote sensing provides to cover large ground surface which makes it valuable as economical and shareable for wide range of environmental interdisciplinary applications. It helped to measure and to understand natural hazards and disasters, and facilitate human being on risk assessment, disaster management and sustainable management. The Earth is dynamic due to having constantly moving ground surface. Numerous phenomena like subsidence, earthquake, volcanic activities, flooding and landslides cause significant surface deformations. Human activities as oil, gas or mine extraction, and excessive usage of water can trigger surface deformation. Ground subsidence which is associated with underground mining activities becomes more serious in Zonguldak settlement, Turkey. Mining based continuous collapses cause loss of life and many other physical problems such as building and road damage. Thus, it is a very serious hazard that government, mining industry and environment are effected (Ng et al, [1]). The subsidence caused by mining where the urban grew over wide areas. The necessity to observe the mining area is come out due to the continues collapses and deaths that happened last decade [International Social Security Association, 2].

Repeat-pass Synthetic Aperture Radar (SAR) interferometry (InSAR) is known as a significant geodetic technique to measure the ground deformation of large scale areas. The main advantage of using InSAR is the ability to access long period data archive.

Differential SAR Interferometry (DInSAR) is used to estimate small-scale movements (at mm-cm accuracy) that occur along the viewing direction (Gens and van Genderen, [3]). It has been achieved for many applications such as deformation estimation of volcanoes (Briole et al. [4]), glacier movements (Goldstein et al. [5]), surface deformation analysis (Manzo et al. [6]), Digital Elevation Modeling (DEM) (Small [7]), and the monitoring of earthquakes (Massonnet et al. [8]), landslides (Fruneau et al. [9], Squarzoni et al. [10]), and subsidence (Strozzi et al. [11]). On the other hand, because of the loss of coherence depending on temporal decorrelation, spatial decorrelation due to large baseline geometry, and changing atmospheric conditions during data acquisition, the information cannot always be extracted. To overcome these limitations of repeat-pass SAR interferometry, the technique of persistent scatterer interferometry (PSI) method is proposed by several groups (Ferretti et al. [12], Werner et al. [13], Hooper et al. [14]; Kampes [15]). This method uses a stack of differential interferograms that belongs to one master image and extracts time-coherent pixels. The PS pixels were extracted with these approaches successfully over the urban areas where has continues small scale deformations (Hooper et al. [16]). Another approach is the small baseline (SB) technique which uses small temporal and spatial baselines to reduce the unwrapping errors (Berardino et al. [17], Casu et al. [18], Hooper [19]).

In Turkey, InSAR is a mostly used tool for determining earthquake deformations (Wright et al. [20], Burgmann et al. [21]; Cakir et al. [22]; Cakir and Akoglu [23]). Although the InSAR method is used in various applications, it generally has not been improved and is used for the purpose of subsidence monitoring in Turkey. There are a few studies on long term time series analysis which are mostly related to earthquake deformation estimation (Motagh et al. [24]; Arikan et al. [25]; Walters et al. [26]) and also land subsidence monitoring (Akarvardar [27]).

In recent years PSI and SB methods are used for the monitoring of mine related displacement extraction (Ng, et al. [1], Chul and Min [28], Mei et al. [29], Gueguen et al. [30], Baek et al. [31]). Detailed information from different coal mining studies is summarized in Table 1.1. In Zonguldak mining region several methods were used for subsidence measurements as leveling and GPS measurements. But these techniques have drawbacks, such as they are point based and short term measurements (Sezer et

al. [32], Akçın et al. [33], Can et al. [34]). InSAR monitoring also performed just for short time periods, and C band fails due to low correlation (Akçın et al. [33], Deguchi et al., [35], Kemaldere [36]).

On this purpose it is aimed to research different technique to overcome this decorrelation using multi temporal InSAR technique. In this study, the goal is to monitor the mining subsidence in Zonguldak Province and to determine its characteristics, such as the direction and velocity, using the InSAR time series analysis which is employed to estimate the ground subsidence rates in mm/year along the line of sight (LOS) direction for long term period. In this frame the temporal evolution of surface deformation between 1993 and 2010 is observed with multi sensor analysis. Due to non/limited a priori knowledge of the subsidence velocity, a displacement analysis with interferometric time series was performed. This analysis will indicate the possibility to acquire first estimation of the deformation behavior in a time series of InSAR data for large areas. Identification of relatively stable areas could be used further for point based analyses as an attribution.

Characterizing the natural hazards and understanding the variation of the Earth's surface over a long time period is very important for the assessment of vulnerability risks. This study is aimed at avoiding the loss of life and property due to subsidence by taking preventative precautions. This interdisciplinary work will also provide a good example for the forthcoming projects that will be carried out in a similar manner in the future.

Table 1. 1 Summarized studies on deformation monitoring at coal mining using multi temporal InSAR

Reference	Data used	Study area	Deformation	Content
Ng et al., 2010 [1]	10 ALOS June 2007- Oct 2008	New South Wales, Australia	85.6 cm as max. subsidence	9 interferograms are calculated by DInSAR and the stack of DInSAR is used with a PSI approach. Depth of mining changes 470 m to 540 m from the surface. Interferograms formed with temporal baselines shorter than 92 days.
Chul and Min 2005 [28]	25 JERS-1 1992-1998	2x2 km-wide Gaeun Korea	0.6 cm/yr	Having perpendicular baseline<1500 m. were considered as point scatterer candidate. After correcting differential interferograms, elevation errors and LOS subsidence rates were computed on a pixel-by-pixel basis. A phase coherence value is considered as a reliability measure for each equation used for phase unwrapping and coherence > 0.7 is identified as PS.
Mei et al., 2008 [29]	28 RADARSAT-1 2000-2006	1x1 km-wide Frank Slide, Alberta, Canada	3.1 mm/yr	Commercial EarthView InSAR Coherent Target Monitoring software as a PSI approach is used. Data is acquired in SLC format. A coherence threshold of 0.65 was used for the process.
Gueguen et al., 2009 [30]	88 ERS 1-2 1992-2002 19 ENVISAT 2004-2007	Nord/Pas-de-Calais coal basin, France	1.25 cm/yr (ERS) 0.3 cm/yr (ENVISAT)	The area has altitudes between 80 and 180 m. Commercial softwares are chosen as Diaposan for DInSAR and GAMMA IPTA for PSI analysis. Focused on urban area of Lens. DInSAR pair 1992-1995 ERS has temporal decorrelation, so displacement could not be extracted precisely.
Baek et al., 2008 [31]	23 JERS-1 1992-1998	Gangwon-do, Korea 22 × 20 km	3.6 cm/yr	DInSAR and SBAS techniques are used. But due to lack some images and temporal baseline limitations good interferograms could not achieved. 25 interferograms are calculated with SBAS. Study area has covered with dense vegetation. SRTM-3 DEM is used to remove topographic phase. Less than 1 km length considered as SB.
Herrera et al., 2007 [37]	24 ERS 1998-2000 14 ENVISAT Mar 2003- Dec 2004	12 × 8 km La Union, Spain	2.3 cm/yr 2.1 cm/yr	A sort of Small baseline subset (SBAS) technique Coherent Pixels Technique is used as an advanced DInSAR method. Depth of mining changes 80 m to 254 m. Interferograms formed with Perpendicular baselines smaller than 130 m and temporal baselines shorter than 900 days. 54 coherent pixels/km ² is identified in average.

1.2 Aim of the Thesis

Zonguldak Province is a coastal settlement area that is prone to human-induced environmental problems such as subsidence due to the coal-mining areas. Severe deformations in the region caused by subsidence have been known since the 1900s, such deformations cause heavy damage on the Earth's surface and to buildings. According to the latest drilling reports, there are still 150 million metric tons of coals under the coastline of Zonguldak province. However, the coastline has now become a residential area with tall buildings, which have also triggered many serious subsidence problems. Although the damage that has occurred in the region is not described in natural hazards regulations in Turkey, the types of damages and the amount of financial loss to citizens caused by building damage shows that the risk is high in Zonguldak Province. Investigation of such spatial and temporal changes would be difficult with conventional methods.

The potentiality of evaluation methods is significant for the prediction of the mechanisms and formation time of subsidence, in order to minimize the economic and social loss. In particular, such methodologies are of vital importance for evaluating man-made topographic deformations like mining activities. Inherently, buildings in a subsidence field are strongly affected and damaged. Generally, mine management organizations complain about damages in the mining basin. Property owners, on the other hand, seek compensation, considering mining managers to be responsible for the damages occurring in the residential areas because of the inconvenience of the ground, architectonics, and cracking or damage due to inadequate building structure materials. In contrast, subsidence after the mining process can be interpreted in a different way. For instance, subsidence on rough surfaces may cause landslides. Although built-up areas may be out of the subsidence area, they could still be damaged due to a landslide that was triggered by the subsidence. These types of incidences are encountered frequently in Zonguldak (Buyurgan [38]).

The rating of damages depends upon the size of buildings, the number of flats, non suitable structural system, and the ground form. Our study area includes large sized and multi-story buildings that were damaged through subsidence. Zonguldak province was built and developed after the pit coal was found. To avoid the effects of urbanization on production, many regulations have been initiated since 1867. Since 1932, these limitations on construction have been strictly applied. In that process, it was noticed that incorrect decisions were made and inaccurate construction areas were chosen. Today, the number of multi-story tower blocks is increasing every day in the city, under which large coal reserves exist. Observations definitely indicate that limestone at the coastline of Zonguldak is the main threatening factor of subsidence. Most of the buildings will be in an uninhabitable situation if coal production continues (Buyurgan [38]). It is obvious that Zonguldak is under the risk of a dangerous disaster.

1.3 Hypothesis

In this study, for the purpose of monitoring of the subsidence, a methodology is going to be developed using the InSAR technique, which will make it possible to determine the rate of the ground deformations for long time period. It is also expected that the prediction of the very-important external factors of subsidence will be achieved. Furthermore, the main triggers of the subsidence will be investigated. The information gathered will help to determine subsidence fields for planning reconstruction areas. Thus, it will be possible to guide the growth of urbanization more carefully.

The evaluation of long term time series of SAR images of mining subsidence in Turkey for the first time in a detailed study. Improving existing deformation monitoring at the case study of Zonguldak province. Assessment of two InSAR techniques, PSI and SB to determine the subsidence phenomena.

1. Sub-objectives and Research Questions

- To indicate the possibility of the continuity of monitoring deformation by InSAR time series analysis

- What is the performance of using multi track InSAR monitoring with ERS, ENVISAT and PALSAR data?
 - Do study areas have enough coherent targets for displacement extraction?
 - What are the scatterer densities over urban and rural areas?
- To produce the deformation maps of the mining region and to interpret the distribution over the province
- What is the subsidence distribution (mm/year) of long time?
 - What are the differences and similarities between PSI and SB methods for the monitoring of coal mining subsidence?
 - What is the difference of C band and L band results on urban and rural areas?
 - Are results agreeing with the previous deformation estimation studies over Zonguldak?
 - Which improvements can be achieved from multi temporal InSAR monitoring?
- To investigate the relation of subsidence with geological structure
- Is natural based deformation as landslides can be monitored?
 - What is the effect of geological properties?

2. Financial Support

During my study on this thesis, I have achieved financial support from different organizations:

- Yildiz Technical University in the framework of the scientific research project 28-05-03-02.
- The European Space Agency (ESA) for providing ERS and ENVISAT data under the project CAT-1 6543.
- The Huygens Scholarship from Nuffic - Netherlands organization for international cooperation in higher education for the period 2009-2011. The research is completed at the Geosciences and Remote Sensing Department of Civil

Engineering and Geosciences Faculty of Delft University of Technology, Delft the Netherlands.

3. Thesis Roadmap

Chapter 1 gives a brief of motivation and research objectives about study as an introduction.

Chapter 2 summarizes the SAR geometry, previous SAR missions and new generation SAR satellites. Main principles of InSAR measurement and limitations of conventional InSAR are also addressed.

Chapter 3 describes the multi temporal InSAR methodology which is used in the study. PSI and SB approaches of StaMPS are presented.

Chapter 4 provides physical information of the study area. Describes what mining subsidence is. Prior studies on study area are presented.

Chapter 5 Data set of study area and the processes are expressed. Mean velocities of the results are presented. Time series analyses of Zonguldak results are compared.

Chapter 6 gives a summary of finding results and conclusions of study. Discuss the results of PSI and SB methods. Figure out the challenging parameters of the study, and suggests ideas as a future work.

A flowchart of roadmap is generalized and described in Appendix-A.

RADAR INTERFEROMETRY: BACKGROUND

2.1 Synthetic Aperture Radar

Spaceborne Radio Detecting and Ranging (RADAR) play an important role since late 1970s, and nowadays is a well-known technique. As an active system radar illuminates the target objects using electromagnetic pulses as microwaves and receives the reflected pulses. Microwave wavelengths range between 1 cm and 1 m in the electromagnetic spectrum (Figure 2.1).

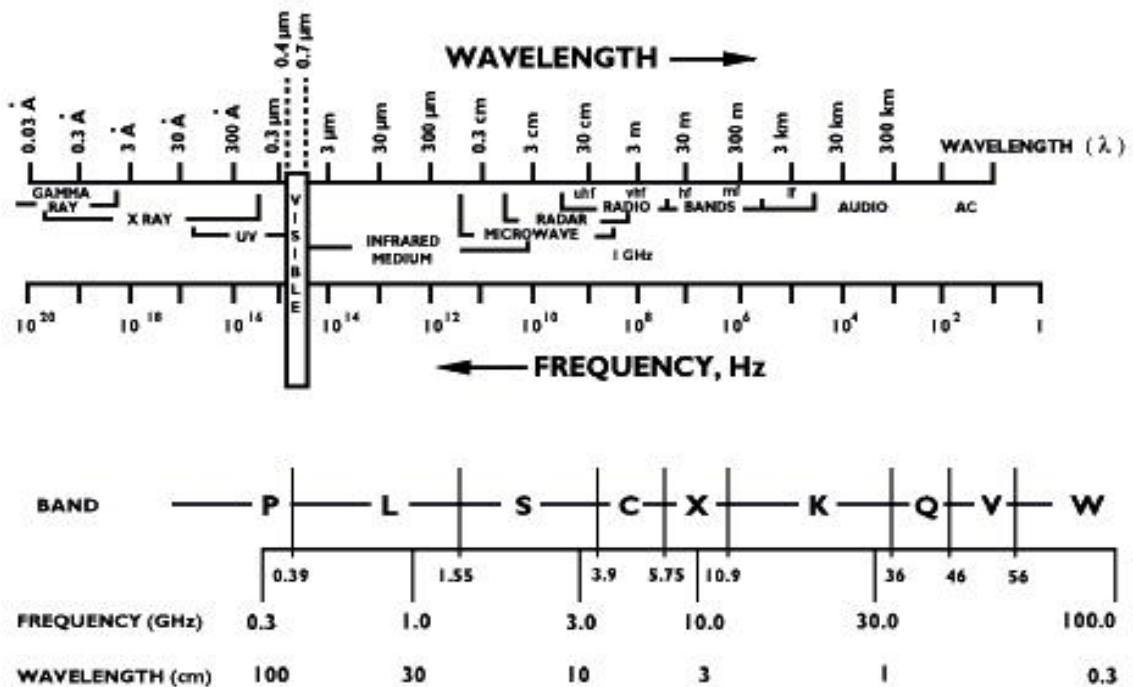


Figure 2. 1 Electromagnetic spectrum (ESA, [39])

Earth observation radar sensors operate with a side looking geometry as known Side Looking (Airborne) Radar (SLR-SLAR) also called Real Aperture Radar (RAR) and Synthetic Aperture Radar (SAR). In SAR systems radar sensor is mounted on an airborne or a spaceborne platform. During the forward motion of the platform, radar illuminates an area on the terrain which is called footprint. The flight direction of the SAR platform is called azimuth. The pulses of radar are sent to the terrain with a look angle (θ) which is perpendicular to the azimuth is called range direction (Figure 2.2). The complementary to the look angle is called depression angle (ψ).

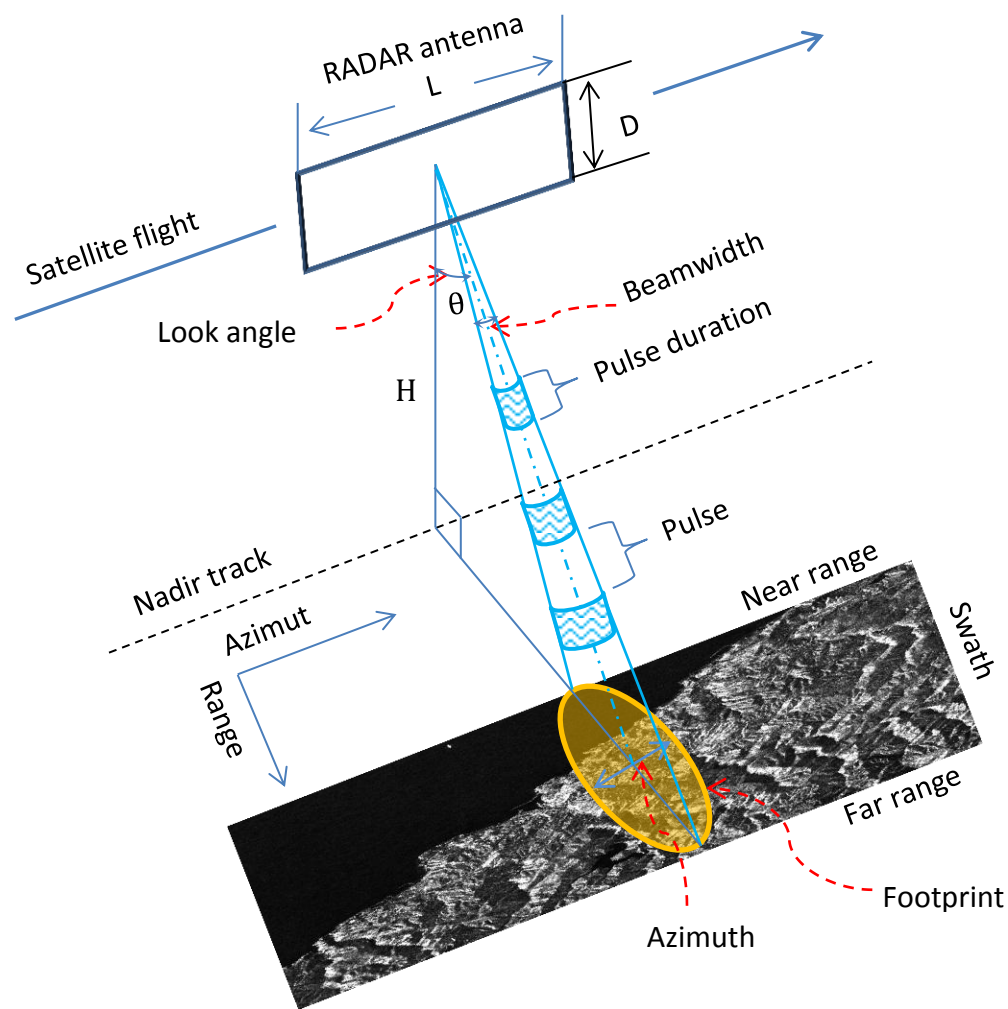


Figure 2. 2 Geometry of RAR (adapted from Cakir [40] and Wright [41])

In radar images both azimuth and range has different resolution. Ground range resolution of radar image is defined the minimum distance to separate two objects along the ground

range. The ground range resolution ΔR_g , depends on the pulse duration τ_p , which is the time between two radar pulses and the incidence angle η , where c is the speed of light,

$$\Delta R_g = \frac{c\tau_p}{2\sin\theta} \quad (2.1)$$

The range resolution and the signal to noise ratio can be improved in case the frequency is modulated. If radar are pulses shortened resolution will be improved. On the other hand pulses should transmit enough energy. For this reason long range radar systems are *chirped*. This approach is used with modulated frequency bandwidth, B_d (Wright [41]). Using this technique the ground range resolution is

$$\Delta R_g = \frac{c}{2B_d\sin\theta} \quad (2.2)$$

The azimuth resolution ΔA_g , depends on the physical antenna length L , the range R and wavelength of the signal λ . If the radar antenna is longer the resolution is better. Beam width $B_w = \lambda/L$ and the swath width on surface is $S_w = \lambda R_m/L \cos\eta$, where R_m is the middle slant range, η is incidence angle. Ground azimuth resolution $\Delta A_g = B_w R$, thus

$$\Delta A_g = \frac{R\lambda}{L} \quad (2.3)$$

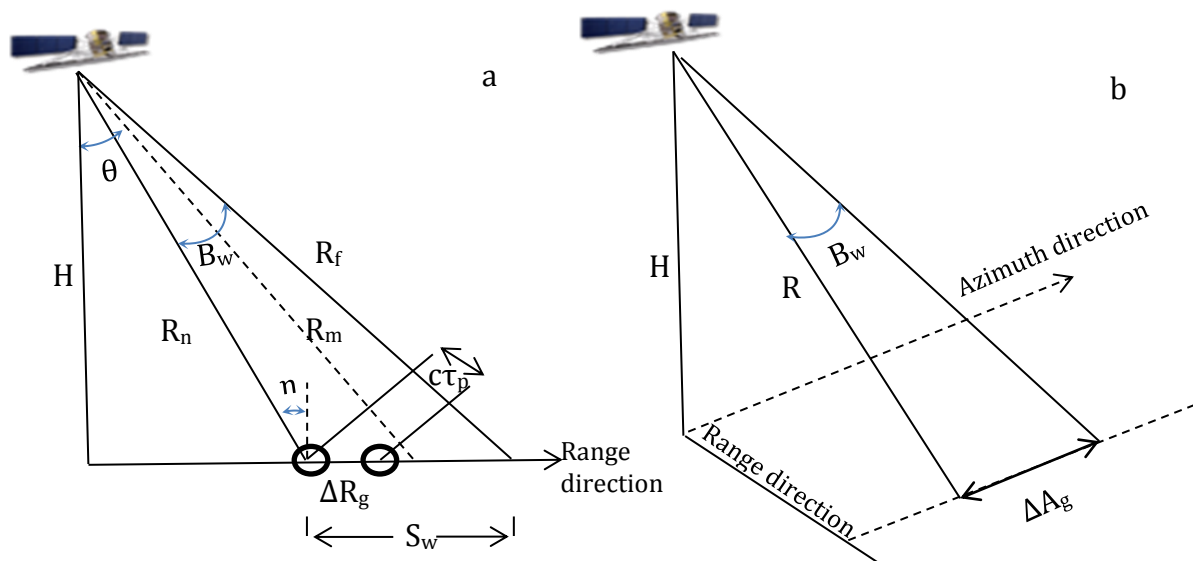


Figure 2. 3 a)Range resolution, b)Azimuth resolution (adapted from Cakir [40] and Wright [41])

Such a long antenna is not practical, due to fact that an advanced technique is developed as known Synthetic Aperture Radar (SAR). It is first represented by Graham [42] that azimuth resolution is improved. The concept comprises of an advanced technique called as *SAR focusing* technique. It is based on shifting the Doppler frequency of the return signal echoes. A large antenna is synthesized during the subsequent pulse returns from the same area illuminated on ground.

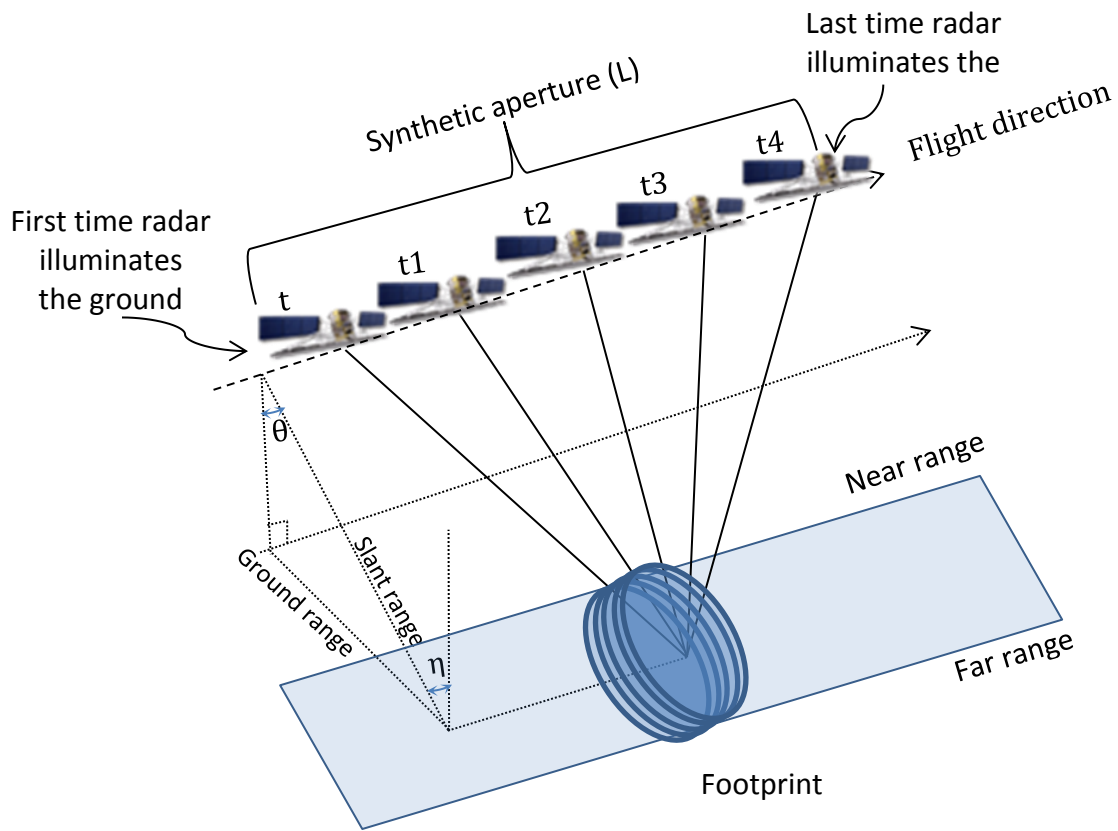


Figure 2. 4 SAR geometry (adapted from Cakir [40])

As shown in figure 2.4 total length of the simulated radar antenna compose synthetic aperture. The target area will be illuminated with many consecutive pulses which have different angles. Each illumination of the target area in each angle has different *Doppler frequency*, f_D (Lazeky [43]). The strong reflection as the Doppler frequency is zero will be received when the range distance is the smallest between the ground object and the radar. It should be smallest when the target is on the perpendicular direction to the radar.

As the radar antenna passes along its flight track the relative velocity between antenna and illuminated area changes and also earth's rotates which are causes a *Doppler effect*. However, there will be a slight angle of the radar platform called squint angle, ω_s (Hanssen [44]). The Doppler frequency for a target object, concerning the squint angle, and platform velocity v_s and look angle will be,

$$f_D = \frac{2v_s}{\lambda} \sin\omega_s \sin\theta \quad (2.3)$$

The Doppler frequency is zero, the zero Doppler, $f_D = 0\text{Hz}$, where the center frequency of the progression of a target through antenna beam is called the Doppler centroid frequency, f_{DC} . As the movement of the target through the beam the variation of the Doppler frequency composes the Doppler bandwidth B_{Dop} , where β_a is the width of azimuth beam of the radar antenna and the v_s is the relative velocity of the radar platform,

$$B_{Dop} = \frac{2\beta_a v_s}{\lambda} \quad (2.4)$$

Meanwhile, the azimuth resolution of a SAR focused image relevant to Doppler bandwidth and the relative velocity of the radar platform,

$$\Delta A_g = \frac{v_s}{B_{Dop}} = \frac{L}{2} \quad (2.5)$$

2.1.1 Properties of SAR Image

The focused SAR data is known as Single Look Complex (SLC) image which consists of amplitude and phase information. The antenna sends electromagnetic waves as pulses to the terrain and the scattered echoes are received. The received signal called backscatter which has both real and imaginary components in a complex format.

The amplitude image records the backscatter of the illuminated area. The backscatter values depend on the characteristics of the surface scatterer like topography, roughness and dielectric coefficient related to moisture of the ground. Tone, texture, size and shape parameters are used to interpretation of SAR images. Radar imagery tone is defined as

the intensity of the backscatter. If a surface is spotlessly smooth, the surface reflects like a mirror effect and radar pulse does not scatter back to the radar. A surface must have enough roughness to backscatter the energy. Roughness is relative and depends on the incidence angle and the wavelength of the radar. A surface is considered rough with the Rayleigh roughness criteria;

$$h > \frac{\lambda}{8\cos\eta} \quad (2.6)$$

where h is mean height of surface roughness feature, λ is wavelength of radar and η is incidence angle [2]. Dielectric coefficient is related to moisture content of the object. If an object has low water content will have low dielectric constant. That causes a high penetration depth, and a small amount of signal return. Wet soil, forest canopy, watered vegetation or young lavas appear dark and the amplitude is zero in SAR images due to the no or low signal return. If energy return to radar that the energy came from higher amplitude which is bright in image is recorded. Shape parameter can be described as the objects' outline as buildings, streets and bridges. Size and texture of the objects can be useful to recognize the features and provide for evaluation of the terrain analysis. Electromagnetic waves are transmitted in phase and during the receiving back the radar pulses interact to the object. The reflection can be a stronger bright return, and also weak dark due to being out of phase. This creates a grainy texture called salt and pepper or speckle. To overcome this situation and obtain better backscatter multi looking is applied on single look images by averaging of several pixels which decrease the pixel size as a result (Wright [41]).

SAR applications depend on the variety of radar wave frequency. Different bands are used for different applications. Satellite sensors have three kinds of bands X, C and L recently. For instance, length of the L-band is longer than C and X; therefore L-band can penetrate deeper than the other bands (Figure 2.5). It is more sensitive to estimate soil moisture and forest biomass than the other bands (Table 2.1).

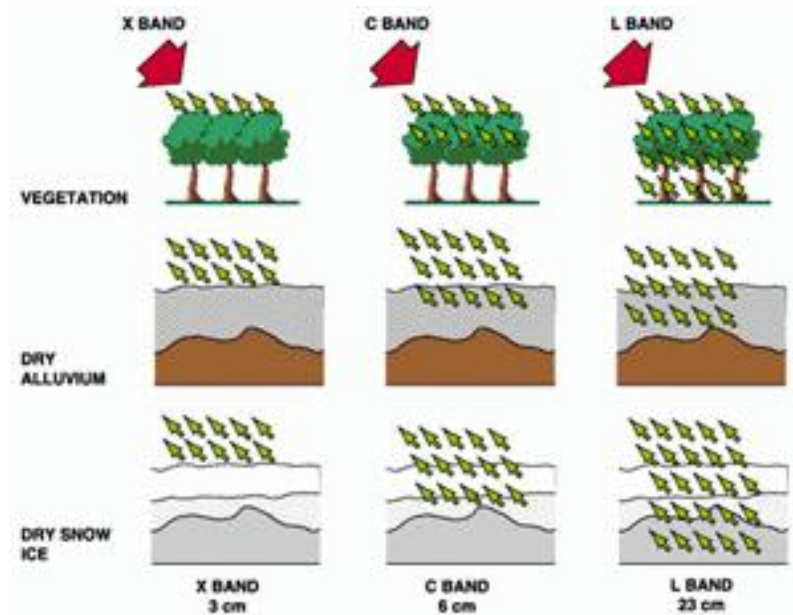


Figure 2. 5 Influence of wavelengths on objects (ESA, [45])

Table 2. 1 SAR bands with frequency and wavelength [46]

Band	Frequency (GHz)	Wavelength (cm)
P	0.225 – 0.39	133–76.90
L	0.39 – 1.55	76.9–19.40
S	1.55 – 3.90	19.4–7.69
C	3.9 – 5.75	7.69–5.21
X	5.75 – 10.90	5.21–2.75
Ku	10.9 – 18	2.75–1.67
K	18 – 26.50	1.67–1.13
Ka	26.5 – 36	1.13–0.83
Q	36 – 46	0.83–0.63
V	46 – 56	0.63–0.53
W	56 – 100	0.53–0.30

Another deterministic parameter is the polarization of the radar wave. It describes the orientation of the transmitted and received SAR wave. Horizontally (H) and Vertically (V) polarized images are used with different configurations as single co-polarization which can be HH or VV and also single-cross HV or VH, dual polarization with HH and HV, HH and VV, VV and VH, VV and HH, and quad polarimetry contains HH+HV+VH+VV. Here first term related to emitted radiation and the second one is received radiation. For some specific applications polarimetry can be a key point for interpretations. Different polarization combinations includes different information, thus it can be useful for the classification of agricultural areas where to separate mixed vegetation [47].

2.1.2 Distortions in SAR Image

Due to having geometry of side looking, geometrical distortions occur on SAR images. Because of the terrain topography on the slant range direction of radar *foreshortening*, *layover* and *shadow* distortions happen (Figure 2.6). Foreshortening depends on the incidence angle of radar and the slope of topography. If the slope is perpendicular to the satellite LOS the distortion gets its maximum.

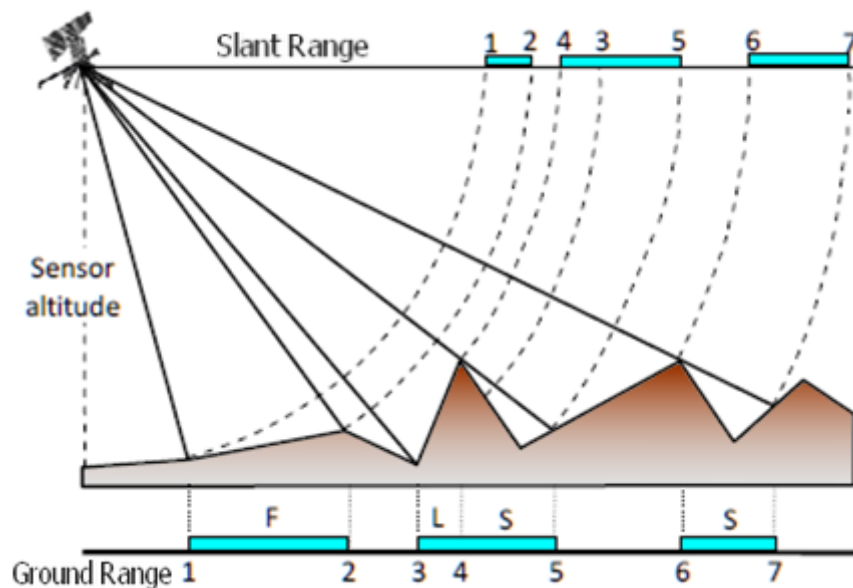


Figure 2. 6 Geometrical distortions in SAR images where F: Foreshortening, L: Layover, S: Shadow (adapted from Sousa [48])

In the radar images tones of foreshortened areas appear bright, and the distance between hill of the slope and bottom is appears shorter (Figure 2.6). If the radar pulses reaches top of a hill before the bottom a reversed slant range image occurs and this is called layover (Figure 2.6). In the image it appears bright where incidence angle is lower than the slope angle. Shadow happens where the slope is away from the sensor (Figure 2.6). The shadow area is not be illuminated so these parts appear dark in the image.

2.1.3 Satellite Acquisitions

Earth based satellite remote sensing of radar is started with the launch of SEASAT by NASA in 1978. Later the Shuttle Imaging Radar A (SIR-A) and SIR-B were launched in 1981 and 1984 respectively by NASA. These L-band space shuttles designed to experiment for monitoring of glacial movements, oceanography and terrestrial analysis. However, they could not have success for long time. In 1987 the former Soviet Union spacecraft Cosmos 1870 was launched as a first S-band SAR satellite, and it completed its mission in 1989. Later in 1991 second S-band satellite ALMAZ-1 which had 15 m ground resolution was launched. Same year European Space Agency (ESA) launched C-band European Remote Sensing satellite (ERS-1) which had 10 years acquisitions. ERS-2 was followed as a second mission which overlapped with the ERS-1, and was launched in 1995. For nine months ERS-2 followed in the same orbit of ERS-1 to compose TANDEM mission with 1 day temporal baseline. Late 2011 ERS-2 provide its last acquisition, and after 20 years ERS mission is completed with a wide archived data.

Japan launched L-band satellite named the Japanese Earth Resources Satellite (JERS-1). It operated from 1992 to 1998. Space shuttle radar observations continued with SIR-C/X-SAR which one launched in 1994. This was the first time that a satellite had three frequencies; X, C and L bands. Canada Space Agency (CSA) operates Radarsat-1 satellite since 1995. It has a very wide swath with 500 km on ScanSAR mode. The Shuttle Radar Topography Mission (SRTM) was designed to perform a single pass interferometry to overcome temporal decorrelation of repeat pass satellites. It was fixed with 60 m baseline between

two antennas. This mission used C and X band to compose Digital Elevation Model (DEM) for 12 days between 11 and 23 February 2000.

The Environmental Satellite (ENVISAT) was launched by ESA in 2002. It has ten different instruments to study on Earth as land, ocean and atmosphere. Advanced SAR (ASAR) is the radar sensor which is an advanced aspect of ERS mission. In 2006 Japan launched second L-band satellite called The Advanced Land Observing Satellite (ALOS) following the JERS-1. In 2007 other new generation SAR satellites were launched as COntellation of small Satellites for Mediterranean basin Observation (COSMO-SkyMed) (June 8th), TerraSAR-X (June 15th), Radarsat-2 (December 14th). COSMO-SkyMed which is operated by Italian Space Agency is the first radar constellation using four satellites equipped with X-band SAR sensor, and it has very short temporal baseline. TerraSAR-X is also an X-band satellite operated by German Aerospace Center (Deutschen Zentrums für Luft- und Raumfahrt - DLR) has an 11 day revisit time. C-band Radarsat-2 is operated by CSA. It has upgraded its routine as left and right looking operations. Spanish Earth Observation Program will launch a high resolution X-band satellite called SAR Observation Spanish Satellite (Satélite Español de Observación SAR - SEOSAR/PAZ) in 2012. ESA is developing new missions with five satellites called Sentinels for Global Monitoring for Environment and Security (GMES) services. Sentinel-1 will be a C-band radar satellite which will be launched in 2013.

Table 2. 2 Characteristics of SAR missions (adapted from [43], [44], [49], [50], [51], [52], [53])

Mission	Agency	Year	Orbit repeat (day)	f(GHz)	Bandwidth (MHz)	Incidence Angle(deg)	Swath (km)	λ (cm)	Polarization *	H _{sat} (km)	G _R (m)
Seasat	NASA	1978	3	1.275	19	20/23/26	100	23.5	HH	800	25
SIR-A	NASA	1981	-	1.275	6	47/50/53	50	23.5	HH	259	40
SIR-B	NASA	1984	-	1.275	12	15-55	20-40	23.5	HH	360/257/224	16-58
Cosmos 1870	RSA	1987-1989	-	3	-	30-60	20-45	9.6	HH	270	20
Magellan	NASA	1989-1992	-	2.385	2.26	18-50	25	12.6	HH	275/2100	120
ALMAZ-1	RSA	1991-1992	-	3	-	30-60	20-45	9.6	HH	270	15
ERS-1	ESA	1991-1992	3	5.3	15.55	21-23-26	100	5.57	VV	790	25
	ESA	1992-1993	35	5.3	15.55	21-23-26	100	5.57	VV	790	25
	ESA	1993-1994	3	5.3	15.55	21-23-26	100	5.57	VV	790	25
	ESA	1994-1995	168	5.3	15.55	21-23-26	100	5.57	VV	790	25
	ESA	1995-2000	35	5.3	15.55	21-23-26	100	5.57	VV	790	25
ERS-2	ESA	1995-2011	35	5.3	15.55	21-23-26	100	5.57	VV	790	25
	ESA	2011	3	5.3	15.55	21-23-26	100	5.57	VV	790	25
JERS-1	JAXA	1992-1998	44	1.275	15	26-35-41	75	23.5	HH	568	18
SIR-C/X SAR	NASA, DLR, ASI	1994	174	9.7	40	15-60	15-40	3.1	VV	225	30
SIR-C/X SAR	NASA, DLR, ASI	1994	174	5.2	20	15-60	15-90	5.8	S _{co} ,D,Q	225	30
SIR-C/X SAR	NASA, DLR, ASI	1994	174	1.28	10	15-60	15-90	23.5	S _{co} ,D,Q	225	30
Radarsat-1**	MDA	Since 1995	24	5.3	11.6/17.3/30	10-58	45-500	5.57	HH	793-821	8-100
SRTM	NASA, DLR, ASI	2000	0	5.3	10	54	225	5.66	HH,VV	233	90
SRTM	NASA, DLR, ASI	2000	0	9.6	10	54	50	3.1	VV	233	30
ENVISAT	ESA	2001-2010	35	5.331	14	15-45	50-405	5.56	S _{cr} , D	800	25-150
ENVISAT**	ESA	Since 2010	30	5.331	14	15-45	50-405	5.56	S _{cr} ,D	783	25
ALOS	JAXA	2006-2011	46	1.27	14/28	8-60	40-350	23.6	S _{cr} ,D,Q	692	7-100
TerraSAR-X**	DLR	Since 2007	11	9.65	150/300	15-60	5-150	3.11	S _{co} ,D,Q	514	1-18
Radarsat-2**	MDA	Since 2007	24	5.405	11.6/17.3/30/50/100	10-60	20-500	5.54	S _{co} ,D,Q	798	1-100
COSMO-SkyMed**	ASI	Since 2007	16	9.66	400	20-60	10-200	3.12	S _{cr} ,D	620	1-100

Mission	Agency	Year	Orbit repeat (day)	f(GHz)	Bandwidth (MHz)	Incidence Angle(deg)	Swath (km)	λ (cm)	Polarization *	H _{sat} (km)	G _R (m)
Kompsat-5	KARI	2012	28	9.66	-	20-55	10-100	3.12	S _{Co} , S _{Cr} D,Q	550	1-20
PAZ-SEOSAR	CDTI	2012	11	9.65	300	15-60	5-100	3.11	S _{Co} ,D	514	1-15
Sentinel-1	ESA	2013	12	5.405	100	20-45	20-400	5.54	S _{Co} ,D	693	5-40
ALOS-2	JAXA	2013	14	1.258	14/28/42/84	8-70	25-350	22.9	S _{Co} , S _{Cr} D,Q	628	3-100
SAOCOM-1A	CONAE, ASI	2014	16	1.275	50	20-50	30-350	23.5	S _{Co} ,D,Q	620	7-100

*S_{Co}=Single Co-polarized, S_{Cr}= Single Cross-polarized, D=Dual, Q=Quad, ** Current Missions

f= radar carrier frequency, λ = Wavelength, H_{sat}=Satellite altitude, G_R=Ground resolutio

2.2 InSAR Principles

Interferometric Synthetic Aperture Radar (InSAR or IfSAR) has phase information beside the amplitude information. Late 1970s InSAR became a very useful tool for earth observation of different applications. First Zisk [54] described one of the first studies on topography mapping of the Moon using interferometric observations in 1972. Graham showed the potential of radar as interferometers to monitor Earth topography by aircraft measurements [42]. Other airborne applications of terrestrial radar interferometry were presented late 1980's by Zebker and Goldstein [55], Goldstein and Zebker [56] (Akarvardar, [27]). Zebker and Goldstein [55] showed the *along track interferometry* which use two antenna mounted on aircraft. Along track interferometry transmits signal by a signal antenna and receive the reflected signal by that antenna and a second antenna at the same time.

Gabriel et al. presented first InSAR application to measure the LOS deformation ranging cm to mm accuracy [57]. They used *differential interferometry* (DInSAR) with three observations which were taken at different times to make two interferograms. One of them is topographic pair and the other one is deformation pair, and then calculated the differences of interferograms. Thus, the effect of topography can be removed. This *three-pass method* can only be used if the common image is correlated with the other two images. However, this condition cannot be possible due to decorrelation of high geometrical baseline or long temporal baseline. A *two-pass approach* and an external Digital Elevation Model (DEM) can be used. But DEM errors will be implicated. In that fact another approach called *four-based method* can be applied, where there is no common SAR image (Hannsen, 2001 [44]).

In 1990 Li and Goldstein also used repeat pass interferometry and an interferometric baseline was created with the passes of satellite revisit. Landers, California earthquake became the first event which was analyzed by DInSAR (Massonet et al., [8]). Since InSAR had success in variety of applications, beside the topographic mapping (Zebker and Goldstein [55], Madsen [58]) many deformation studies have been developed by DInSAR such as earthquakes, landslides, volcanoes, glacier motion, and land subsidence.

2.2.1 InSAR Geometry

The basis of the InSAR depends on difference of two SAR images which were taken from slightly different viewing positions. The difference pattern is called as *interferogram*. An Interferogram can be achieved by two ways, single-pass (along-track) interferometry and repeat-pass (across-track) interferometry. In the single-pass approach two SAR antennas are mounted on a single platform where first and second signals are acquired at the same time. In the repeat-pass interferometry one antenna is mounted on a platform which is mostly satellite passes over the same scene in different time with a slightly repeating orbit. In this work I will focus on repeat-pass interferometry where Figure 2.7 shows the configuration of SAR geometry;

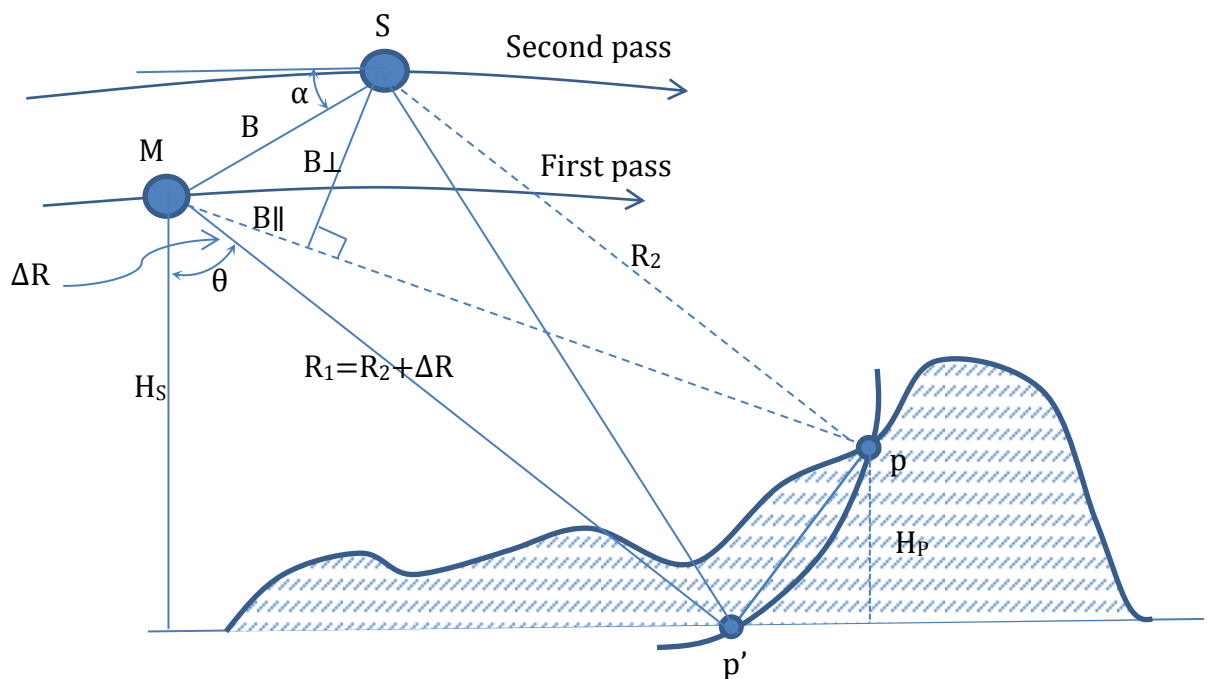


Figure 2. 7 InSAR Geometry

First SAR acquisition is called as *Master* image and the second one is referred as *Slave* image. The distance between these two acquisitions is called the interferometric baseline, the baseline vector B is composed of parallel ($B_{||}$) and perpendicular baseline (B_{\perp}). The time difference between two SAR acquisitions is called the temporal baseline. For the same pixel amplitude and phase components of two SAR images can be represented as A_1, A_2 and Φ_1, Φ_2 respectively. Interferogram is formed by cross-

multiplying pixel by pixel of complex conjugate of master image to slave image. The complex pixel C_p is described as below where Φ is the phase difference,

$$C_p = A_1 A_2 \cos \phi + i \sin \phi = A_{12} e^{i\phi} \quad (2.7)$$

$$\phi = \phi_1 - \phi_2 = -\frac{4\pi}{\lambda} \Delta R \quad (2.8)$$

ΔR is the range difference of two SAR acquisitions and α is the orientation angle of the baseline, it is not possible to derive ΔR directly from the geometry due to orbital inaccuracies and the 2π phase ambiguity,

$$(R_1 + \Delta R)^2 = R_1^2 + B^2 + 2R_1 B \sin(\theta - \alpha) \quad (2.9)$$

$$\Delta R \approx B \sin(\theta - \alpha) \quad (2.10)$$

Height of the target H_p can be given by,

$$H_p = H - R_1 \cos \theta \quad (2.11)$$

2.3 Deformation Monitoring by DInSAR

InSAR uses difference of two SAR phases to monitor the surface deformation. If the two measurements are taken within a temporal delay and a deformation occurs during this time, it is possible to detect deformation by the difference of the phases. If a subsidence occurs through the LOS direction second wave will travel longer than the first wave to the radar. Beside the deformation phase interferometric phase ϕ contains components as

$$\phi = \phi_{topo} + \phi_{def} + \phi_{atm} + \phi_{orb} + \phi_n \quad (2.12)$$

where ϕ_{topo} is the phase contribution of topographic profile, ϕ_{def} is the phase change due to surface deformation, ϕ_{atm} phase delay due to the atmosphere, ϕ_{orb} is the orbital errors, ϕ_n is the phase noise due to the decorrelation of baseline, thermal differences.

2.3.1 Topographic Phase Contribution

Due to having two SAR observations, an elevation contour like lines occur in an interferogram where the phases have equal lines (Akarvardar [27]). This sensitivity of topography is called as the altitude of ambiguity h_A is

$$h_A = \frac{R_2 \lambda \tan \theta}{2B_{\perp}} \quad (2.13)$$

It is actually the elevation difference which leads a 2π wavelength change in phase. Topographic phase can be removed by using an external DEM with two-pass method or DEM can be produced with three-pass method. After geocoding one of the SAR image DEM should be simulated with the same height ambiguity as in the interferogram and removed from the interferogram.

2.3.2 Atmospheric Delay

Interferometric phase measurements can be disturbed by the atmospheric effects which can cause phase delay in the observations. Water vapor, temperature, pressure in the troposphere can effect on signals. Due to atmospheric heterogeneities during the SAR acquisitions at different times extra fringes appear in the interferogram. Because of space and time variations of atmospheric water vapor, interferometric phase can be effected. If water vapor increase, signal will travel slower. As a result range will be increased and the phase will be delayed. It is presented that nighttime scenes have less affected than the daytime scenes by the atmosphere which is statistically more stable at night (Massonnet and Feigl [59]). Atmospheric phase signal is correlated with the topography of the area.

If phase signal is just appear in one interferogram and do not appear in other interferograms for the same time period, the phase change can be refer to atmospheric artifacts. To remote this affect GPS meteorology technique, water vapor measurements can be used. Another approach is using multi temporal interferograms which isolates phase variation due to atmospheric effects.

2.3.3 Orbit

As mentioned before SAR interferometry depends on relative measurements of two satellites which were spatially separated by different orbits. This separation leads a shift in the phase that is coming from the same surface. Some SAR systems do not have accurate information on their platform position and orientation which are needed to determine the topographic contribution. In an interferogram the orbital errors appears as near linear trends. If there is not deformation the interferometric phase should be expected flat over the interferogram (Wright [41]). If there is orbital errors deformation maps include the errors. The flat-earth trend should be removed by using precise orbits of satellites which were provided by ESA and the Delft Institute for Earth-Oriented Space Research.

2.3.4 Surface Deformation

If the phase contributions from topography, orbital effects and atmospheric delay removed any change in range direction correspond to surface deformation. The ground displacement (deformation) on LOS direction P_D of a p point between two SAR orbits is shown in Figure 2.8.

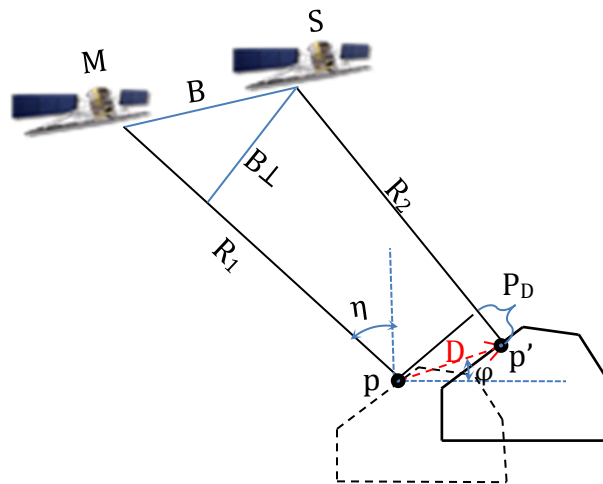


Figure 2. 8 Repeat-pass DInSAR geometry (adapted from Sousa [48])

The range of first orbit is R_1 and after the deformation the range of second orbit is R_2 . From the figure 2.8 the a deformation vector D in φ direction will give us the component of slant range deformation P_D ,

$$P_D = |D|\cos(\eta - \varphi) \quad (2.14)$$

In the estimated differential interferogram deformation is represented as homocentric circles which are called *fringes*. Each fringe gives length of half wavelength surface displacement along the LOS. This change is a relative change between 0 to 2π . Measurement of correct slant range distance depends on the correct integer numbers of phase cycles which should be added to each phase measurement. The absolute phase is fractional wrapped and has an ambiguity problem due to having an interval between 0 to 2π and solving this ambiguity is called *phase unwrapping*. This process finds the correct number of whole cycles and gives metric values of land deformation.

For the steps of DInSAR such as image registration, filtering and unwrapping there are many approaches described well in the literature, which will not be detailed here. Only the approach that I applied in this thesis will be detailed in the 3th chapter. Besides, these main references on the application and the theory of InSAR can be found in Gens and Van Genderen [3], Hanssen [44], Madsen et al. [58], Massonnet and Feigl [59], Bamler and Hartl [60], Rosen et al. [61].

2.3.5 Sources of Decorrelation in InSAR

As described in previous section, for the interferometric monitoring two sequent SAR images, which can be gathered in different times or simultaneously, are used. A correlation function of an interferogram is defined as coherence γ to compute the correlation coefficient between two SAR where $E\{\cdot\}$ is the operator of mean, S_1 is a pixel from the master image S_2 is the twin pixel in the slave image, and $*$ indicates complex conjugation,

$$\gamma = \frac{E\{S_1 S_2^*\}}{\sqrt{E\{|S_1|^2 E\{|S_2|^2\}}}}, 0 \leq \gamma \leq 1 \quad (2.15)$$

The coherence magnitude can be described as a function of Signal to Noise Ratio (SNR) of the interferogram (Hanssen [44])

$$|\gamma| = \frac{SNR}{SNR+1} \quad (2.16)$$

SNR is expressed as the ratio the power of received signal P_S to the power of the noise P_N ,

$$SNR = \frac{P_S}{P_N} \quad (2.17)$$

Every pixel in the interferogram specified with an absolute coherence value ($|\gamma|$) which can be used to accuracy of the interferogram. Its amplitude change between 0 and 1, and 1 indicates the highest coherence such as urban area where surface properties are identical in two SAR images. Conversely, zero values will be dark such as sea, river in the image and indicates that two images are decorrelated.

Source of decorrelations:

In repeat-pass InSAR one of the major reasons of loss in coherence is *temporal decorrelation*. This is caused due to change of terrain which affects the characteristics of surface scattering. These changes can be because of physical change as or a change of dielectric properties between two acquisitions. Correlation can be maintained long time in urban areas, rocky or rare vegetated areas. On the other hand decorrelation can occur within one day as landslide, harvest of crop, snowing. A convenient temporal baseline should be chosen for the application and the characteristics of the surface. When producing a deformation map long term gap between the acquisitions is required, short temporal baseline is needed for generating DEM.

Geometric decorrelation increases when baseline between two SAR orbits increase. This geometric decorrelation occurs if the difference of incidence angle between master and slave image is large. Baseline of the interferogram affects the topography estimation. Smallest perpendicular baseline can be acquired if the both images gathered almost from the same position. For the SAR imaging a *critical baseline* B_{crit} is described below which is cause to decorrelation. This baseline concerning to a spectral shift having the equal as the bandwidth B_d ,

$$B_{crit} = \lambda \left(\frac{B_d}{c} \right) R \tan(\theta - \zeta) \quad (2.18)$$

Here λ is the wavelength of the radar, ς is the topographic slope, θ is the incidence angle, R is the range and c is the speed of light. The geometric decorrelation γ_{geo} can be written as

$$\gamma_{geo} = \frac{B_{crit} - B_{\perp}}{B_{crit}}, B_{\perp} \leq B_{crit} \quad (2.19)$$

$$\gamma_{geo} = 0, B_{\perp} > B_{crit} \quad (2.20)$$

For flat terrain the $B_{crit} \cong 1.2$ km for ERS and ENVISAT satellites, and $B_{crit} \cong 13$ km for ALOS satellite.

Doppler centroid decorrelation γ_{DC} occurs due to the differences in the Doppler centroids between master and slave images Δf_{DC} ,

$$\gamma_{DC} = \begin{cases} 1 - \frac{\Delta f_{DC}}{B_d}, & \text{for } |\Delta f_{DC}| \leq B_d \\ 0 & \text{for } |\Delta f_{DC}| > B_d \end{cases} \quad (2.21)$$

where B_d is the bandwidth in the azimuth direction (Sousa [48]). If the Doppler centroids of two acquisitions do not overlap it cause the decorrelation. The coherence decreases with the increase of decorrelation.

Thermal decorrelation γ_T is a systematic effect of the device, and described by the SNR,

$$\gamma_T = \frac{1}{1 + SNR^{-1}} \quad (2.22)$$

Interferograms contain *volume decorrelation* related to the scattering medium of radar signals. The decorrelation increases with increasing volume scatter. Decorrelations can also be caused during the processing of chosen algorithms such as coregistration and interpolation. As interferometric SAR affected by many parameters which were described above, multi-temporal InSAR techniques have been developed to overcome these decorrelations, which will be detailed in the next section.

METHODOLOGY OF INSAR PROCESSING

3.1 Multi Temporal Time Series with InSAR Analysis

Conventional deformation monitoring by InSAR technique has been discussed in Chapter 2 with its pros and cons. The repeat pass InSAR technique has been under investigation by the end of 1990s to overcome the limitations. The main idea is to minimize the decorrelation effects as known long temporal and geometric baseline, and atmospheric inhomogeneity using multi temporal SAR images in a stack. A time series analysis can be applied to estimate the temporal evaluation of surface displacement over a period using multi temporal SAR images.

One approach is known as *persistent scatterer* (PS) pixels which show stable scattering in time are proposed by several groups (Ferretti et al. [12], Hooper et al. [14], Kampes [15]). Another approach which is known as *small baseline* (SB) method uses stack of conventional InSAR interferograms to obtain displacement change over time (Berardino et al., [17], Hooper [18], Schmidt and Burgmann [62]). In persistent scatterer InSAR (PSI), a single point scatterer is identified in ground resolution cells where SB approach identifies distribution of scatterers for resolution cells.

In this study SAR images are gathered in raw format and converted to SLC images with ROI_PAC public software (Rosen et al. [63]) interferogram processing is applied with the public domain Delft Object-Oriented Radar Interferometric Software (DORIS) (Kampes et al. [64]). For the estimation of geometrical baselines satellite orbit positions are needed. In this study interferograms are produced by using Delft precise orbits. The topographic effect is reduced by an external DEM as 3'' arc SRTM data

which has $\sim 90 \times 90$ m resolution. Geocoding is referred with World Geodetic System 1984 (WGS84) reference system.

PSI and SB approaches has been successfully applied for the detection of deformation at coal mining in recent years (Ng et al. [1], Mei et al. [29], Gueguen et al. [30], Baek et al. [31]). In this chapter, basic concepts of PSI and SB methods of Stanford Method for Persistent Scatterers (StaMPS) approach which extract deformation successfully from all terrains is represented (Hooper [65], [Hooper [66]).

3.1.1 Persistent Scatterer Interferometry of StaMPS

In this approach a set of N SAR images are used and $N-1$ interferograms are formed respect to one master SAR image. A stack of interferograms which have a common master is created. The master selection is based on to achieve higher coherence which depends on temporal baseline, geometrical baseline and the Doppler centroid frequency.

Due to terrain changes surface characteristics are effected which cause to loss of coherence. Decorrelation in a pixel depends on the backscatter distribution from the ground surface to this pixel. In SAR images the reflected energy from a resolution cell is composed from the total coherent contributions of different scatterers. Due to relative movement of these scatterers or view angle change can cause this decorrelation. The electromagnetic characteristics of the ground surface should not be changed from image to image. If one of the scatterer in the pixel is much brighter this dominant scatterer provides more contribution to the phase. The movement of the scatterer can be measured by the phase echo (Hooper [66]). Figure 3.1 shows the distributed and dominant scatterers in one pixel and below them simulated phase for 100 iterations.

In general two approaches of PS processing are defined. The first one extract the pixels which have stable phase in time (Ferretti et al. [67], Crosetto et al. [68], Kampes [15]). Atmospheric and orbital contributions are removed by phase difference of adjacent candidate pixels. From this double difference deformation and DEM error contributions are modeled for the time series. Lastly, noise level is estimated from

difference of the model and the double differenced phases (Hooper et al. [69]). This approach is not useful for non-urbanized areas.

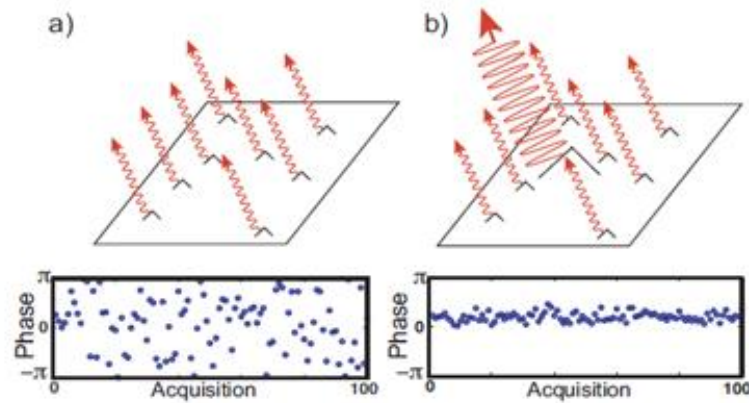


Figure 3. 1 a) Distributed scatterers that contribute to the phase in one pixel b) dominant PS in one pixel (Hooper [65])

The second approach searches for pixels that have spatial correlation with phase (Hooper et al. [14], van der Kooij et al. [70]). A spatial filter is applied to each candidate of PS to estimate spatially correlated phases as deformation, orbit error and atmospheric error. These contributions are subtracted and then from the remaining phase DEM error contribution is modeled for the time series. The noise for the pixel is estimated from the residual between the model and the phase.

In StaMPS first candidate PS points are selected from the stack of interferograms. For this amplitude dispersion index (D_A) (Ferretti et al. [67]) as the ratio of the standard deviation of the amplitude image (σ_A) to the mean of SAR amplitude images (μ_A) is calculated pixel-by-pixel with a given threshold value.

$$D_A = \sigma_A / \mu_A \quad (3.1)$$

After the selection of PS candidates StaMPS searches phase stability where pixels have almost zero noise. Phase stability depends on the assumption that deformation is correlated spatially. A phase observation is followed the adjacent PS candidates are filtered and which have the low residual noise are selected as PS points. In urban areas these PS points might be man-made structures as building, roofs, roads, bridges which most of the energy is directly reflected. In rural area also scatterers can occur as rocks or tree trunk.

Spatially uncorrelated DEM errors are estimated with an external DEM, and removed. Unwrapping is applied after DEM error removal and noise of each interferogram can be obtained with standard deviation estimation. Spatially correlated orbital errors are removed using precise orbital information.

In this approach deformation is correlated in time where atmosphere is correlated in space. Noise is uncorrelated in both time and space. Using filter in space and time, deformation phase can be separated from atmosphere phase and noise. Last product is the mean velocity at LOS direction in rate mm/year.

3.1.2 Small Baseline Interferometry of StaMPS

SB approach of StaMPS is similar to PSI approach. Here, less decorrelated phase is estimated from short intervals such as in time and in geometry. Thus, interferograms are calculated with a defined small temporal and geometrical baseline. Besides the PSI approach in SB there is not just one common master data. Interferograms are formed with a low noise minimizing the time interval, geometry and look angle. If the temporal difference is small between two images than the interferogram includes less temporal decorrelation. First SB approaches are used multilook to decrease decorrelation noise (Berardino et al. [17], Schmidt and Burgmann [62]). But multilooking also decrease the resolution. Further developments on SB provide full resolution process Hooper [19], (Lannari et al. [71]).

In SB method phase stability is given by the threshold amplitude difference dispersion index ($D_{\Delta A}$) which is ratio of standard deviation of master – slave difference in amplitude ($\sigma_{\Delta A}$) is divided by mean amplitude (μ_A).

$$D_{\Delta A} = \sigma_{\Delta A} / \mu_A \quad (3.2)$$

Filters are used in time and space to separate the deformation and atmospheric phase which is similar to PSI approach. A flowchart for the StaMPS multi temporal InSAR processing is given below in Figure 3.2.

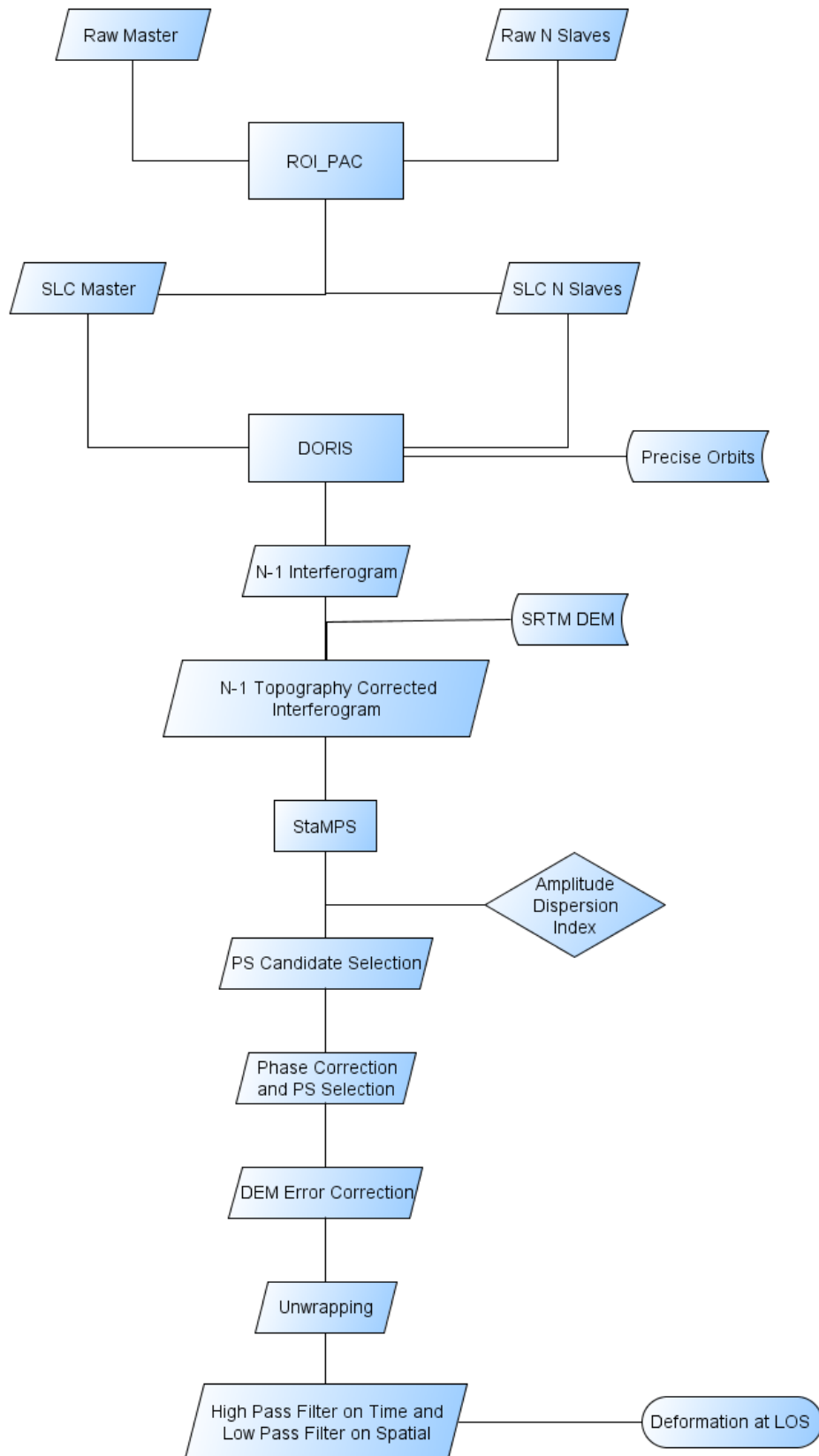


Figure 3. 2 Flowchart of StaMPS steps (adapted from Sousa [48] and Hooper [66])

SUBSIDENCE IN ZONGULDAK COAL MINE AREA

4.1 Study area

The study area, Zonguldak Province is the largest coal mining located in the north-west part of Turkey. Zonguldak city is the capital of Zonguldak Province in the west of Black Sea. The adjacent provinces of Zonguldak are Bartın in the east, Karabük in the southeast, Bolu in the south, and Düzce in the southwest. The population of the province is 612.406, and of 286.032 lives in 3.310 km². In the province there are 6 local authorities named Alaplı (185 km²), Çaycuma (392 km²), Devrek (935 km²), Gökçebeş (190 km²), Ereğli (972 km²) and the Zonguldak center (631 km²) (Figure 4.1) (TCE, [73]).

The province has a rough topography that of 56 % is composed of mountains, and the other parts are covered with plateaus and plain with the percentages of 31 % and 13 % respectively. In Zonguldak, forest areas covers the 52 % of the province area, and approximately 80 % of it is effective and 20 % of it is classified as poor forest. Agricultural fields covers 30 % of the province, and the rest of the area is covered with meadow and non-agricultural areas. Besides, Zonguldak is very rich about stream sources. There are five main streams namely Filyos, Yenice, Devrek, Aydınlar and Alaplı which are divided by valleys to many short streams. With three lakes and two ponds, total water surface is 16.06 km². Also there are underground water sources with a reserve of 90 hm³/year which of 10.5 hm³/year part are used by human (Governorship of Zonguldak, [74]).

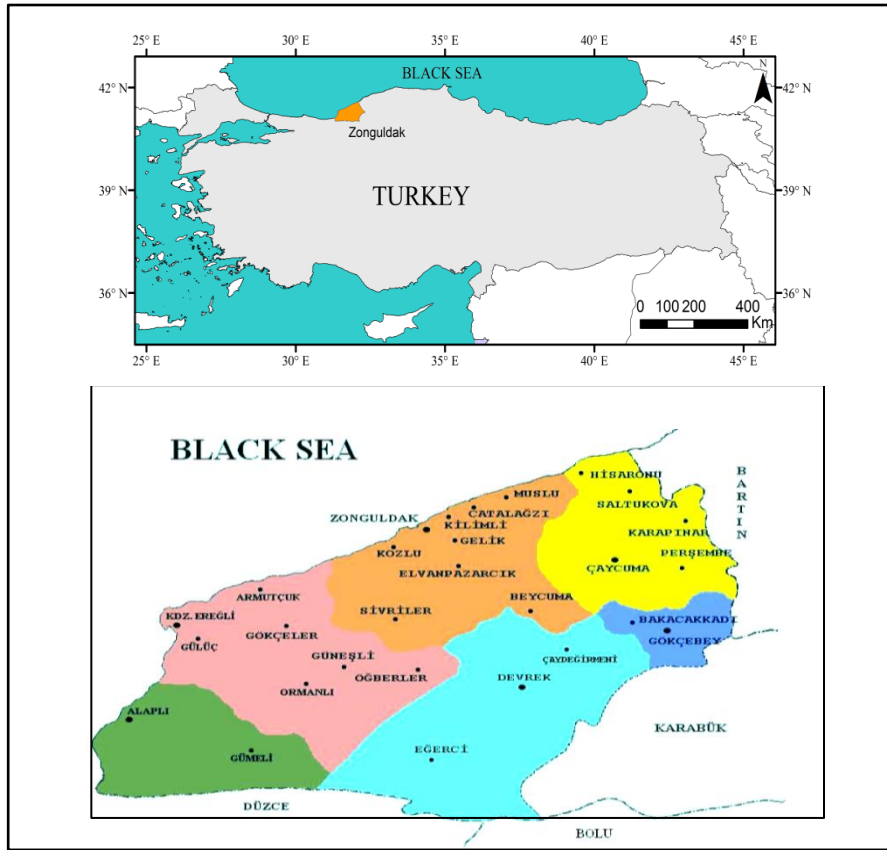


Figure 4. 1 Study area (TCE, [73])

Zonguldak has an oceanic climate (maritime climate), as precipitation distributed almost evenly through the year. Monthly average of the minimum and maximum daily temperatures and number of days with precipitation for the period 1975 and 2010 are shown in the Figure 4.2. Rainy season is mostly in autumn and winter. The mean humidity reaches up to 70 %.

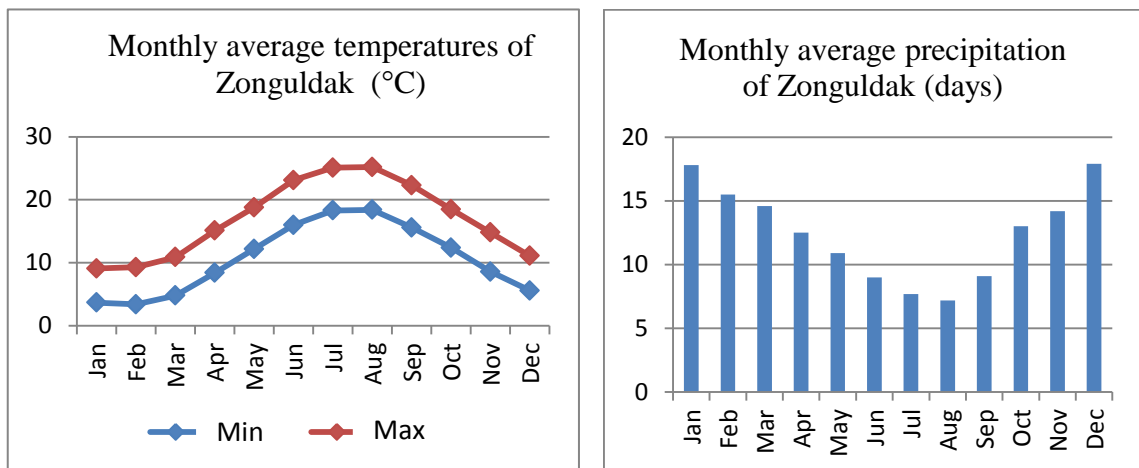


Figure 4. 2 Weather conditions of Zonguldak (adapted from Turkish State Meteorological Service [75])

In Zonguldak, there are many minerals such as boxite, barite, copper, colomit, limestone, basalt, manganese, quartzite, schiefertone and coal. Coal mining is active since 1848, and it is one of the main energy sources for Turkey. The study area is the center of the Zonguldak and has a size of about 25 km x 20 km with a steep topography (Figure 4.3). The altitude of mountains, which are line up parallel to the sea, ranges between 0 and 986 m. The DEM, slope and aspect of the study area are shown in Figure 4.3, Figure 4.4 and Figure 4.5 respectively within the subsidence area and potential subsidence area which are described by TTK.

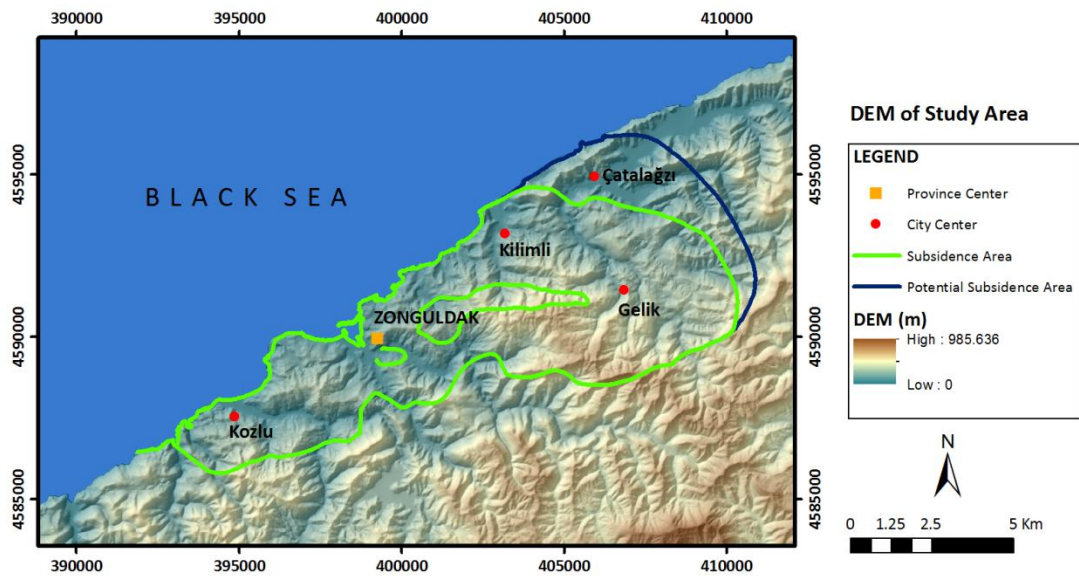


Figure 4. 3 DEM of Zonguldak city center

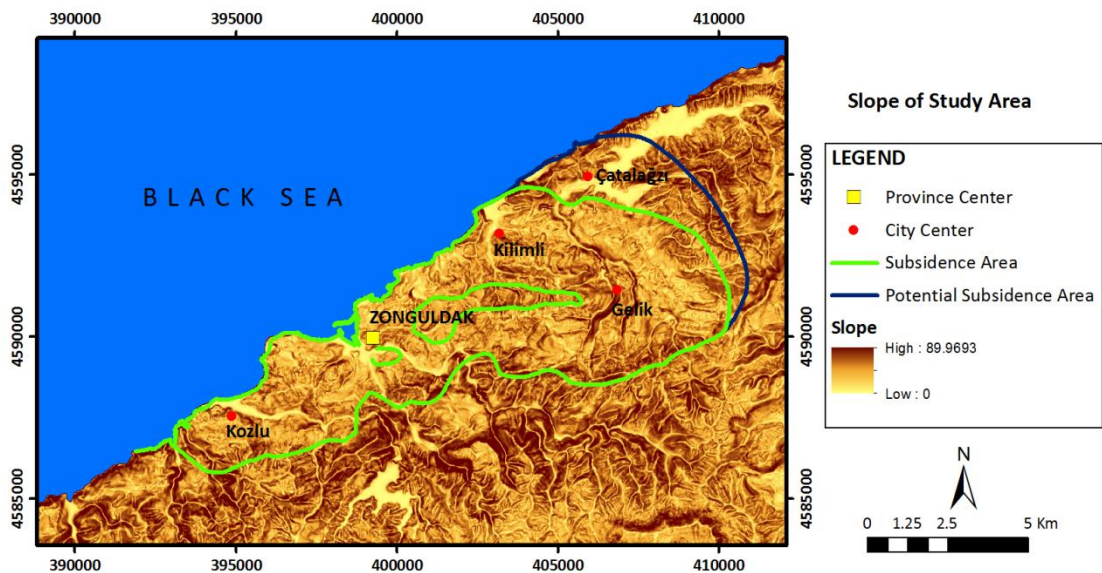


Figure 4. 4 Slope of the study area

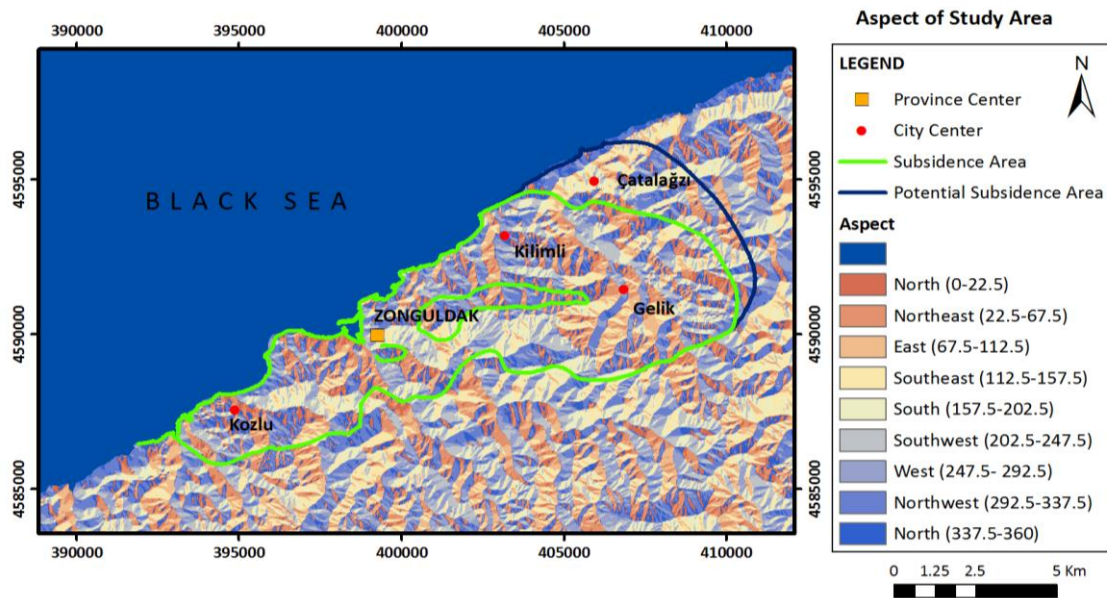


Figure 4. 5 Aspect of the study area

The population in Zonguldak increased after the coal mining activities. Rapid population as well as characteristics of topography caused an unplanned urbanization. Cities which are located at the coastline have higher population than other cities. Table 4.1 shows the population growth of Zonguldak versus Turkey.

Table 4. 1 Population growth of Zonguldak and Turkey (TSI, [72],[76])

Year	Population of Turkey	Annual Growth Rate of Population in Turkey (%)	Population of Zonguldak Center	Annual Growth Rate of Population in Zonguldak Center (%)
1965	31.391.421	-	148.041	-
1970	35.605.176	2.52	173.217	3.14
1975	40.347.719	2.50	194.700	2.34
1980	44.736.957	2.06	231.580	3.47
1985	50.664.458	2.49	250.164	1.54
1990	56.473.035	2.17	249.610	-0.44
2000	67.803.927	2.52	218.422	-1.33
2011	74.724.269	1.42	215.407	-0.12

4.1.1 Geological Background

The Zonguldak is located in the West Anatolian Pontides which is a part of Istanbul zone. In study area there are different lithological units belonging to Paleozoic, Mesozoic, and Cenozoic era. It has four main rock system which are formed from bottom to up in the order of Paleozoic Carboniferous, Mesozoic Upper-Jurassic,

Mesozoic-Cretaceous and Cenozoic-Quaternary (Figure 4.6). Above of the carboniferous period, there are karstic limestone forms at the lower cretaceous period. The Zonguldak basin is consist of limestone, volcanic rocks, clastics, and claystone forms. The coal seams are formed in Namurian to Westphalian stages of the coal bearing Carboniferous system of Paleozoic period (Duzgun [77], Turer et al. [78]). A general geology map is shown in Figure 4.7.

ERA	SYSTEM	SERIES	STAGE	FORMATION	THICKNESS	LITHOLOGY	EXPLANATION
Cenozoic	Quaternary	Holocene		Alluvium	10-60	Qal	
Mesozoic	Cretaceous	Lower		Yemişliçay	1000	Ky	Volcanogenic sandstone, tuff, agglomerate, basalt, andesite,
			Cenomanian	Tasmaca	0-400	Kk	Marlstone
			Albian	Sapça	500	Kkt	Claystone, limestone glauconite sandstone,
			Aptian	Kilimli	700	Kks	Sandstone, shale
				Velibey	250	Kkv	Sandstone
		Barremian	İnciğez	50-150	JKI	Conglomerate, sandstone, mudstone	
		Jurassic	Upper		İnaltı	300-400	JKIj
Paleozoic	Carboniferous	Lower	Westphalian-B,C	Karadon	350-550	Cka	Sandstone, coal conglomerate, claystone, diatomite,
			Westphalian-A	Kozlu	700-900	Cko	Conglomerate, sandstone, shale, mudstone, coal
			Namurian	Alacaagzı	300-1000	Ca	Shale, mudstone, sandstone, coal
		Upper	Visean	Yılanlı	500	DCy	Limestone, dolomitic limestone, dolomite

Figure 4. 6 Stratigraphic section of the study area (adapted from [36], [79], [80])

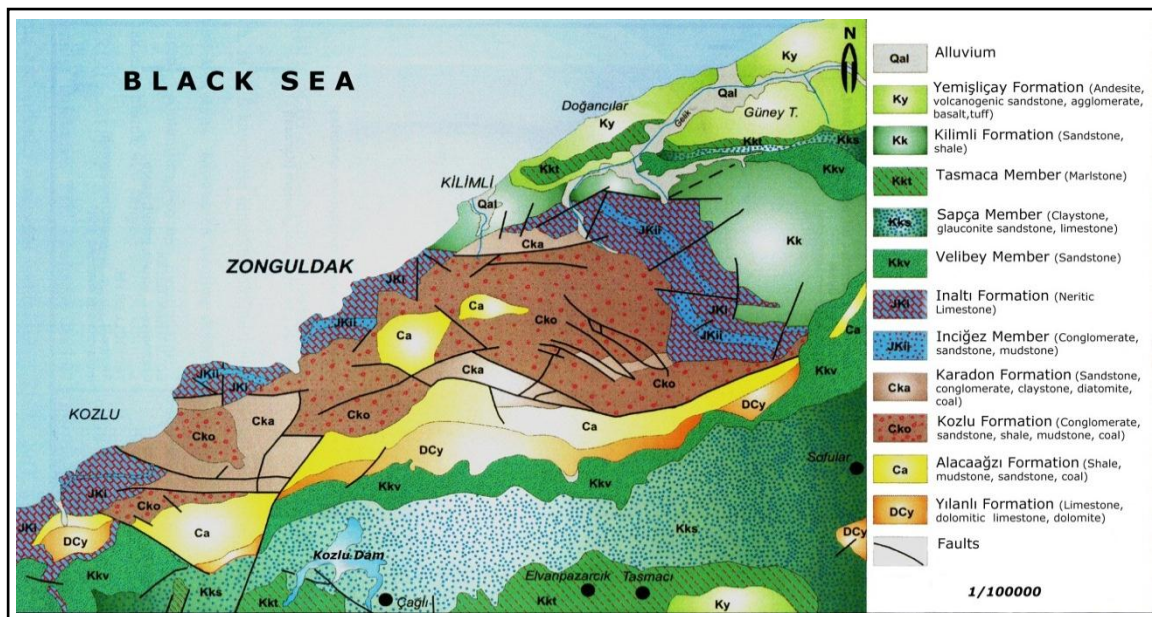


Figure 4. 7 The geological map of the Zonguldak city (adapted from [36])

The Kozlu formation which has about 700 m thickness consists of conglomerate, sandstones, shale, mudstone, and coal lithology with sequence. It is the most important one that has coal at carboniferous unit. Upper of Kozlu Karadon, İnalti and Kilimli formations exists with the sequence. Karadon formation shows similarities to Kozlu formation as conglomerate, sandstones, claystones, diatomite, and coal. But it has thinner coal seams than Kozlu. The İnalti formation consists of conglomerate, limestone and mudstone. The thickness of ranges between 2 to 4 m (Ciritoglu and Baysal [81]). Another coal included formation is Alacağzı which is at Namurian stage of carboniferous system. Alacağzı overlain on Yılanlı formation which is visean aged of carboniferous system. It consists of limestone, dolomitic limestone and dolomite. Two main facts as burial and subsequent uplift erosion are seen in this region at the carboniferous units (Hosgormez [82]). Volcanic and sedimentary rocks are formed at Eocene which are more suitable forms for landslides. The youngest lithological part is alluvium that occurs where streams fall to the sea.

In Zonguldak, karstic structure observable in paleozoik and mesozoik area. Moistured temperate weather triggers the formation of karstic generations as caves, dolines and sinkhole such as İnalti formation. In Zonguldak city, there are many big cave systems which include lakes and underground rivers. Most of them are in the mining area as shown in the Figure 4.8.

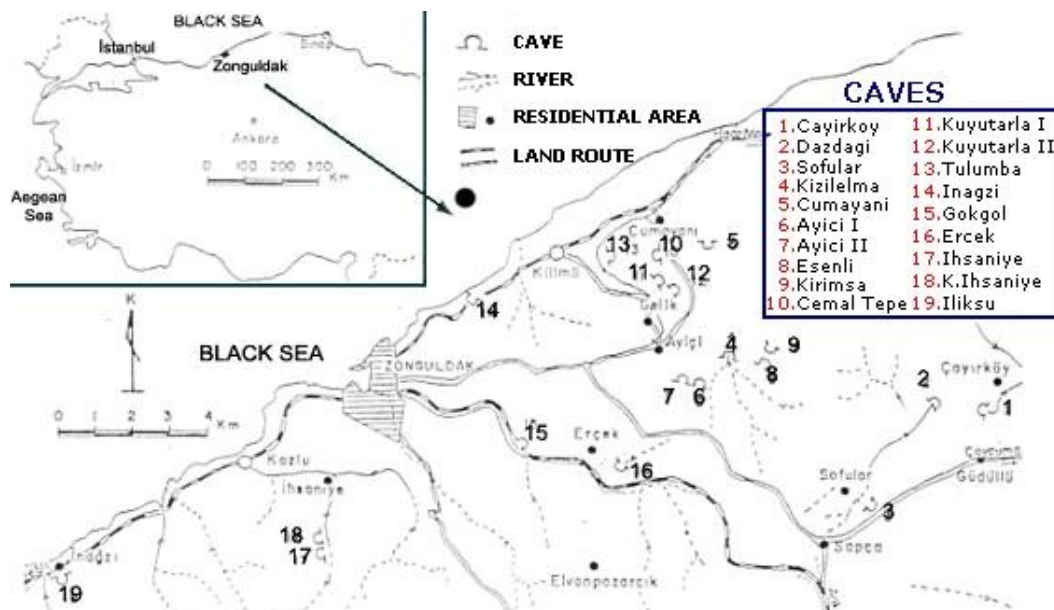


Figure 4. 8 Caves of Zonguldak (Bülent Ecevit University, [83])

One of the very well known cave is Gökgöl Cave which is formed in limestone of Yılanlı formation at visian age. The cave is located at 3 km away from the center of Zonguldak, and to the 1 km south of the coal mining area. It has a 3350 m lenght and 11 m depth. First 875m of it was opened to tourism. The cave includes three parts as fosil at the entrance, active and semi-active structures. There are many stalactite forms reaches to 2-5 m and underground streams.

Here some other caves which are in the center are described. One of them is Cumayanı which is located at 1km away from the district of Zonguldak Cumayanı. It has a 10 km length with all short branches, and has three entrances. This cave collects water from Ayıçin Aydın stream and a doline at Kızılelma. İnağzı cave is the another one, that is at the center of Zonguldak in İnağzı district. It is approximately 600 m and has short streams. Kızılelma is in Gelik disctriict where mining galleries are also located. It has a length of 6.5 km, and has stalactite and column structures (Bülent Ecevit University, [83]).

4.2 Coal Mining Activities in Zonguldak

Mining operations started in Zonguldak in 1848, in the time of the Ottoman Empire (Güney [84]). After mining operations, as a coastal settlement Zonguldak became an important province for Turkish industry. It has developed and became a district first and then a province in 1899 and in 1924 respectively. In 1983 Turkish Coal Enterprises (TTK-Türkiye Taşkömürü Kurumu) was founded. Zonguldak coal mining basin has two working fields where Area 1 has a 5.420 km² that of 3.000 km² is under the sea and 2.420 km² is on the land, and Area 2 has 1.465 km² working fields. Mining activities continue in 6.885 km² area is total (TCE, [73]). The border of the basin expands from Ereğli to İnebolu at the coastline with a length of approximately 200 km (Figure 4.9).

Approximately three million tons of coal is produced every year, and about 400 million tons of coal has been produced since 1848. From 1941 to 2011 378.400.902 ton raw coal produced and 229.668.436 ton are processed as salable. In Figure 4.10 the total amount of coal is shown as raw and processed. There are five underground coal-mining areas in the Zonguldak and Bartın provinces which are namely Kozlu, Karadon, Üzülmez, Armutçuk and Amasra. Amasra mine is located in Bartın province.

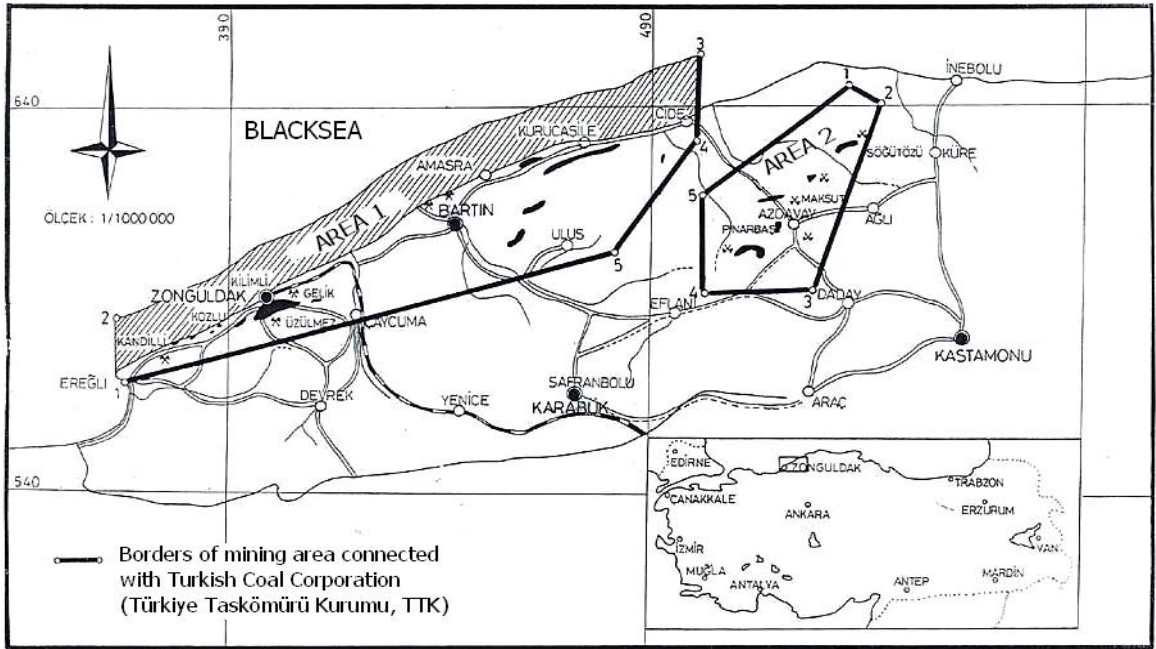


Figure 4. 9 Zonguldak coal basin (TCE, [73])

For these five regions, the raw coal productions and the processed coal productions are shown in Figure 4.11a and 4.11b respectively. Underground coal mining activities was continued from 1941 to 1974 with increasing production, and reached maximum in 1974 with an amount of 8.5 million ton.

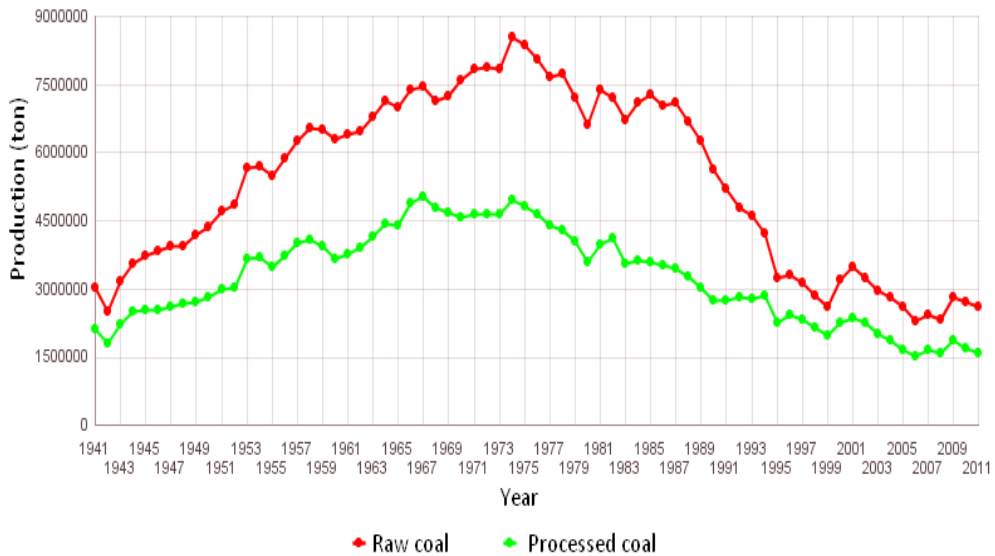


Figure 4. 10 Coal production of TTK in Zonguldak Province between 1941 and 2011 (TCE, [85])

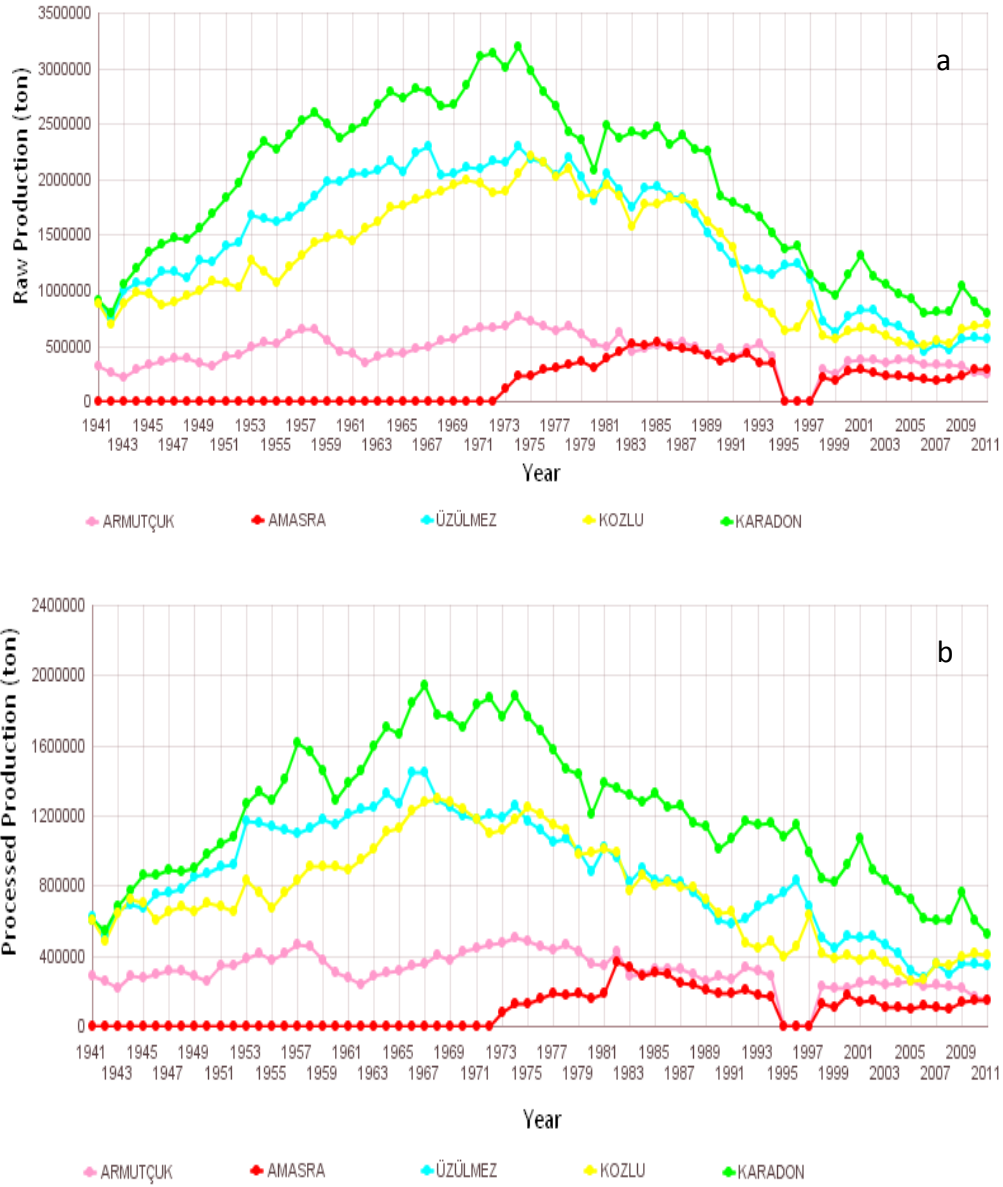


Figure 4. 11 Coal productions of TTK in 5 regions a) Raw b) Processed (TCE, [85])

As illustrated in Figure 4.11, until mid 70s coal productions were continued at 4 regions except Amasra, and production coal production was decreased after 1974. Although the mining has been started in Amasra in 1973, it started to decrease after 1982. After 2004 reserves which were not operated by TTK were given under control of private companies. According to the TTK report 2011 approximately 1.3 billion ton reserves are determined in total (Table 4.2) (TCE, [73]).

		2011							
		AMASRA	ARMUTÇUK	KARADON		KOZLU	ÜZÜLMEZ		
		RESERVE	RESERVE	Gelik RESERVE	Kilimli RESERVE	RESERVE	Asma-Dil. RESERVE	Bağlık-İnağzı RESERVE	
Depth									
Available		413.900	1.100.725	3.080.326	2.526.106	2.346.694	1.383.640		10.851.391
Available Total		413.900	1.100.725	3.080.326	2.526.106	2.346.694	1.383.640		10.851.391
Proved	-30/-550	170.828.066							170.828.066
	200/-650		9.033.413						9.033.413
	Mostra/-460			50.621.818	80.837.034				131.458.852
	Mostra/-700					67.690.363			67.690.363
	Mostra/-600						136.140.603		136.140.603
Proved Total		170.828.066	9.033.413	50.621.818	80.837.034	67.690.363	136.140.603		515.151.297
Probable	-100/-550	115.052.000							115.052.000
	-150/-650		15.859.636						15.859.636
	-460/-760			65.983.000					65.983.000
	-460/-860				93.179.000				93.179.000
	-700/-900					40.539.000			40.539.000
	-600/-800						32.060.000		32.060.000
	0/-1200							62.282.000	62.282.000
Probable Total		115.052.000	15.859.636	65.983.000	93.179.000	40.539.000	32.060.000	62.282.000	424.954.636
Possible	-550/-1200	121.535.000							121.535.000
	-200/-650		7.883.164						7.883.164
	-760/-1200			53.900.000					53.900.000
	-860/-1200				63.134.000				63.134.000
	-900/-1200					47.975.000			47.975.000
	-800/-1200							74.020.000	74.020.000
Possible Total		121.535.000	7.883.164	53.900.000	63.134.000	47.975.000		74.020.000	368.447.164
Total Amount		407.828.966	33.876.938	173.585.144	239.676.140	158.551.057	169.584.243	136.302.000	1.319.404.488

Table 4. 2 Reserves of Zonguldak coal basin (tonnes) (TCE, [73])

In this study I have focused on three mining areas as Kozlu, Karadon and Üzülmöz which are in the center city of Zonguldak and Kozlu, Kilimli, Gelik towns (Figure 4.12). Kozlu mine is 8 km west of Zonguldak city in Kozlu town and has a 12 km² area. In Kozlu region there are five coal seams with thickness from 1 to 3 m between -200 to -630 m depths under the city (Figure 4.13) [Can et al. 34]. Second location Karadon which located on Kilimli and Gelik towns, is 15 km east of center and has a 32 km² area. Coal productions are operated in Kilimli and Gelik enterprices. Operations are continuing between 130 and -540 m on 11 different coal seams which have thicknesses 1 to 3.3 m (Figure 4.14) (TCE, [73]). The last region Üzülmöz is in the city center of Zonguldak and has about 28 km² mine area. Mining production is continuing between -90 and -250 m. depth (Figure 4.15). There are seven coal seams and their thicknesses are changing 1.2 to 4 m.

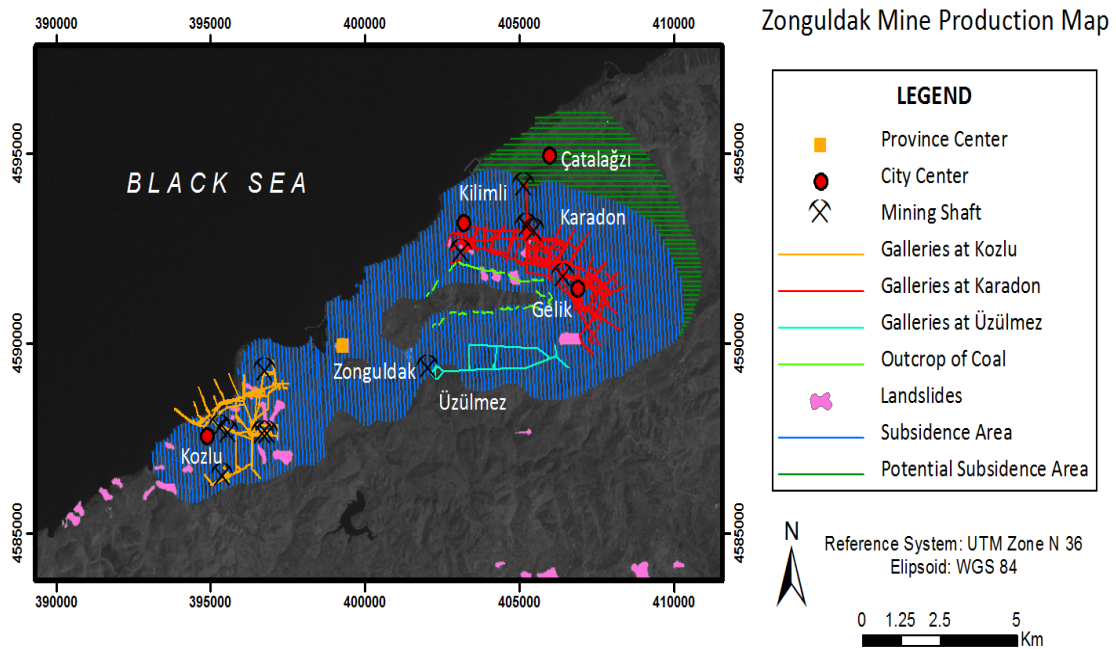


Figure 4. 12 Location of mining tunnels at the study area of Zonguldak showed on 20070724 dated panchromatic Landsat-ETM image (15 m ground resolution).

A subsidence area and a potential subsidence area are defined by TTK. The Subsidence Area includes three mining regions. The Potential Subsidence Area is located at the north of Karadon mining which includes Çatalağzı town (Figure 4.10). Between Üzülmöz and Karadon mining regions outcrop of coal are exist where coal can be extracted over the surface.

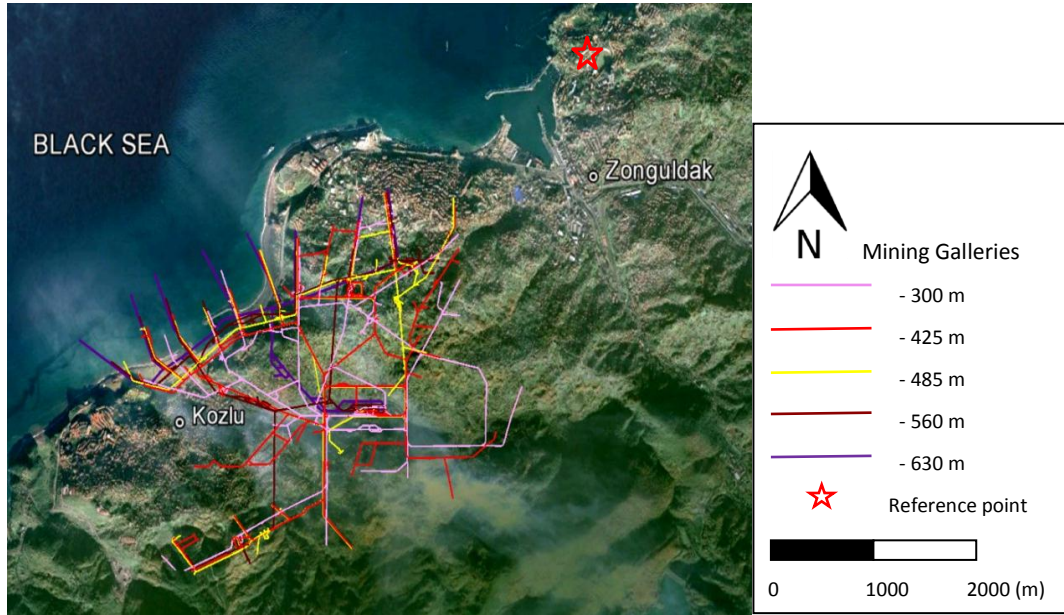


Figure 4. 13 Mine galleries in Kozlu (Background optical image is GoogleEarth)

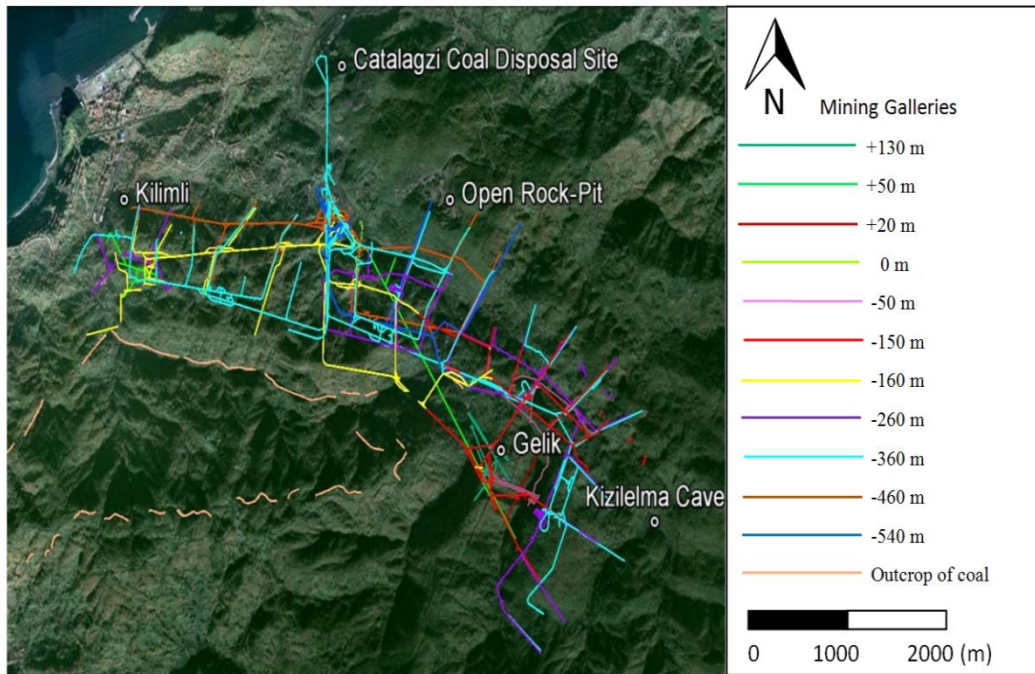


Figure 4. 14 Mine galleries in Karadon (Background optical image is GoogleEarth)

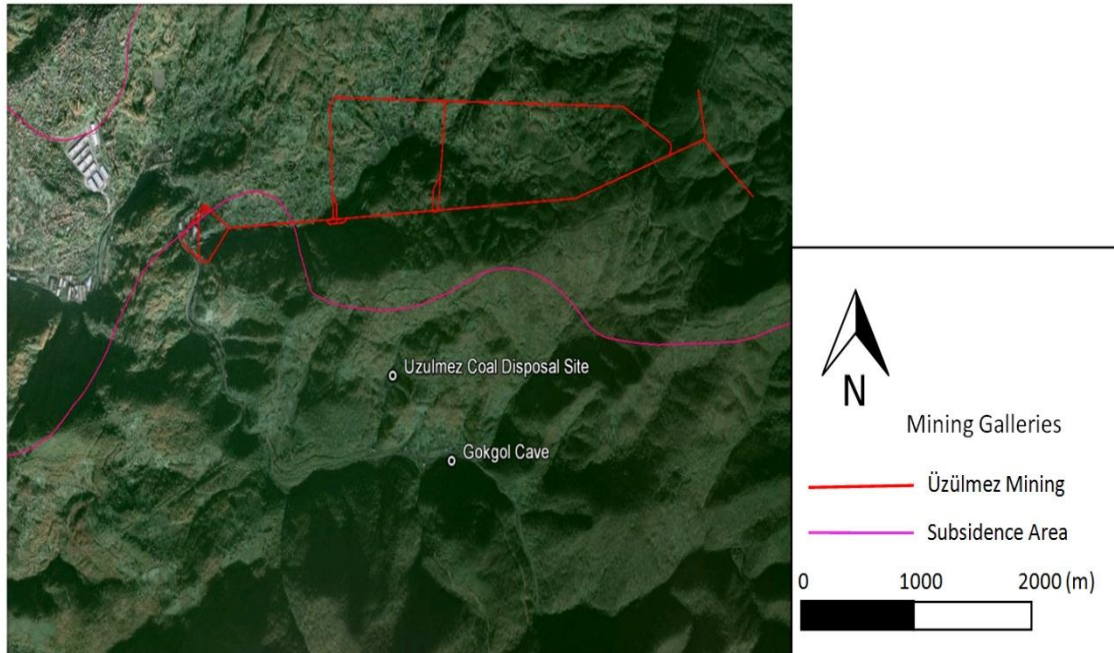


Figure 4. 15 Mine galleries in Üzülmöz (Background optical image is GoogleEarth)

4.2.1 Definition of Problem

At the beginning of the 20th century human-induced environmental problems such as subsidence was being caused due to mining from coalfields. Severe deformations in the region caused by subsidence have been known since the 1900s. Such deformations caused heavy damage on the Earth's surface, buildings, roads and ports that were on very large, expansive areas (Figure 4.16).

The effects of the subsidence of underground mining usually appear denser at settlements. Moreover, subsidence effects the balance of the geomorphological structure of the nature. The forest management and the drainage system should be considered as under danger. For the area where many flooding and landslides happen it is important to know the characteristic of the surface displacements.

In 1933, the Turkey Coal Basin Management Agency (TCBMA) provided maps including the locations of mining operation borders. Improved technologies were used as well, and the borderlines of the basin were extended with additional drilling. Nevertheless, because necessary precautions were not taken when making the reconstruction plans, the city grew over the operational mining areas.



Figure 4. 16 a-Deformations on building (Turer et al. [78]) and b-Deformations on ground (Can et al. [34])

The study area includes large sized and multi-story buildings that were damaged through subsidence. Zonguldak province was built and developed after the pit coal was found. To avoid the effects of urbanization on production, many regulations have been initiated since 1867. Since 1932, these limitations on construction have been strictly applied. In that process, it was noticed that incorrect decisions were made and inaccurate construction areas were used.

Today, the number of multi-story tower blocks is increasing every day in the city, beneath which large coal reserves exist. Observations definitely indicate that limestone at the coastline of Zonguldak is the main threatening factor of subsidence. Most of the buildings will be in an uninhabitable situation if coal production continues (Buyurgan [38]). It is obvious that Zonguldak is under the risk of a dangerous disaster.

The reconstruction plans of the Zonguldak Province areas that are on coalfields were revised in 1975 and again in 1990. However, because of a lack of coordination these plans could not be considered by the TCBMA, and today the urban area has a large problem with building damage that is irreversible. The drilling research showed that under the limestone-covered coastline of Zonguldak, which is from Kozlu to Kilimli, and also in Üzülmöz and Karadon million metric tons of pit coal existed. In the study area

the reserves of coal in Zonguldak city center reaches approximately 704 million ton according to the TTK report 2011 (Buyurgan [38], TCE [73]) (Figure 4.17).

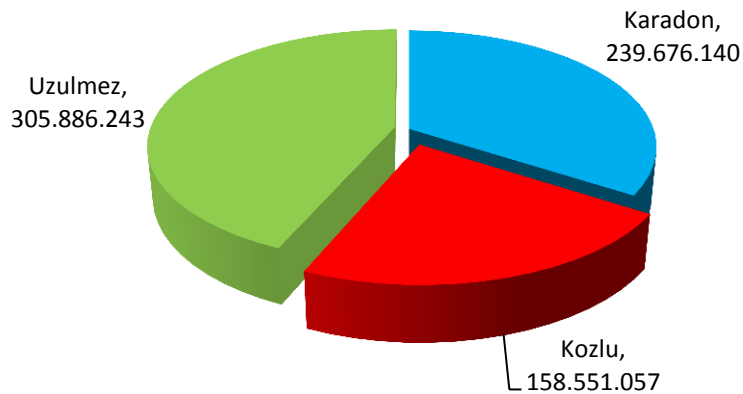


Figure 4. 17 Reserves in Zonguldak center

The shorelines of Zonguldak have a large amount of coal reserves and also have an attractive panorama. After a while, this area became built up as a high-rise residential region. This evolution has brought problems relating to both subsidence and mass movements. Especially with coastline mining, ancient cretaceous limestone has caused subsidence in the urban region. In the urban area of the study region many buildings and ground surface of structures have been strongly affected and damaged.

Due to geological structure Zonguldak underground coal mines suffer many roof falls. Detected roof falls in Kozlu, Karadon, Amasra, Üzülmez and Armutcuk are 5630, 12439, 3275, 6927, 1860 respectively between 1986 and 2003, and a lot of people lost their lives in Zonguldak region due to mining operations (Düzgün [77]). From 1941 to 2011 3754 person lost their lives and many people injured during the mining operations (Figure 4.18).

Storage of mining wastes is another important geo environmental problem (Table 4.3). The amount of waste reached to 139 million ton from 1865 to 2000 (Akçın et al. [87]). From 2004 to 2010 mining waste is increased %61 (Akçın and Çakır [88]). The waste is stored in forest area or at shoreline. But tides move them to seabed with effects the population of sea habitants. Forest is also polluted which is another increasing danger for nature and human.

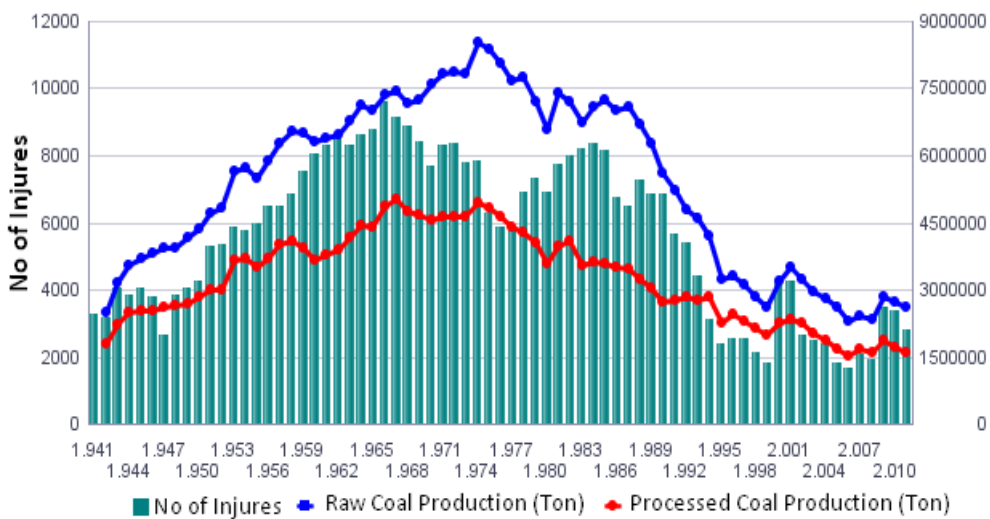
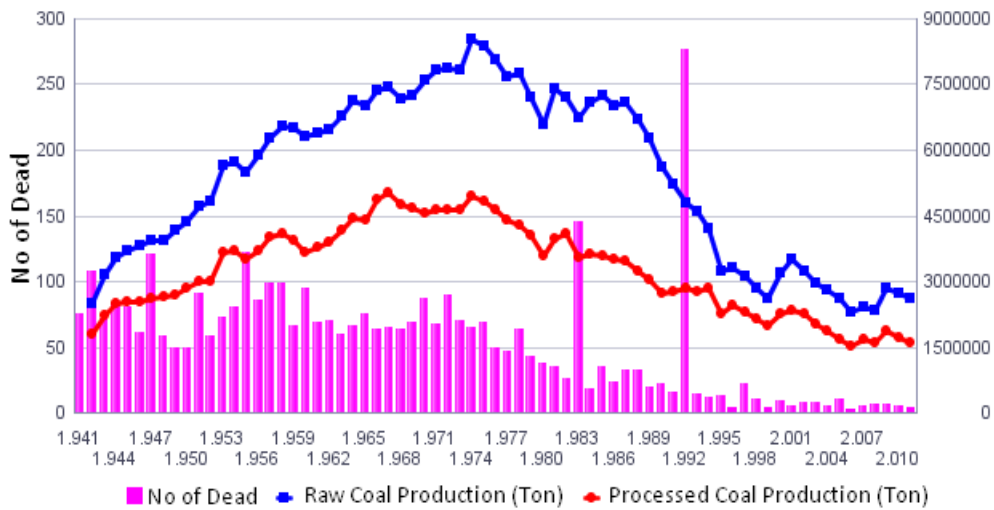


Figure 4. 18 a) No of dead per year and coal production, b) No of injures per year and coal production (TCE,[86])

Other problems due to geological structure are landslides, flooding and sinkholes. It is very proper to occur flooding and landslides in the city due to many water sources, geological properties and consistent precipitation. General Directorate of Mineral Research and Exploration (MTA) completed Landslide Inventory Map of Turkey Project in 2005 (Duman, et al [89]). For Zonguldak province 423 km² of province is determined as landslides (Turer et al. [78], Duman, et al [89]) (Figure 4.19). It is known this area is suitable for sinkhole development due to karstic terrain. Last time in 1st January of 2012 a sinkhole took place in Gelik region with about 8 m radius and 30 m depth (Posta, [90]).

Table 4. 3 Discharged waste water amounts of mining operations (TCE, [73])

Locations	Discharge of waste water (m ³ /day)	Treatment facility
TTK Kozlu mine	14500	None
TTK Karadon mine	14300	None
TTK Üzülmez mine	16438	None
TTK Coal plant center	1500	None
TTK Coal plant Catalagzi	1800	None

Firedamp and underground mine fire are the other disasters occur in mining. The biggest firedamp explosion happened in 1992 and 263 employee lost their lives. The last one happened in May 2010 at Karadon –540 m depth and 30 people lost their lives. Beside the official mining areas there are also illegal mining activities which also play an important role of risk on human life and settlements (Kutoğlu et al. [91]). Every year because of illegal mining people lost their lives in the mining due to undependable and uncontrolled conditions.

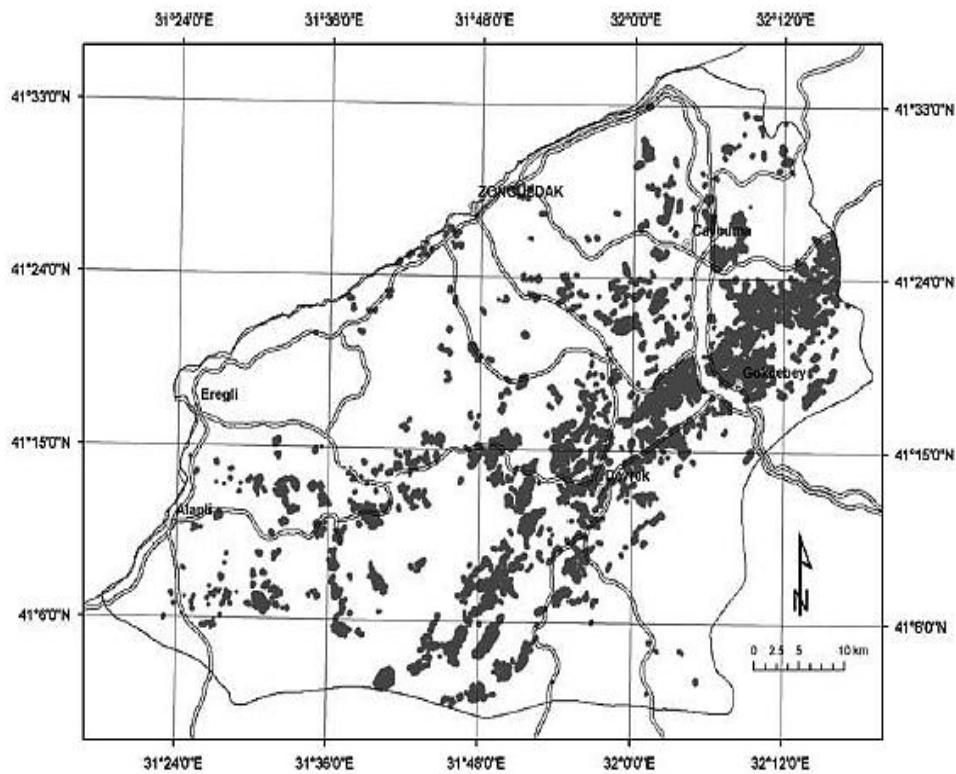


Figure 4. 19 Landslide map of Zonguldak province (Turer et al. [78])

Other factor is coal fire which happened last time in November 2007 in Gelik mine of Karadon. An underground coal fire was occurred, and many roofs collapsed (Çakır and Barış [92]).

It is obvious that observation of the area due to continuing collapses that have happened frequently in the last decade is necessary. Monitoring this area is thus of high importance to the government, mining industry and environment. Although the damage that has occurred in the region is not described in natural hazards regulations in Turkey, the types of damages and the amount of financial loss to citizens caused by building damage shows that the risk is high in Zonguldak Province.

The existence of residential areas is also a risk element that can increase subsidence effects to the point of a disaster. Some parts are still under serious risk due to the unorganized extension of urbanization. For this reason, it is very important to prevent loss of life and property due to the subsidence.

Mining subsidence does not just effects on buildings and roads also have effects on water, communication based underground pipelines which reduce the gradient of a watercourse, and as a consequence decrease the agricultural profit. Also land cover is affected due to surface deformation. Because of the effects on buildings, legal problems occur between owner of the building and the mining corporation. In the area of subsidence real estate is exposed to economic lost.

This thesis will not only contribute to preserve human life but also the country's economy. The study is aimed to investigate the subsidences that are damaging dwelling units in urban and also surface deformations in rural areas. At the end of the study, the magnitude of subsidence that is initiating surface deformations will be evaluated. The velocity of subsidence will also be estimated using the InSAR remote sensing technique and geological vision. The motivation of the proposed research is to estimate the effects of subsidence in order to further risk assessments and to contribute to the safety of the urbanization taking place in the region. It is assumed that the results are going to represent a new point of view for the research on change of geomorphological structure.

4.2.2 Formation of Mining Subsidence

Mining subsidence occurs on condition that enough space is created after the human based mineral deposits extractions such as salt or coal subsidence. After the extraction of minerals like coal, it leaves caverns behind. With the compression and the forces of surrounded rock strata a bowl shaped collapse happens, and the upper surface subsides. The amount of subsidence is always less than the depth of the mine. Subsidence can occur during the excavation but mostly happen a few days, weeks or year after the excavation. The movement of the surface can be vertical, horizontal or both. Subsidence happens where coal seam exists but the effect of the subsidence covers larger area on the surface.

The width of the effected surface depends on the geology between the center of the subsidence and surface, dimensions of mined area (depth, length, and width), slope of coal seam (limit angle, τ), mining method, and speed of mining operation. The relation between the width of the coal seam and the effect of subsidence is shown in Figure 4.20. If width of seam gets wider the possible surface subsidence also gets larger. Subcritical area is called when w/h rate is lower than 1.4. Where h is the depth of the coal, and w is the width of the extraction coal seam (Kemaldere [36]).

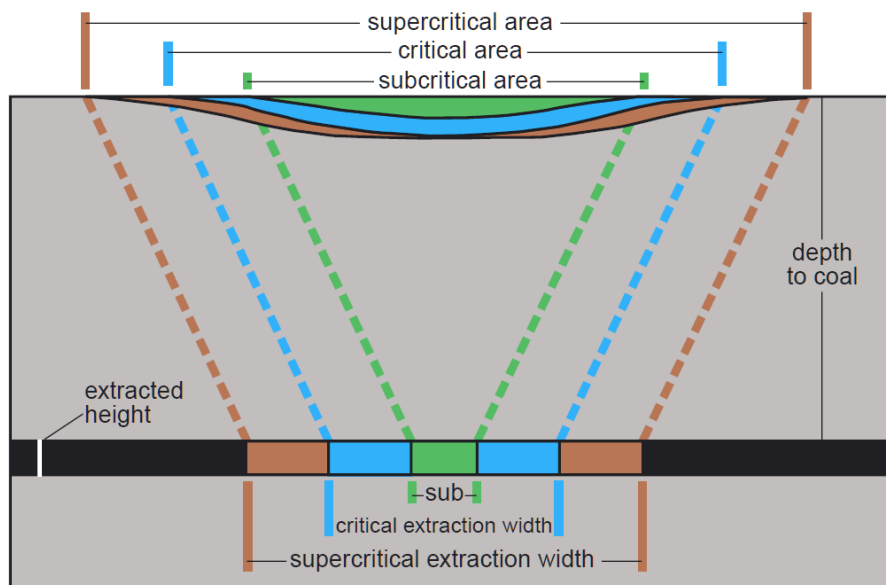


Figure 4. 20 Relationship between width of coal seam and the surface subsidence (Bauer [93])

Figure 4.21 depicts the subsidence bowl where the coal seam is flat, and its effect on the surface, where S_M is maximum subsidence. Figure 4.22 shows the subsidence of sloped coal seam, and the affected surface area.

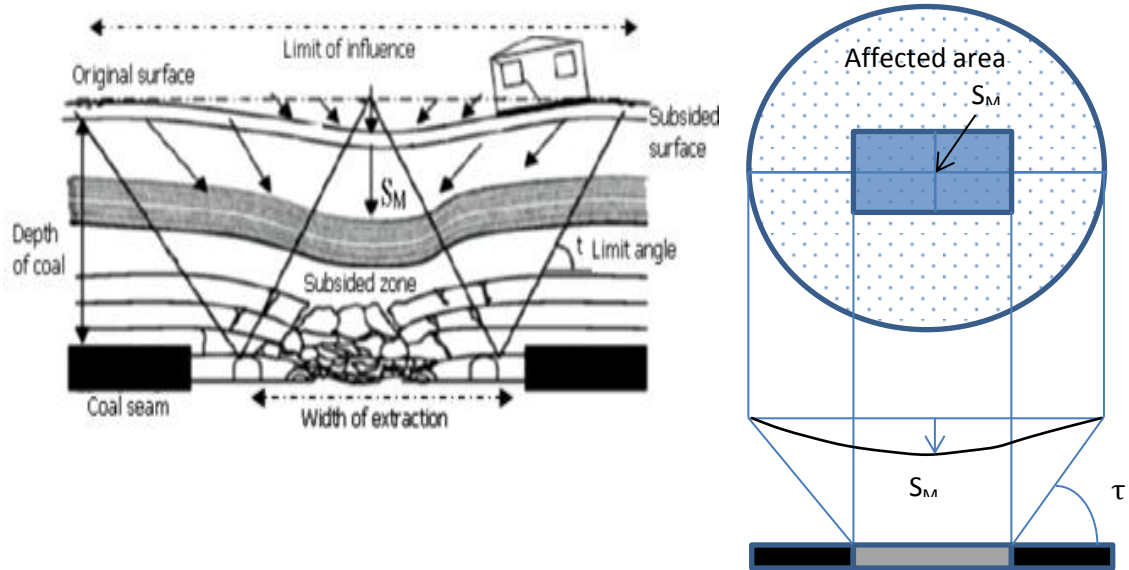


Figure 4. 21 Subsidence at flat coal seam (adapted from Kutoğlu et al [91], Can et al. [94])

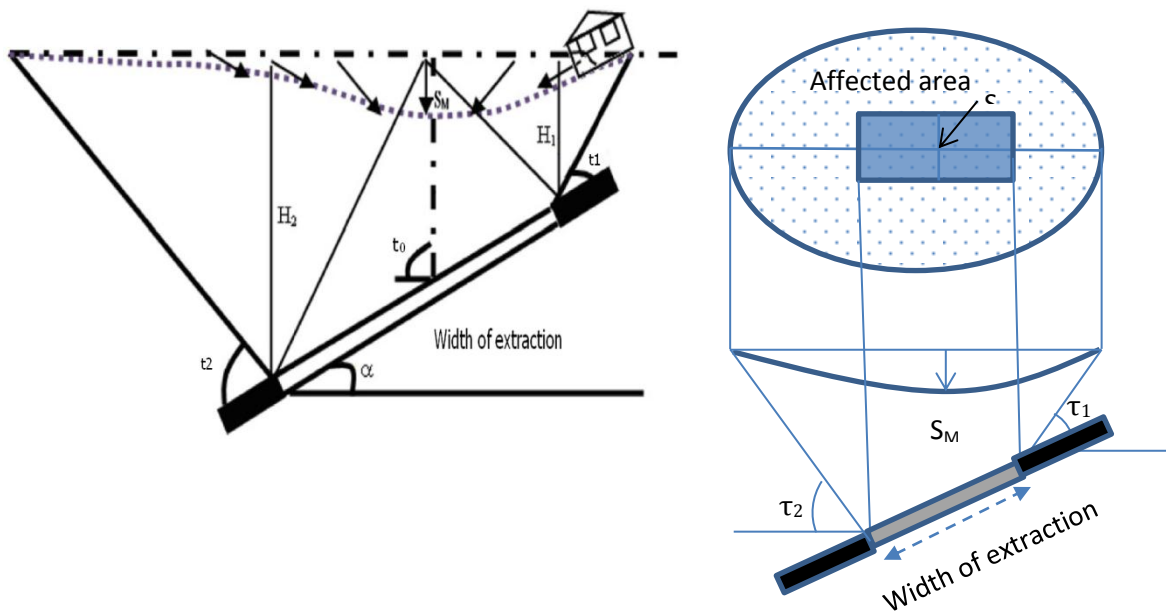


Figure 4. 22 Subsidence at sloped coal seam (τ_1 and τ_2 are the slopes of the coal seam, τ_0 is the slope where subsidence is maximum) (Adapted from Can et al. [94])

4.2.3 Prior Subsidence Studies at Zonguldak Mine

In Turkey Zonguldak province is a well-known region where continuous subsidences occur. In Zonguldak mining region several methods were used for subsidence measurements as leveling and GPS measurements. But these techniques have drawbacks, such as they are point-by-point based and short term measurements (Sezer et al. [32], Akçın et al. [33], Can et al. [34]). These are also time consuming and localized studies. Regional deformation monitoring is difficult with conventional geodesic techniques (Düzgün and Demirel [95]). GPS and leveling measurements have not been applied at Karadon and Üzülmöz regions. In the Zonguldak region, subsidence was monitored by previous InSAR studies (Akçın et al., [33], Deguchi et al. [35], Kemaldere [36]) which gives information about the deformation in short term time periods. Previous studies are summarized with Table 4.4. A detailed comparison is composed in Chapter 6.

Table 4. 4 Previous subsidence monitoring studies on Zonguldak

Referans	Method	Period	Data	Kozlu	Karadon	Üzülmöz
Deguchi et al [35]	DINSAR	Sept-May 1995	JERS 1 pair	204 mm/ 4.5 months	204 mm/ 4.5 months	204 mm/ 4.5 months
Akçın et al. [33]	DINSAR	2005-2006	RADARSAT 15 images	44mm/year	None	None
Akçın et al. [33]	GPS	2005-2006	-	61 mm/year	None	None
Deguchi et al [35]	DINSAR	Aug-Sept 2006	PALSAR 1 pair	none	30-40 mm/ 1.5 month	30-40 mm/ 1.5 month
Kemaldere [36]	DINSAR	Sept 2006 Dec 2007	PALSAR 1 pair	95 mm/year	None	None
Kemaldere [36]	DINSAR	Dec 2007 Mar 2010	PALSAR 1 pair	88 mm/year	53 mm/year	None
Kemaldere [36]	DINSAR	Oct 2008 May2009	ENVISAT 1 pair	50 mm/7months	None	None
Kemaldere, [36]	DINSAR	May 2009 Nov 2009	ENVISAT 1 pair	40 mm/6 months	None	None
Kemaldere [36]	DINSAR	Nov 2009 Apr 2010	ENVISAT 1 pair	50 mm/4.5 months	None	None
Can et al. [34]	GPS	Aug 2009 May 2010	-	10-78 mm/9 months	None	None
Can et al. [96]	Levelling	2 periods 10 months	-	25-75 mm	None	None

MULTI TEMPORAL InSAR OBSERVATIONS RESULTS

In this chapter the data used and the results determined by multi temporal InSAR monitoring on Zonguldak region are presented. All available SAR data of ERS, ENVISAT and PALSAR were processed using StaMPS approach of PSI and SB methods. For the mining area time series of the subsidence is evaluated for urban and rural areas. Application of multi temporal InSAR approaches provided similar results, however some limitations and differences are also obtained. Details of the evaluation are presented in Section 5.2 and the discussions are presented in Chapter 6.

5.1 Available SAR Dataset

All SAR data achieved within ESA archives for 17 years period were monitoring between 1993 and 2010 (Table 5.1). Except the SLC images of ERS data all data were acquired in raw format. While selecting the data the orbits were chosen which have as many images as possible for the same frame (Figure 5.2). Because of that seasonal distinction was not under consideration. One of the advantages of SAR monitoring is being capable of acquiring in ascending and descending orbits. It is achieved that 10 ERS-1 and 16 ERS-2 images which are from descending orbits. Furthermore two tracks of ENVISAT ASAR images are gathered in each two passes, 17 ascending and 26 descending passes. Moreover 23 images of ascending L band ALOS PALSAR were also investigated for the subsidence phenomena. Beside the SAR data for the processing SRTM data, vector data of galleries of the mining areas, meteorological data for each acquisition of SAR data were used.

Table 5. 1 Specifications of available dataset

Sensor	Swath km	Orbit	Track No	Frame No	λ cm	Pol.	Scene No	Time period
ERS	80	Descending	21	2773	5.6	VV	33	19930418-20010110
ENVISAT	I2-105	Descending	21	2770	5.6	VV	29	20031126-20100113
ENVISAT	I2-105	Ascending	343	824	5.6	VV	17	20040506-20100729
PALSAR	70	Ascending	604	820	23.6	HH	13	20070118-20100428
PALSAR	70	Ascending	604	820	23.6	HH+HV	10	20070905-20100613

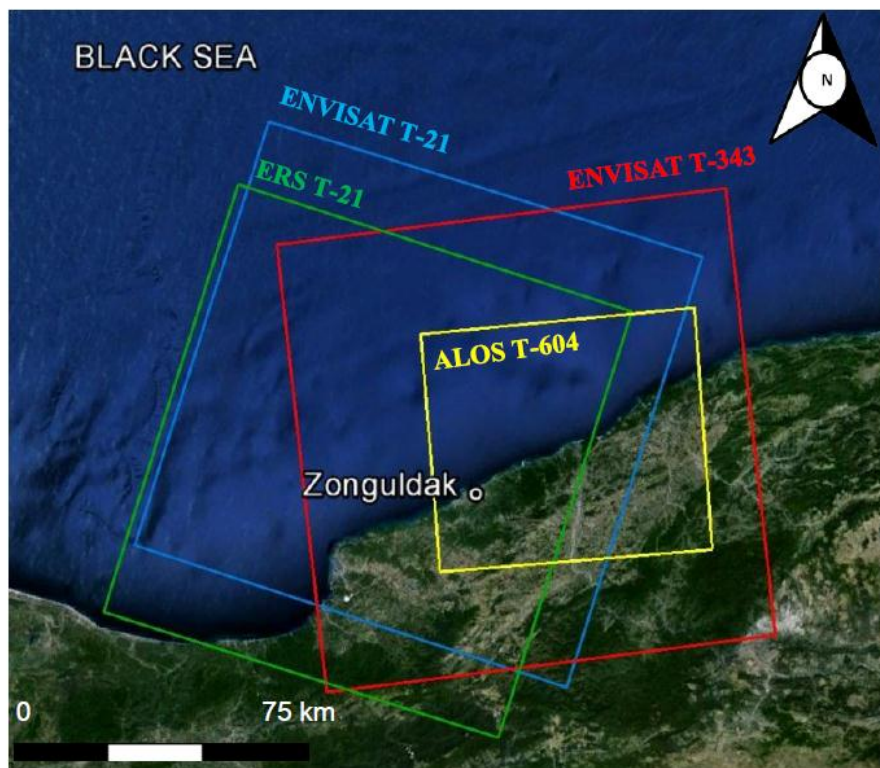


Figure 5. 2 Available SAR data frames which cover the study area Zonguldak

5.1.1 ERS Data Acquisitions

ERS data compose the first long period of subsidence monitoring in Zonguldak. The SAR data used in this research was acquired between 1993 and 2001. Due to having gyroscopes problems which caused high Doppler baseline, ERS-2 satellite Doppler is not stable after January 2001 (Akarvardar [27], Lazecký [43]). Perpendicular baseline, temporal baseline and Doppler centroid of images are shown in Figure 5.3. There are temporal gaps which trigger decorrelation such as there is not image in 1994 and 1998, and there is just one image in 1996 (Figure 5.3).

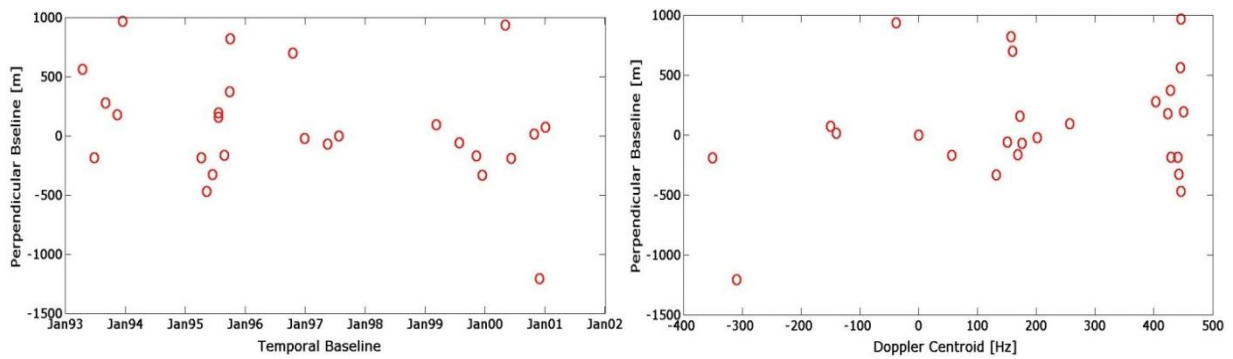


Figure 5. 3 ERS descending orbit track 21

5.1.2 ENVISAT/ASAR Data Acquisitions

Satellite ENVISAT which is developed by ESA is not just designed to continue ERS mission also designed to collect other kinds of data such as about atmosphere and ocean. It has ten sensors and one of them is ASAR which is used to gather SAR images. It is an advanced version of ENVISAT satellite that has different polarization modes and image swath varieties (Table 5.2). Since October 2010, ENVISAT acquisitions were not suitable due to having changed the orbital configurations [97].

Table 5. 2 Specifications of ASAR image swaths (ESA, [98])

Image swath	Swath width (km)	Ground position from nadir (km)	Incidence angle
IS1	105	287-292	15.0-22.9
IS2	105	242-347	19.2-26.7
IS3	82	337-419	26.0-31.4
IS4	88	412-500	31.0-36.3
IS5	64	490-555	35.8-39.4
IS6	70	550-620	39.1-42.8
IS7	56	615-671	42.5-45.2

Over the study area there were only IS2 swath images, thus two tracks of IS2 archive images were used. For the descending orbit track 21 which is same track as the ERS is gathered. In figure 5.3 shows the achieved 29 ENVISAT images. Less number of images were achieved from track 343 as 17 images. There are also temporal gaps in ENVISAT images which may cause temporal decorrelation, especially in ascending orbit.

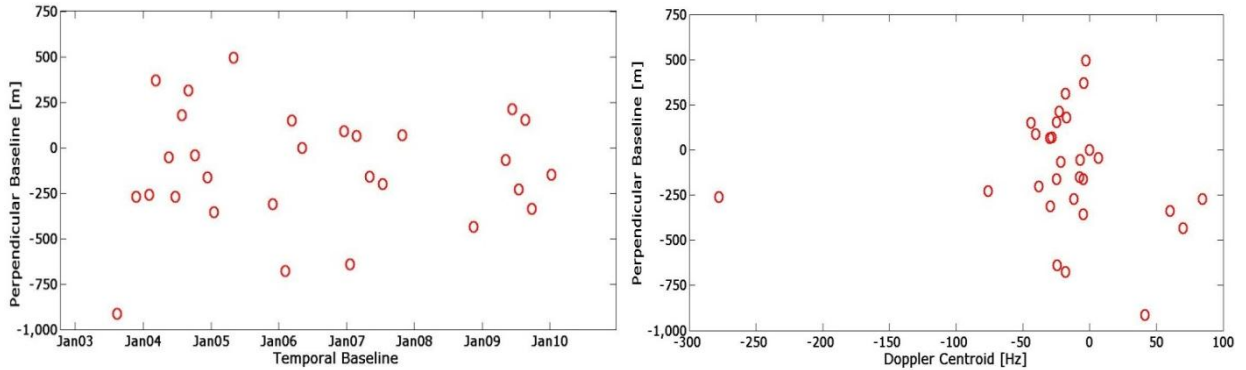


Figure 5. 4 ENVISAT-ASAR descending orbit track 21

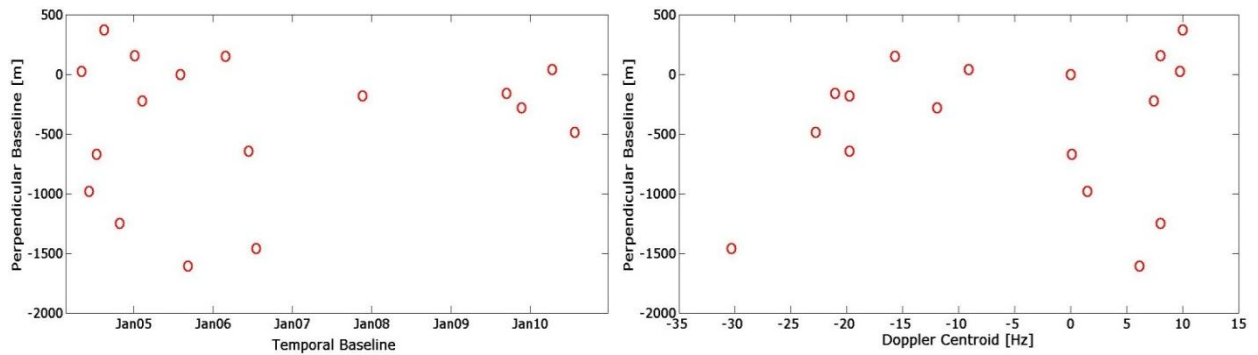


Figure 5. 5 ENVISAT-ASAR ascending orbit track 343

5.1.3 ALOS/PALSAR Data Acquisitions

ALOS is developed by the cooperation of Japanese Ministry of Economy, Trade and Industry with Japan Aerospace Exploration Agency. It includes three remote sensing sensors such as Panchromatic, AVNIR and PALSAR. Panchromatic remote-sensing Instrument for Stereo Mapping is designed to produce high precision DEM. The Advanced Visible and Near Infrared Radiometer type 2 (AVNIR) is a multispectral sensor that is designed to produce precise land use and land cover maps. The third sensor is the Phased Array type L-band Synthetic Aperture Radar (PALSAR), which has L-band. The different modes of PALSAR sensor are listed in Table 5.3.

Table 5. 3 Specifications of PALSAR image modes [52]

Mode	Fine Beam		ScanSAR	Polarimetry
Bandwidth	28MHz	14MHz	28MHz/14MHz	14MHz
Polarization	Single polarization HH or VV	Dual Polarization HH+HV or VV+VH	HH or VV	HH+HV+VH+VV
Incidence angle	8°-60°	8°-60°	18°-36° (3 scan) 18°-40° (3 scan) 18°-43° (3 scan)	8°-30°
Range resolution	7-44 m	14-88	100 m	24-89 m
Swath (km)	40 -70	40 -70	250-350	20-65

It was acquired in total 23 fine beam mode of PALSAR images between 13.06.2010 and 18.01.2007. 13 of these were acquired in Fine Single Beam (FSB) and 10 of were in Fine Dual Beam mode (FDB) (Figure 5.5). In PALSAR images perpendicular baselines are larger than the ERS and ENVISAT. Although the critical baseline for PALSAR is quite large, as the critical baseline is described in chapter 2.

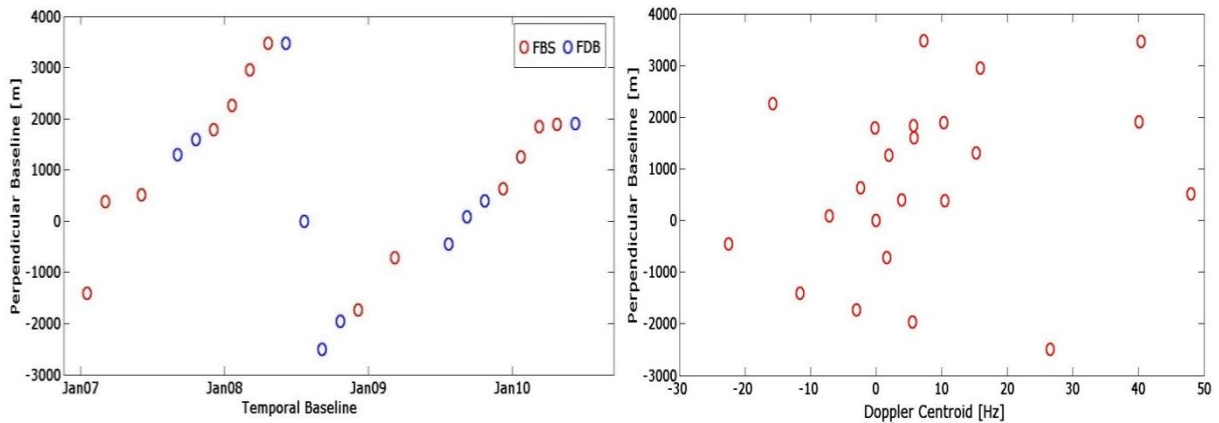


Figure 5.5 ALOS-PALSAR ascending orbit track 604

5.2 ERS Multi Temporal InSAR Results

5.2.1 ERS PSI Processing

In the process of PSI 26 available images were used and 25 interferograms were produced related to master image of 30 July 1997 (Table 5.4). The master selection is based on the perpendicular and temporal baselines of the data stack in order to have high coherence. As expected large baselines caused high phase unwrapping errors.

Due to fact that I have dropped interferograms as 19930418, 19931219, 19950411, 20000510 and 20001206, which have low coherence with master image (Figure 5.6a). PS process was applied with 20 interferograms with the pairs which were limited with a 704 m perpendicular baseline and 1494 days temporal baseline. For the PSI analyses amplitude dispersion index was chosen as 0.3.

Table 5. 4 ERS data used in PSI approach

No	Sensor	Date	Temp B (day)	Perp B (m)	$\sigma_{\text{Noise}}(^{\circ})$
1	ERS-1	19930418	1564	567	69.126
2	ERS-1	19930627	1494	-183	61.095
3	ERS-1	19930905	1424	282	58.933
4	ERS-1	19931114	1354	180	53.734
5	ERS-1	19931219	1319	972	78.868
6	ERS-1	19950411	841	-184	52.748
7	ERS-1	19950516	806	-467	65.661
8	ERS-1	19950620	771	-326	57.264
9	ERS-1	19950725	736	197	46.795
10	ERS-1	19951003	666	376	46.267
11	ERS-2	19950726	735	159	49.555
12	ERS-2	19950830	700	-164	54.532
13	ERS-2	19951004	665	821	69.645
14	ERS-2	19961023	280	704	68.262
15	ERS-2	19970101	210	-22	47.972
16	ERS-2	19970521	70	-69	48.535
17	ERS-2	19970730	0	0	57.470
18	ERS-2	19990317	-595	94	49.766
19	ERS-2	19990804	-735	-59	53.734
20	ERS-2	19991117	-840	-170	51.564
21	ERS-2	19991222	-875	-332	58.827
22	ERS-2	20000510	-1015	938	76.612
23	ERS-2	20000614	-1050	-189	67.389
24	ERS-2	20001101	-1190	17	56.430
25	ERS-2	20001206	-1225	-1207	80.437
26	ERS-2	20010110	-1260	75	58.845

5.2.2 ERS SB Processing

As criteria to shorten baselines in SB approach, I have limited the spatial and temporal baselines in critical baseline description which was approximately 1100 m for ERS and ENVISAT. The minimum coherence was chosen 0.3, and temporal baseline is chosen as five years to extract more pairs. However due to decorrelations perpendicular baseline was limited smaller than 400 m to reduce spatial decorrelation and to estimate good

coherence. Therefore, 55 ERS interferograms were calculated from 23 images (Appendix-B). The amplitude difference dispersion is chosen as 0.6.

The networks of the PSI and SB are shown in Figure 5.6. In Figure 5.6.a the blue baselines show the five dropped data in PSI process. Figure 5.6.b depicts the acquisitions that were used in the processing of SB. Three blue points represents the data which could not be used due to decorrelation.

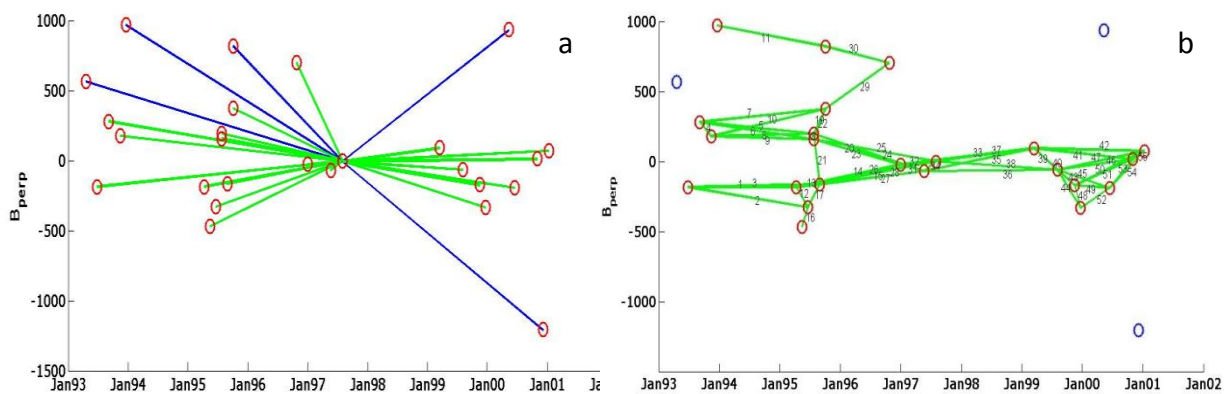


Figure 5. 6 Perpendicular baselines relative to 19970730 of ERS dataset a) PS baselines
b) SB baselines

5.2.3 ERS PSI-SB Comparison

As noted before, land cover has influence on InSAR processing. In Zonguldak region coherence along the steep areas was poor which probably happen due to layover, shadow and forest cover. Besides, the city gave high coherence at the Kozlu region and along the coastline. For the analysis three main areas Kozlu, Karadon and Üzülmöz which are shown in Figure 5.7 were decided to focus on. As expected, PS and SB points were identified mostly at the urbanized areas. The number of 2582 and 2353 points were detected in PSI and SB methods respectively. These scatterers mostly belong to buildings, but there are also other scatterers in the port, mine and roads.

From 1993 to 2001 approximately 24 million ton coal is extracted from Kozlu, Karadon and Üzülmöz mines (TCE, [85]). For the same period surface subsidence of mining areas are obtained as mm/year through the LOS direction (Figure 5.7).

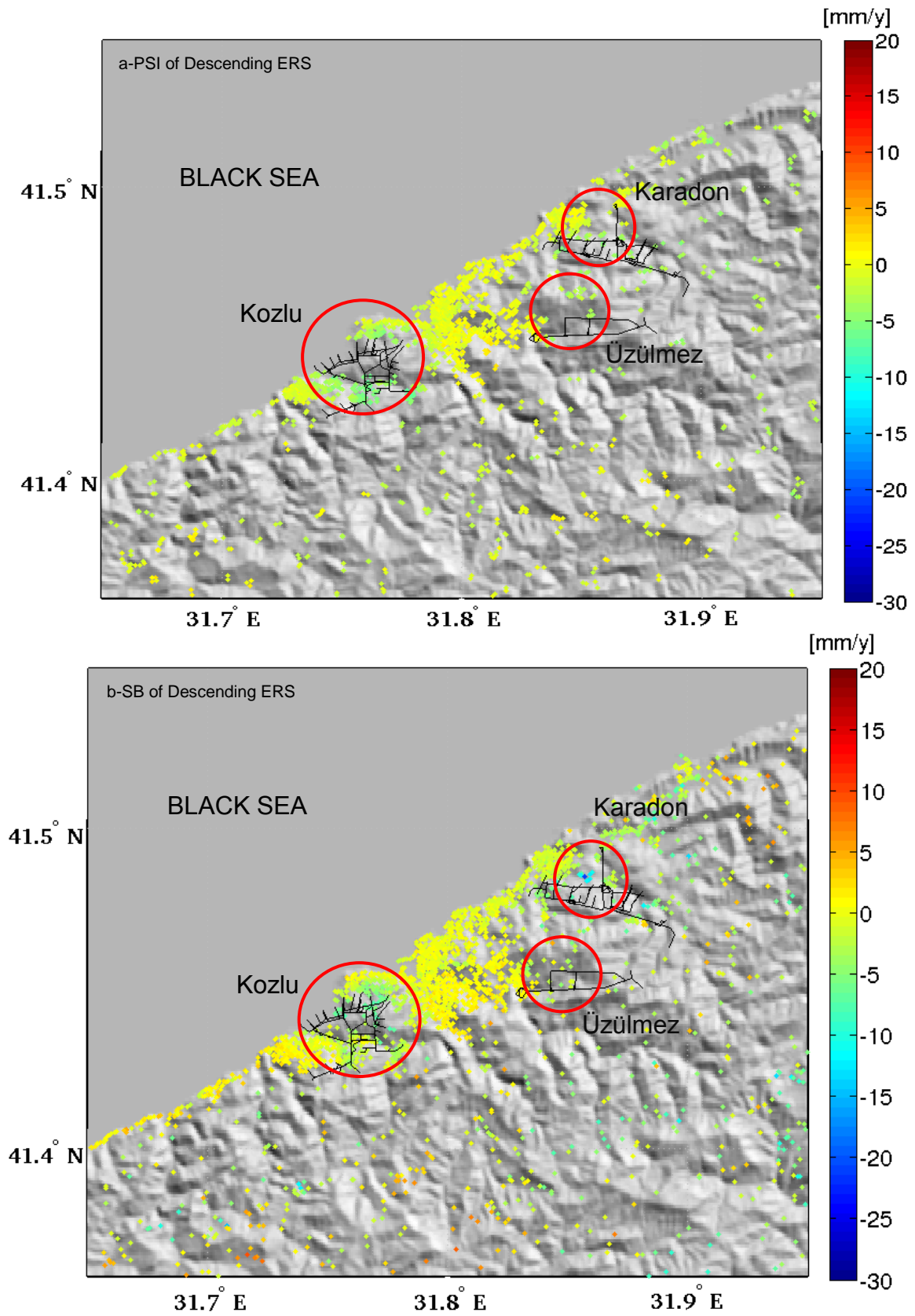


Figure 5. 7 ERS PSI and SB subsidence results along LOS from 1993 to 2001

The main lobe of the coal mining was detected in two methods at Kozlu town where the main mining galleries are located (Figure 5.7.a and 5.7.b). The Kozlu area is subsiding in both PSI and SB results. The level of the urbanization can be clearly identified by the density of the points. Karadon and Üzülmöz mines are located in a rarely urbanized and forested environment. In the results of PSI subsidence estimated rates are less than in SB results at Karadon and Üzülmöz regions.

For the analysis cross-section profiles were applied to show the deformation in space and time series of the points were computed to show evolution of the deformation in time. However, subsidence is fairly noticeable in Karadon and Üzülmöz when we look at the profile over the area (Figure 5.8b and 5.9b) and the time series of the selected points (Figure 5.10). High subsidence rates were obtained in Karadon and Kozlu where movements are up to 19.5 mm/year and 7.5 mm/year respectively with SB results. PSI results presented low velocity in Karadon as 6 mm/year, and in Kozlu it was 7.5 mm/year as in SB results. In Üzülmöz a slight displacement was monitored rating to 4-5 mm/year with each method.

In two results same cross-section profiles were obtained on Kozlu, Karadon and Üzülmöz where the mining galleries were located on, to indicate the spatial behavior of the displacement. Due to having less point in Kozlu at PSI results, there were gaps on profile of Kozlu (Figure 5.8a), meanwhile the velocity was better noticed in SB (Figure 5.8b). Although less points were determined at Karadon in PSI results a slight deformation was observed (Figure 5.8c). For the same cross-section maximum deformation was monitored in SB result of ERS data (Figure 5.8d).

The evolution of the displacement for the regions Kozlu, Karadon and Üzülmöz an area was chosen with radiuses 2km, 1km and 500 m respectively in PSI and SB results. The results of the time series analysis are shown in Figure 5.9, and they presents the deformation in each region clearly.

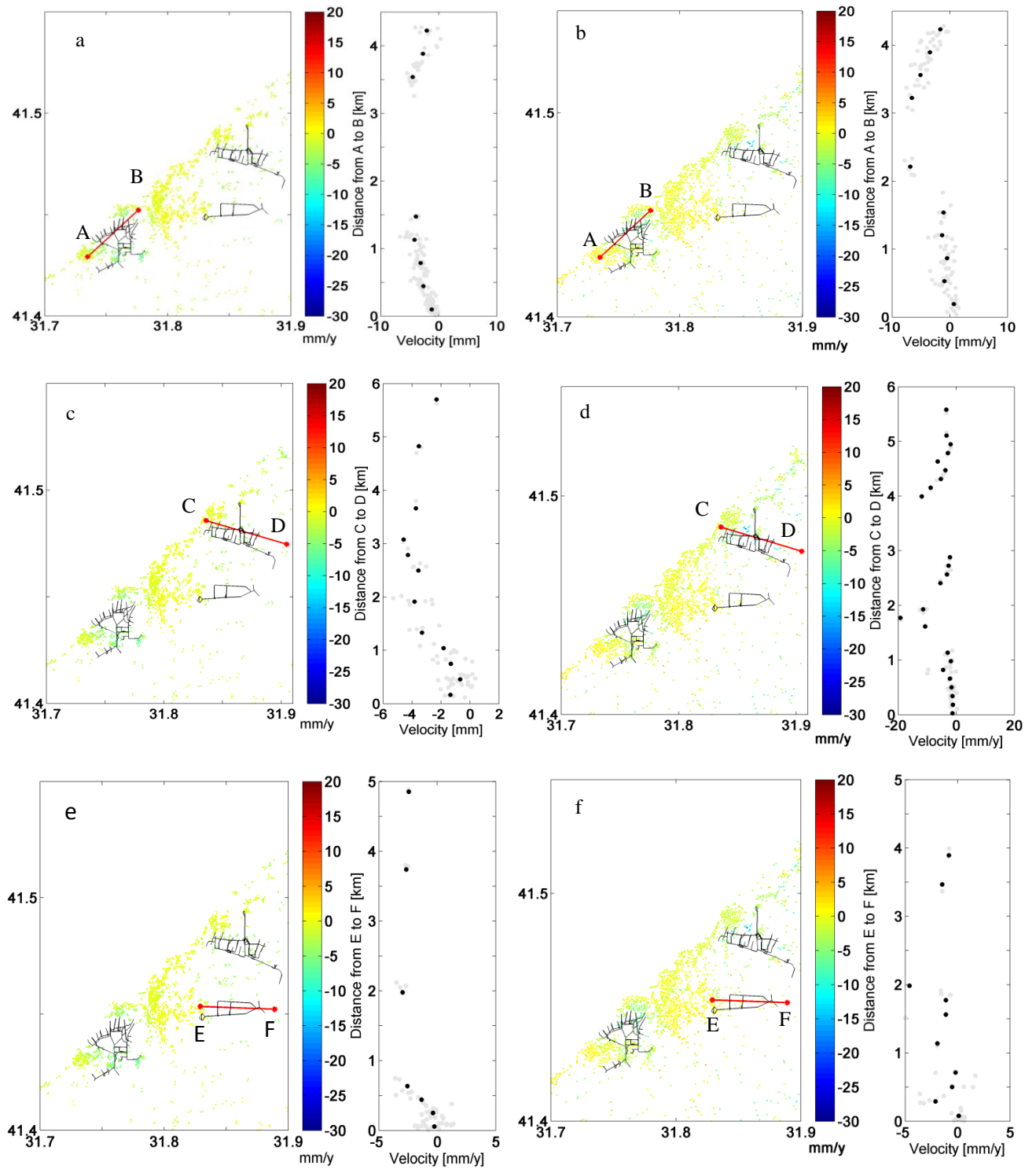


Figure 5. 8 Profile at Kozlu on ERS a) PS result, b) SB result; at Karadon c) PS result, d) SB result; at Üzülmöz e) PS result, f) SB result

The evolution of the displacement for the regions Kozlu, Karadon and Üzülmöz an area was chosen with radiuses 2km, 1km and 500 m respectively in PSI and SB results. The results of the time series analysis were given in Figure 5.9, and they show the deformation in each region clearly.

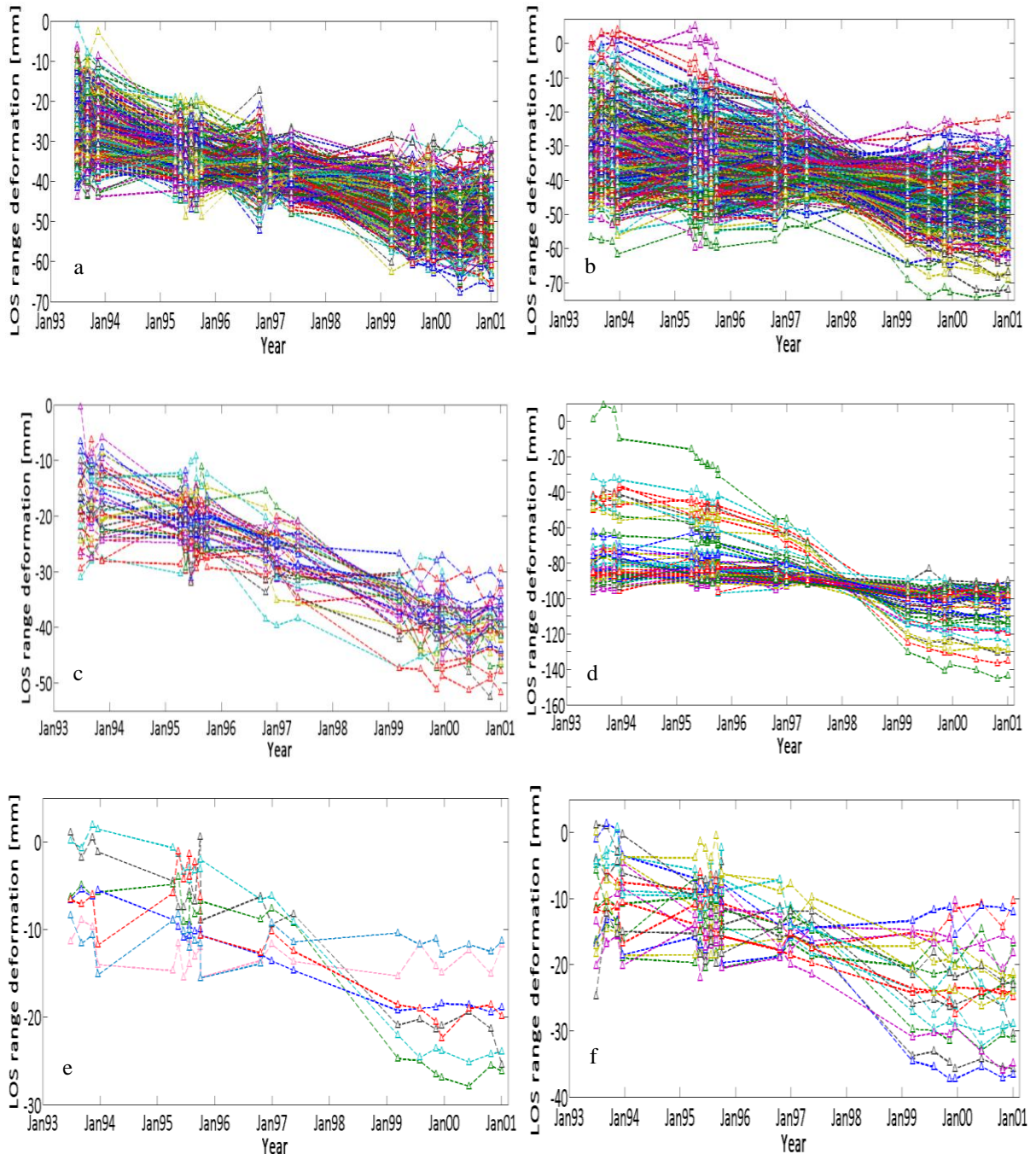


Figure 5. 9 Time series analysis from descending ERS for the regions Kozlu a) PSI results, b) SB results; Karadon c) PSI results, d) SB results; Üzülmöz e) PSI results, f) SB results

In ERS results deformation was monitored 60 mm in Kozlu region for eight years by both PSI and SB methods (Figure 5.9a-5.9d). There are also sparsely urbanized towns surrounding the center in Üzülmez and Karadon towns. In Üzülmez region 40 mm deformation was determined in both PSI and SB results (Figure 5.9a, 5.9b), meanwhile in Karadon region (Figure 5.9e) deformation reached up to 145 mm with slightly denser points (Figure 5.7b) with SB method. In Üzülmez region both PSI and SB results produced a few points, though displacements reached up to 30-40 mm (Figure 5.9c, 5.9f).

5.3 ENVISAT Multi Temporal InSAR Results

In InSAR processing 2 tracks of C-band ENVISAT data covers the mining region of Zonguldak were acquired. 29 images and 17 images were gathered in the descending and ascending geometry respectively. SLC images were produced by ROI_PAC software. DORIS software was used to compute the interferograms and, PSI and SB approaches were produced by StaMPS. Spatial decorrelation was removed by multiple interferograms. Phase due to atmospheric delay, orbit and DEM errors was estimated for each process and removed.

5.3.1 ENVISAT Descending PSI

For the PSI analyses I have used 26 archived raw ENVISAT images of 29 which have descending geometry acquired between December 2003 and January 2010. 17 August 2005 dated SAR data was chosen as master and 25 interferograms were calculated from this master image. 20030813, 20060208 and 20070124 are the images which have the largest perpendicular baselines. These iamges were dropped during the process due to cause low coherence (Figure 5.10a). Temporal baseline was limited as 1610 days and amplitude dispersion index is chosen as 0.3 (Table 5.5).

Table 5. 5 ENVISAT descending data used in PSI approach

No	Date	TempB (day)	PerpB(m)	$\sigma_{\text{Noise}}(^{\circ})$
1	20030813	-735	-915	85.460
2	20031126	-630	-272	53.502
3	20040204	-560	-261	55.650

Table 5. 5 is continuing

No	Date	TempB (day)	PerpB (m)	$\sigma_{\text{Noise}}(^{\circ})$
4	20040310	-525	371	59.248
5	20040519	-455	-55	42.525
6	20040623	-420	-271	50.516
7	20040728	-385	180	46.036
8	20040901	-350	313	50.698
9	20041006	-315	-43	40.854
10	20041215	-245	-162	42.746
11	20050119	-210	-355	55.921
12	20050504	-105	495	68.528
13	20050817	0	0	46.620
14	20051130	105	-312	48.102
15	20060208	175	-677	92.35
16	20060315	210	150	40.726
17	20061220	490	89	37.654
18	20070124	525	-640	87.165
19	20070228	560	64	38.549
20	20070509	630	-160	42.505
21	20070718	700	-201	46.529
22	20071031	805	68	46.758
23	20081119	1190	-435	71.141
24	20090513	1365	-67	49.228
25	20090617	1400	211	54.076
26	20090722	1435	-228	55.132
27	20090826	1470	153	52.888
28	20090930	1505	-336	64.034
29	20100113	1610	-149	52.503

5.3.2 ENVISAT Descending SB

Using the same dataset, 73 pairs were succeeded on the limitation for perpendicular baselines as smaller than 400 m and for temporal baselines as smaller than two years. Maximum perpendicular baseline and maximum temporal baseline were included as 365 m and as 665 days respectively. During the process coherence was chosen as 0.3. Figure 5.10b shows the network of the InSAR pairs and the Appendix-B shows the baseline information for each pair. The amplitude difference dispersion was chosen as 0.6.

5.3.3 ENVISAT Descending PSI-SB Comparison

Most of the coherent scatterers are located in the urbanized center of Zonguldak and Kozlu regions. There are sparsely distributed points surrounding the town of Kilimli and

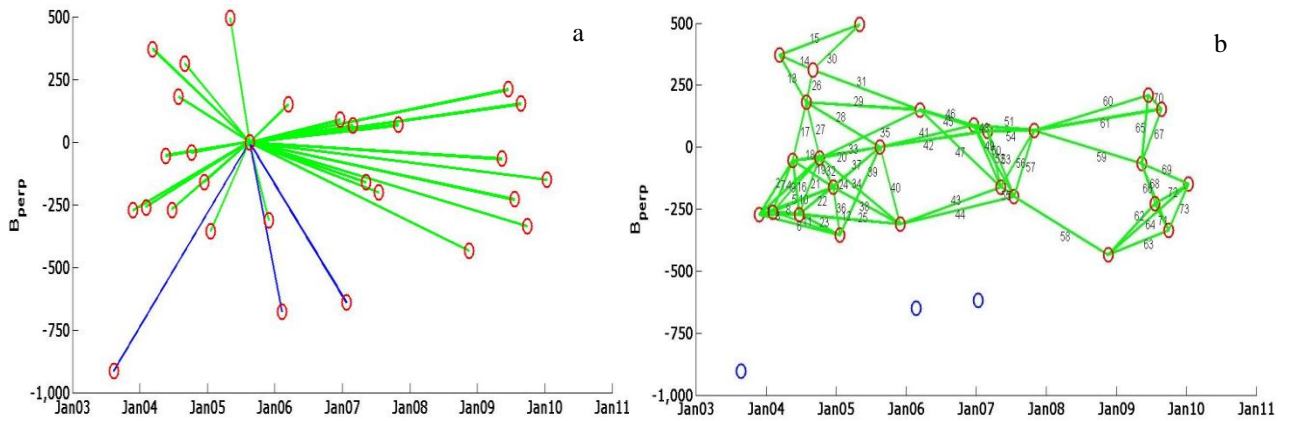


Figure 5. 10 Perpendicular baselines relative to 20050817 of ENVISAT descending dataset a) PSI baselines b) SB baselines

Gelik where Karadon mine is located. In total 3694 and 3094 points were identified from PSI and SB results respectively. These points were also identified mostly at the urbanized areas as identified in ERS. The main lobe which of the Earth surface deformation was extracted in ERS results, was detected with both methods in Kozlu town (Figure 5.11). The subsidence reaches high rates as 7.5 mm/year and 25 mm/year in Kozlu in PSI and SB results respectively. There are fewer points where Karadon and Üzülmöz mining tunnels are located. In the results of PSI velocity of deformation is 6 mm/year in Karadon and in Üzülmöz (Figure 5.11a). In the result of SB monitoring the velocity increases up to 10 mm/year in Karadon, and to 17 mm/year in Üzülmöz regions within the selected fields. Meanwhile, as well as the mining regions the distributed points indicating deformations were detected also in two areas with SB method (Figure 5.11b). Velocities of 15 mm/year and 13 mm/year were extracted from Area-1 located south of Kozlu and Area-2 located at south-east of Üzülmöz respectively (Figure 5.11b). For the analysis of extracting continued deformation the cross-section profiles which were applied on ERS results were also applied on ENVISAT results. In both cross-sections of the Kozlu, the deformation was seen clearly (Figure 5.12a and 5.12b). The cross-section of Karadon and Üzülmöz do not show the deformation very clearly in PSI results whereas in SB results both of Karadon and Üzülmöz cross-section present the deformation in space.

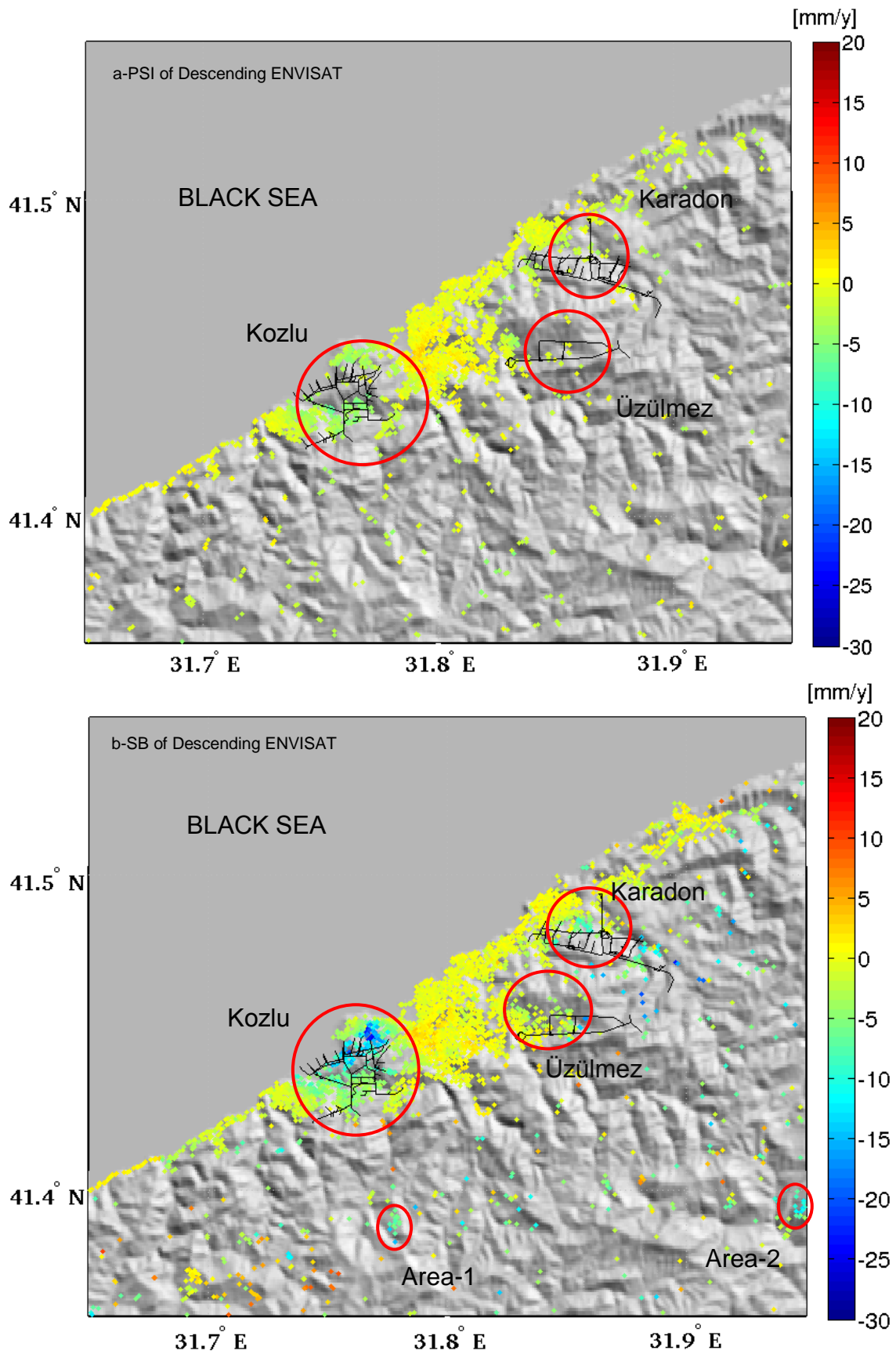


Figure 5. 11 ENVISAT descending track PSI and SB subsidence results along LOS from 2003 to 2010

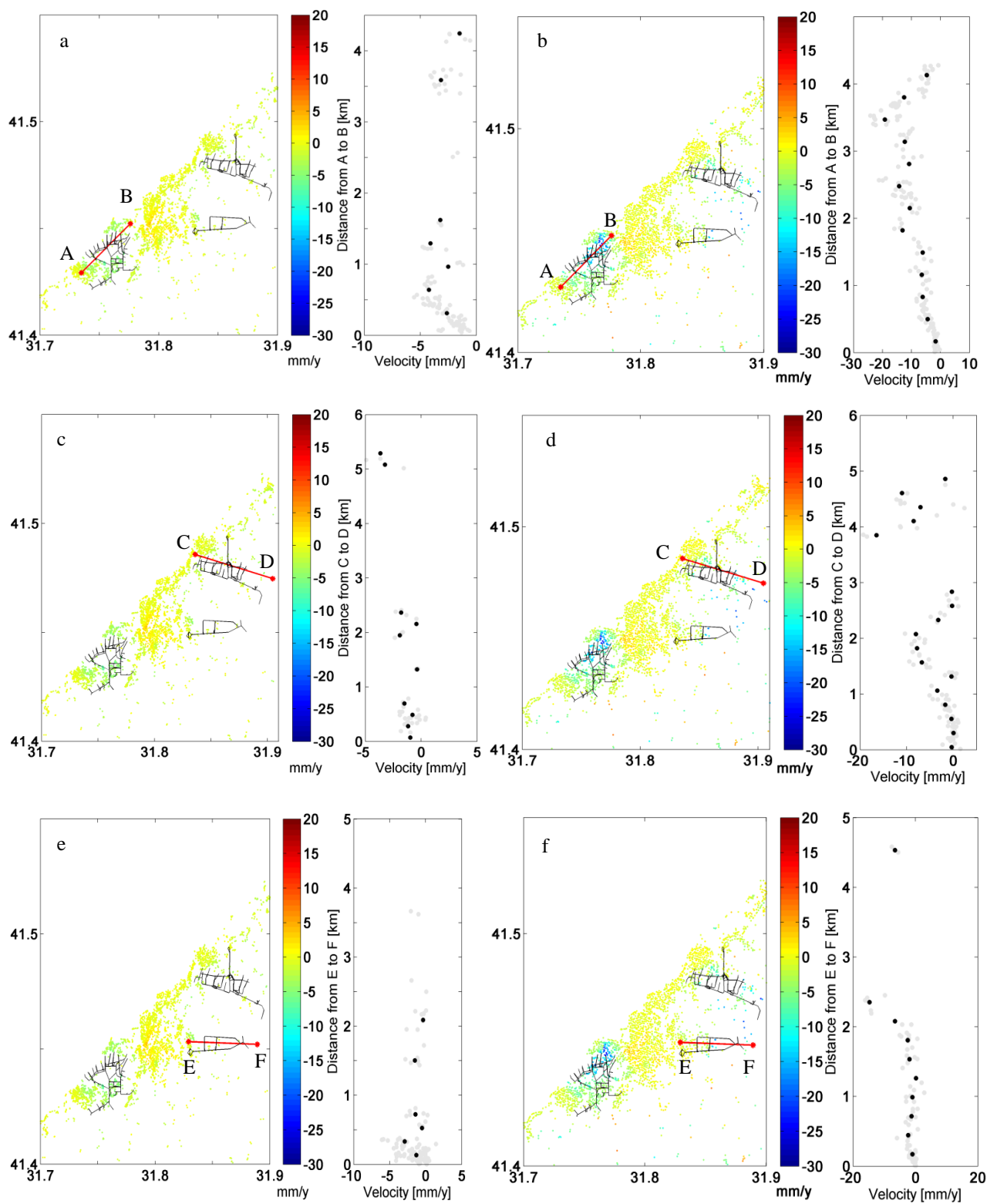


Figure 5. 12 Profile at Kozlu on descending ENVISAT a) PS result, b) SB result; at Karadon c) PS result, d) SB result; at Üzülmöz e) PS result, f) SB result

The estimated deformation rates in SB results are higher than PSI results in all regions. Although having fewer points in regions Karadon and Üzülmöz, deformation is observed in time for six years. To observe the evolution of the displacement for the regions an area was chosen in Kozlu with a radius of 2 km and in Karadon and Üzülmöz of 500 m for both PSI and SB results. The time series analysis depicted that at the town of Kozlu deformation was monitored as 45 mm and 150 mm by PSI and SB results respectively (Figure 5.13a-5.13b). In Karadon deformation was extracted 35 mm and 60 mm by PSI and SB methods respectively (Figure 5.13c-5.13d). Meanwhile, in Üzülmöz region the deformation is extracted around 35 mm by PSI method, while it reaches up to 95 mm in SB results (Figure 5.14a-5.14b). In the time series 90 mm and 80 mm deformation were determined in a chosen size as 500 m and 1km for Area-1 and Area-2 respectively (Figure 5.14c-5.14d). These areas, which are small villages, are most probably affected by a mass movement as landslides.

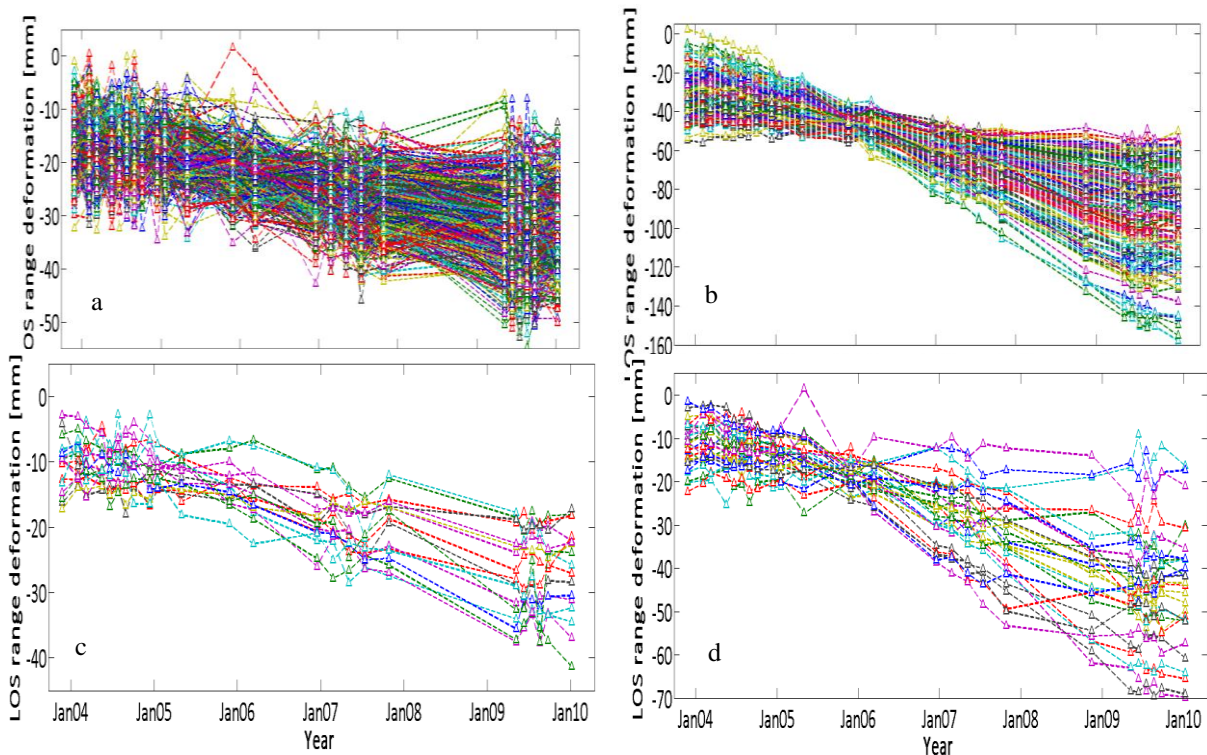


Figure 5. 13 Time series analysis from descending ENVISAT for the regions Kozlu a) PSI results, b) SB results; Karadon c) PSI results, d) SB results

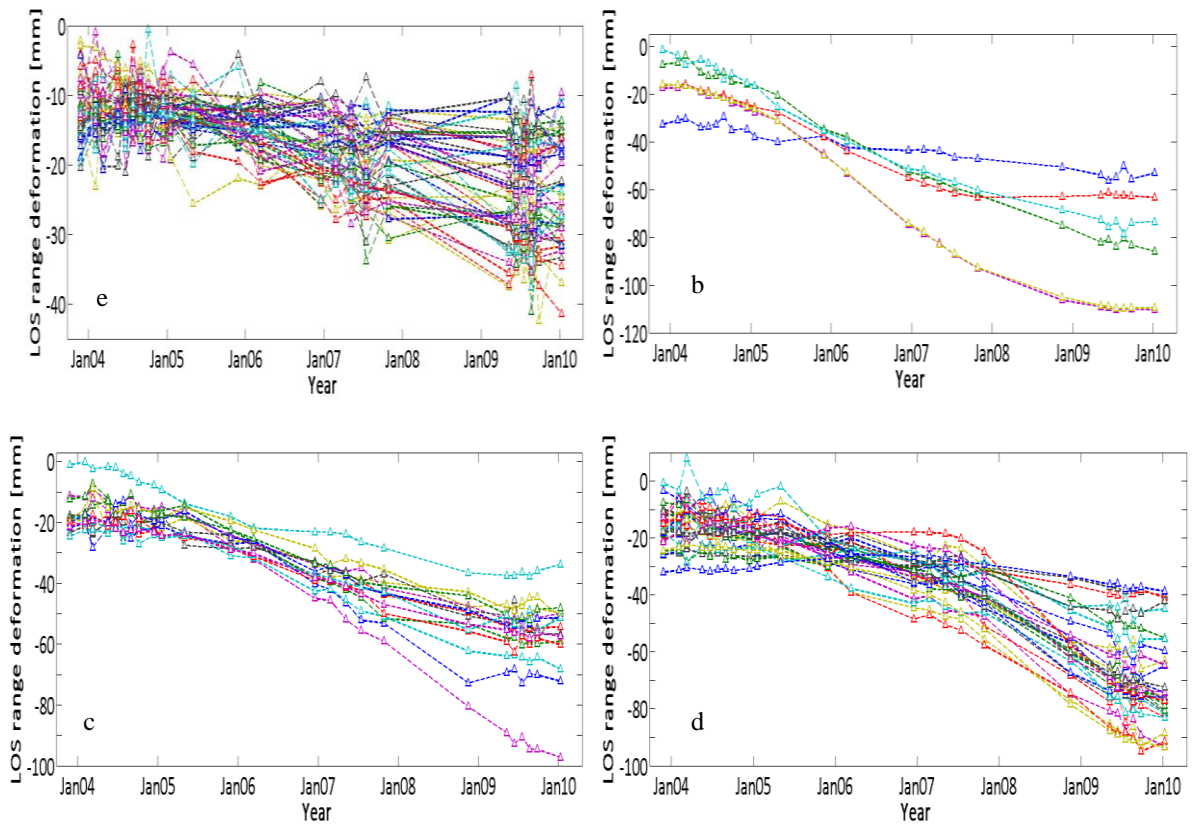


Figure 5.14 Time series analysis from descending ENVISAT for the regions Üzülmöz a) PSI results, b) SB results; c) Area-1; d) Area-2

5.3.4 ENVISAT Ascending PSI

Ascending track of ENVISAT frames are overlapping with descending track of ENVISAT frames both on the region and in the time. However, in the archive there are not many frames available in descending track. Thus 17 images were acquired but out of 14 were suitable for the PSI analyses. The images acquired in 20041028, 20050908, and 20060720 were dropped since having higher perpendicular baselines than critical baseline (Table 5.6). The master image which was acquired in 17 August 2005, and the selected dataset are showed in Figure 5.15a.

5.3.5 ENVISAT Ascending SB

In the SB monitoring of the ascending dataset, all of the 17 images were included and 32 interferograms were computed with perpendicular baselines less than 600 m and temporal baselines limited to two years. Here coherence was chosen as 0.25 to compute more interferograms, however lack of data in time span caused loss of

decorrelation. The amplitude difference dispersion was chosen as 0.6. Figure 5.15b shows that the network of the SB pairs were not configured as strong as descending SB network. All SB pairs and the baselines can be seen in Appendix-B.

Table 5. 6 ENVISAT ascending data used in PSI approach

No	Date	TempB (day)	PerpB (m)	$\sigma_{\text{Noise}}(^{\circ})$
1	20040506	-455	28	48.839
2	20040610	-420	-979	57.850
3	20040715	-385	-670	54.317
4	20040819	-350	376	51.885
5	20041028	-280	-1251	58.051
6	20050106	-210	158	47.167
7	20050210	-175	-218	49.395
8	20050804	0	0	65.056
9	20050908	35	-1610	59.513
10	20060302	210	152	47.512
11	20060615	315	-642	53.164
12	20060720	350	-1458	59.526
13	20071122	840	-180	48.192
14	20090917	1505	-159	50.237
15	20091126	1575	-277	51.061
16	20100415	1715	44	51.297
17	20100729	1820	-483	54.927

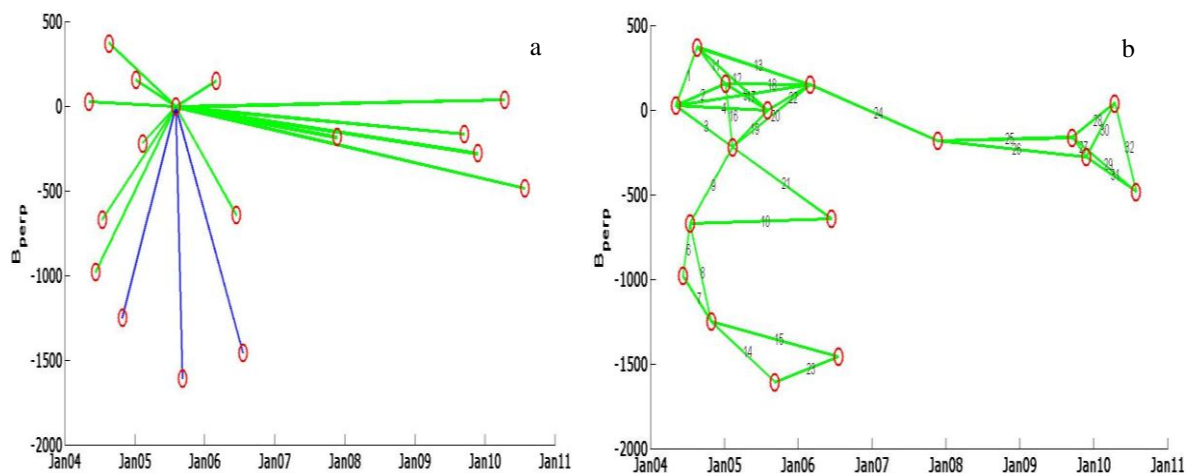


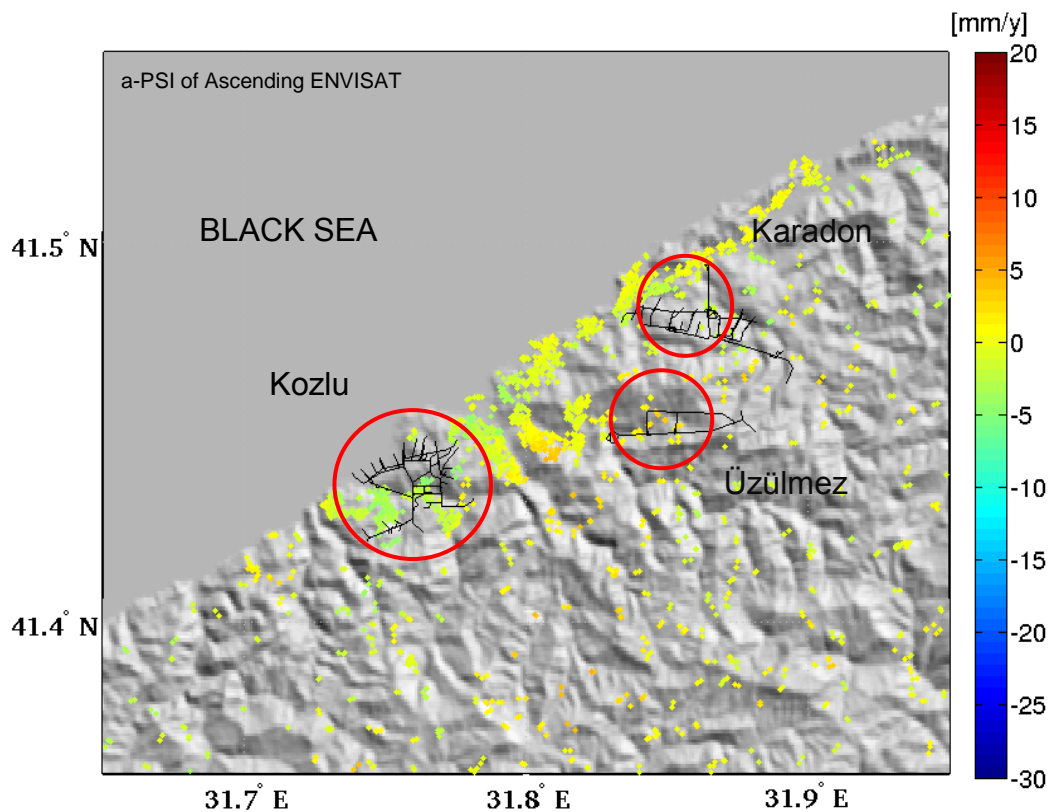
Figure 5. 15 Perpendicular baselines relative to 20050804 of ENVISAT ascending dataset a) PSI baselines b) SB baselines

5.3.6 ENVISAT Ascending PSI-SB Comparison

The ascending track of ENVISAT data resulted in the same deformation pattern in Kozlu as observed in both ERS and the descending track of ENVISAT results. However it is not

clear in Karadon and Üzülmez mining. There are low density of points in both PSI and SB results (Figure 5.16). This is most probably due to lack of coherence. The PSI dataset has less images and gaps in the acquisition period (Figure 5.15a). In SB network the distribution of network is not homogeneous which causes lack of redundancy and loss of coherence. Coherent distributed scatterer points were mostly identified in the city center of the Zonguldak and Kozlu region. 2249 and 1315 points were detected using the ENVISAT ascending images with PSI and SB approaches respectively. Here reliable results were not extracted very clearly due to having low and temporal decorrelated dataset as expected. However, in the urban area of Kozlu the surface subsidence pattern is monitored with low density of PSI and SB results.

The subsidence at Kozlu is determined as 5 mm/year in PSI results and reaches up to 12 mm/year in SB results. The velocities of 5 mm/year and 13 mm/year were extracted in PSI and SB results respectively at Karadon mining. A slight velocity as 1 mm/year and 1.5 mm/year was monitored both with PSI and SB results. The cross-section profiles present the displacement in Kozlu clearly. In Karadon and Üzülmez profiles are not very distinct due to lack of low density of points. On this purpose time series analyses in three regions were presented in Figure 5.19.



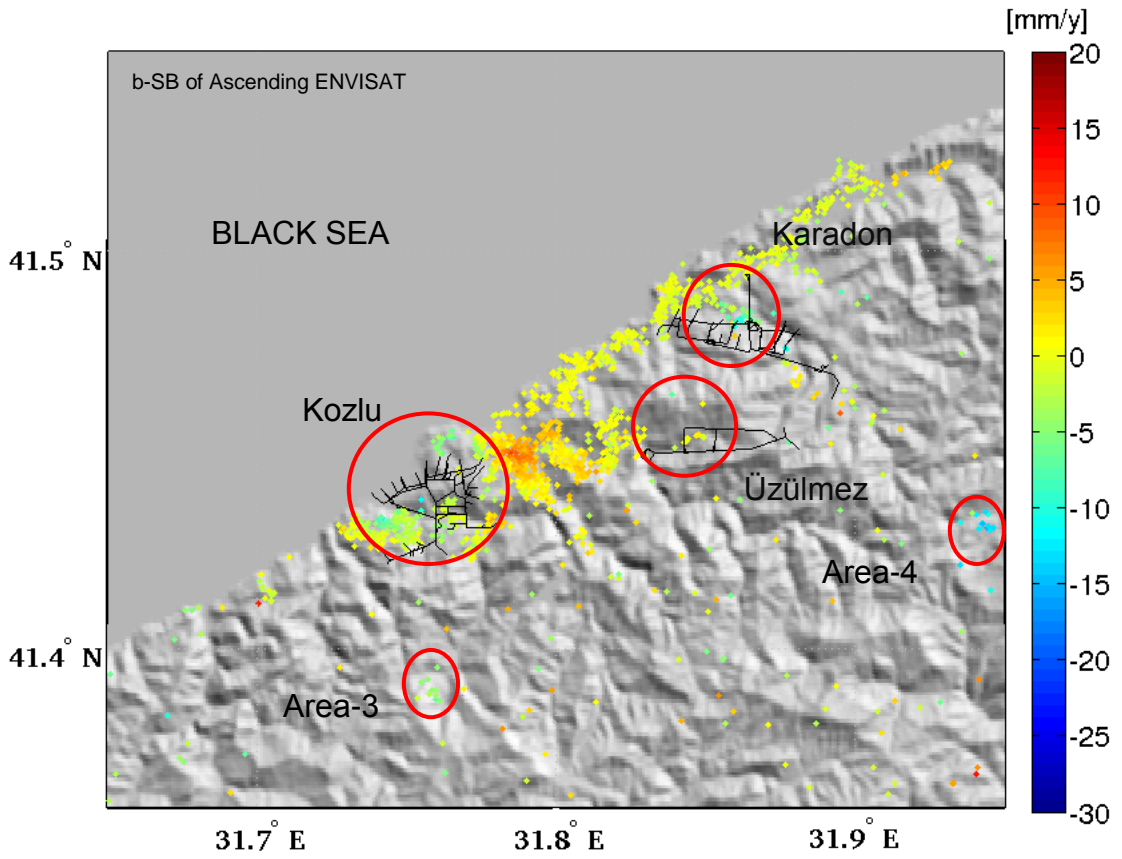


Figure 5. 16 ENVISAT ascending track PSI and SB subsidence results along LOS from 2004 to 2010

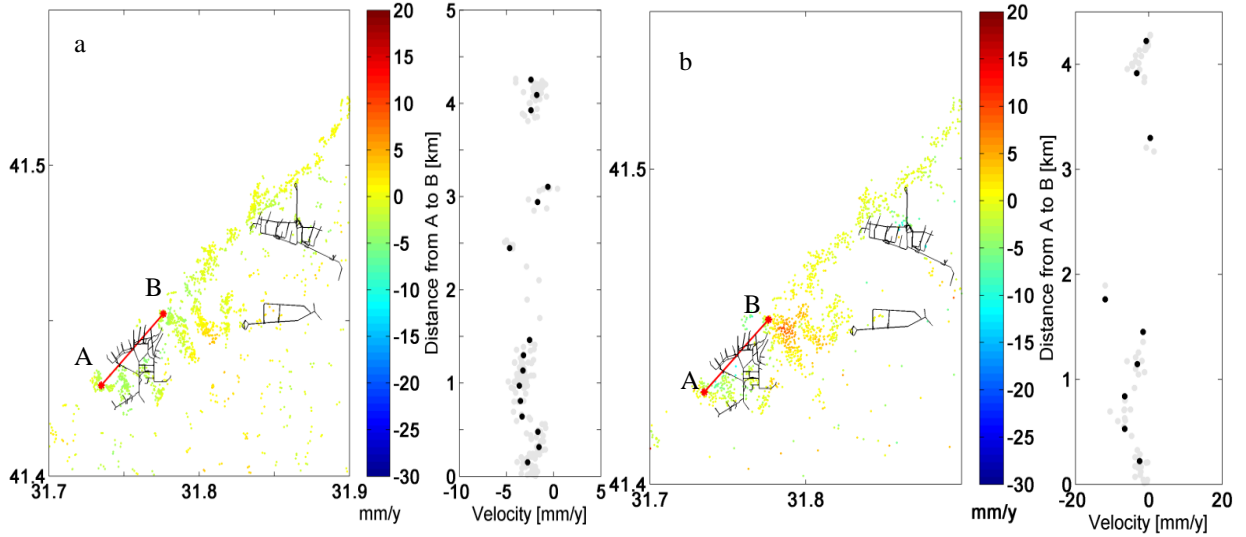


Figure 5. 17 Profile at Kozlu on ascending ENVISAT a) PS result, b) SB result

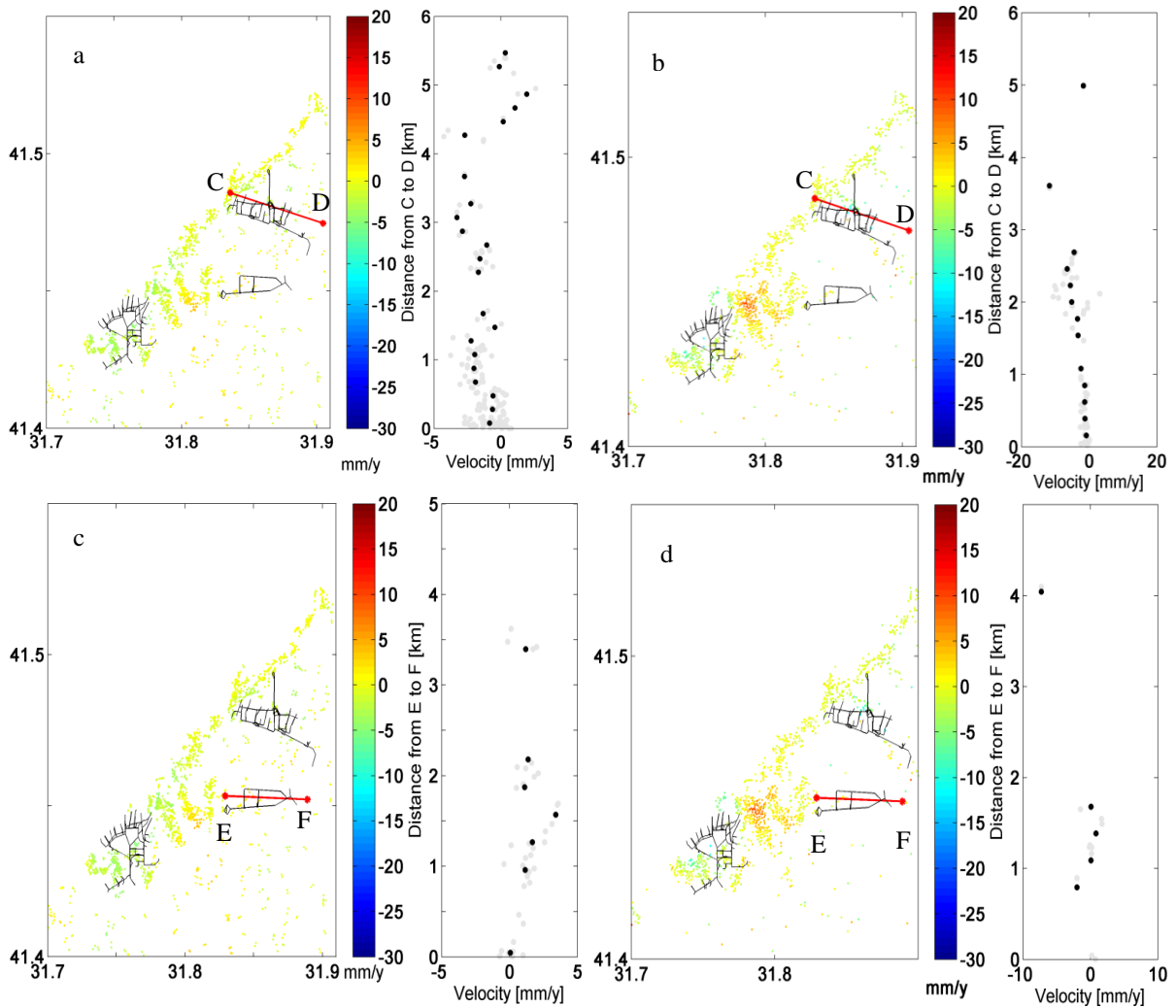


Figure 5. 18 Profile at Karadon on ascending ENVISAT a) PS result, b) SB result; at Üzülmez c) PS result, d) SB result

To check the evaluation of deformation in time, time series of points were obtained from 2004 to 2010 from the selected areas over the mining galleries. The size of the areas were same as chosen before, in Kozlu with a radius of 2 km and, in Karadon and Üzülmez with 500 m in both PSI and SB results. For Area-3 and Area-4 a 500 m and 1 km radius regions were chosen, and time series were analysed. Deformations of the 30 mm and 90 mm in LOS were detected in Area-3 and Area-4 respectively (Figure 5.19g-5.19h). These areas covering small villages are most probably affected by a mass movement as landslides.

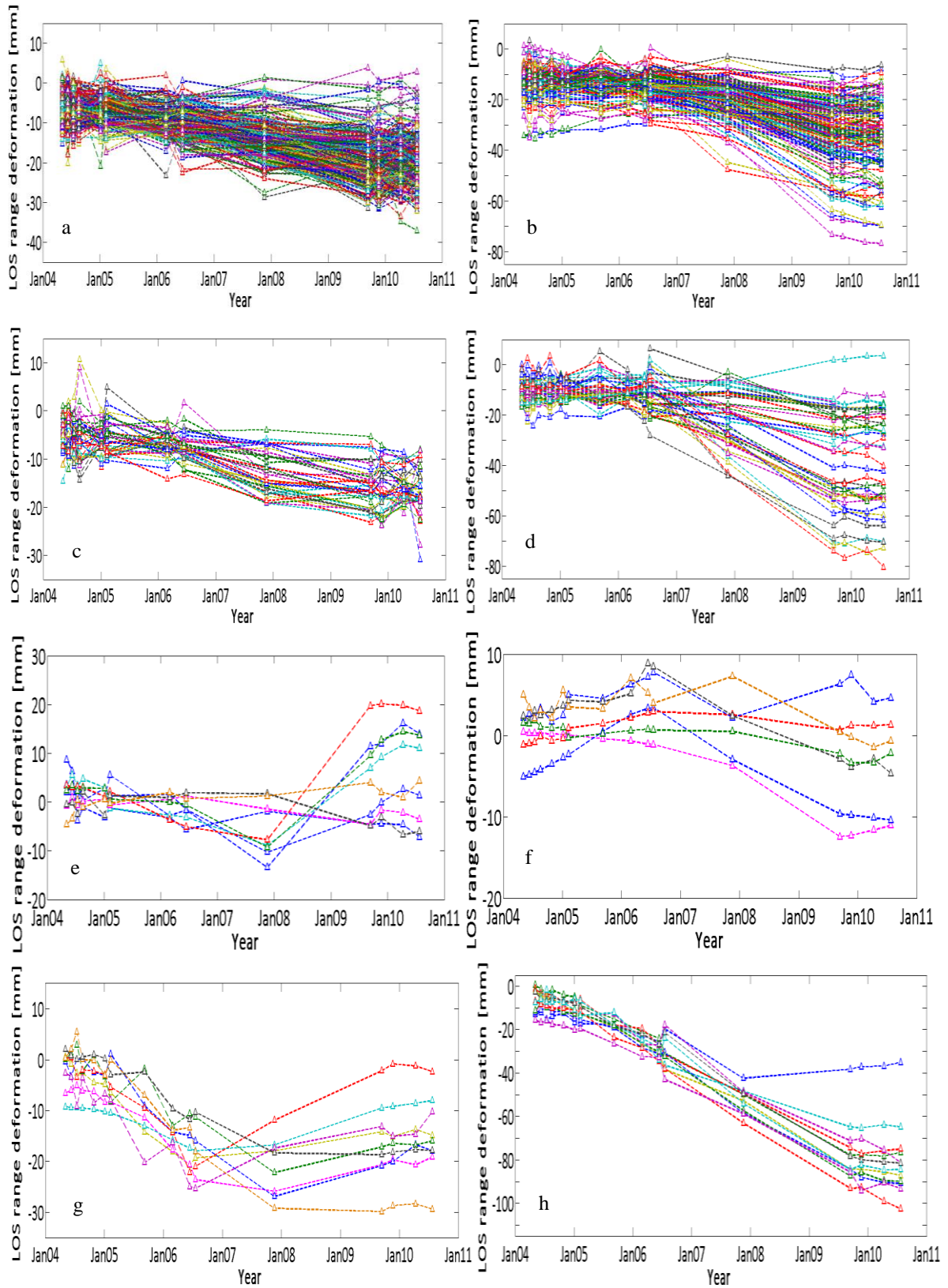


Figure 5. 19 Time series analysis from ascending ENVISAT for the regions Kozlu a) PSI results, b) SB results; Karadon c) PSI results, d) SB results; Üzülmöz e) PSI results, f) results ; g) Area-3; h) Area-4

5.4 PALSAR Multi Temporal InSAR Results

The 10 data of PALSAR were gathered in FBD mode and the 13 data were gathered in FBS mode from September 2007 to June 2010. FBS mode has two times better range resolution than FBD, and in order to process all ALOS data together FBD to FBS conversion was applied during the focusing in ROI_PAC (Sandwell et al. [99]). In total 23 HH polarized PALSAR images were used.

5.4.1 PALSAR PSI Processing

PALSAR images were gathered in ascending orbit overlapping with the ERS and ENVISAT orbits. 23 July 2008 dated data was chosen as master, and related to this master 22 interferograms were computed (Table 5.7). Even having small perpendicular and temporal baselines five interferograms as 20080307, 20080422, 20080607, 20080907 and 20100126 were removed from the process due to their low coherences.

Table 5. 7 PALSAR ascending data used in PSI approach

	Date	TempB (day)	PerpB (m)	6Noise(°)
1	20070118	-552	-1407	54.917
2	20070305	-506	383	56.172
3	20070605	-414	518	49.210
4	20070905	-322	1301	44.181
5	20071021	-276	1602	41.427
6	20071206	-230	1793	47.373
7	20080121	-184	2262	51.445
8	20080307	-138	2951	66.618
9	20080422	-92	3475	74.208
10	20080607	-46	3470	75.689
11	20080723	0	0	55.764
12	20080907	46	-2497	74.107
13	20081023	92	-1961	52.549
14	20081208	138	-1736	55.290
15	20090310	230	-716	46.969
16	20090726	368	-449	41.728
17	20090910	414	89	38.826
18	20091026	460	395	36.677
19	20091211	506	632	41.500
20	20100126	552	1261	65.600
21	20100313	598	1842	43.991
22	20100428	644	1895	46.827
23	20100613	690	1905	52.747

PS process was applied with 17 interferograms where pairs have limited perpendicular baseline and temporal baseline as 2262 m and 690 days (Figure 5.20a). For the PSI analyses amplitude dispersion index was chosen as 0.4.

5.4.2 PALSAR SB Processing

At the process of PALSAR data with SB method perpendicular baseline was limited with 4500 m, temporal baseline was limited with two years and minimum coherence was chosen as 0.45. Three images as 20080422, 20080607 and 20080907 were not able to overcome this limitations and were dropped before the process (Figure 5.20b). Therefore, 129 interferograms were computed from 20 images (Appendix-B). The amplitude difference dispersion was chosen as 0.6

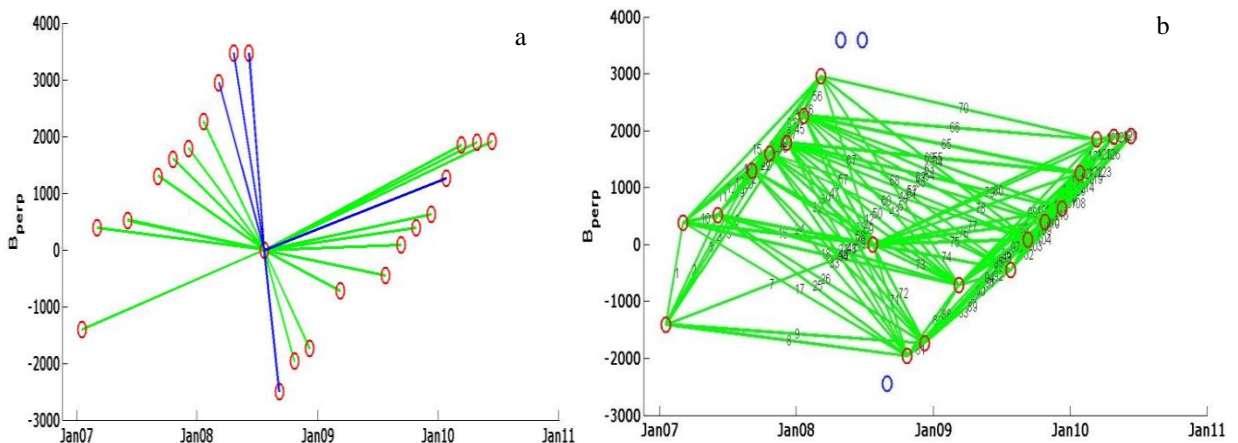


Figure 5. 20 Perpendicular baselines relative to 20080723 of PALSAR ascending dataset
a) PSI baselines b) SB baselines

5.4.3 PALSAR PSI-SB Comparison

Both methods identified dense points over the both urban and rural areas which even has forest land cover. The scatterers mostly belong to settlements of Zonguldak city center and Kozlu town, but there are also other scatterers in the port, mine, roads and rural areas where Karadon and Üzülmöz mining are located. The number of points as 72399 and 16024 were detected with PSI and SB methods respectively. The main lobe of the subsidence over the Kozlu coal mining was detected in both PSI and SB results. Also in Karadon and Üzülmöz regions surface displacement was obviously detected with the two methods (Figure 5.21).

Moreover, besides the mining regions subsidence was monitored to the south of Üzülmöz mining in SB result of PALSAR. As presented in part 4.1.1, in Zonguldak there are many formations of karstic generations. This subsidence pattern is located over one of the caves in Zonguldak named Gökgöl Cave which is located very close to the Üzülmöz mining. And apart from the comparison area selected in Karadon, a dense deformation was extracted in PSI result.

Within the selected regions in Kozlu, high rates of deformation was extracted as 30 mm/year and 28 mm/year with PSI and SB methods respectively (Figure 5.21a and 5.21b). The rural areas where Karadon and Üzülmöz are located, covered with high dense points. The results of PSI velocity present the deformation as 31 mm/year in Karadon and 28.5 mm/year in Üzülmöz. In SB results the subsidence velocity were extracted as 28.5 mm/year and 30 mm/year in Karadon and Üzülmöz regions respectively. Beside the selected regions in mining areas in Karadon deformation reaches up to 44 mm/year and 35 mm/year maximum in Area-5 in Figure 5.21a and 5.21b. In SB result significant deformation was monitored over Gökgöl Cave as 77 mm/year. Moreover, in the Üzülmöz mining region 98 mm/year deformation which was also very close to Gökgöl Cave was monitored as maximum amount (Figure 5.21b). For the comparison same cross-section profiles were applied over three regions. In all of the six profiles the subsidence at space was clearly observed (Figure 5.22). For the evaluation of the deformation over the 3.5 years, time series were determined. In Kozlu, Karadon and Üzülmöz same regions were chosen with different radius as 500 m, 1km and 500 m respectively, due to having dense points. The time series were depicted that the deformation was monitored 105 mm and 100 mm by PSI and SB methods respectively at the town of Kozlu (Figure 5.23a-5.23b). In Karadon deformation was extracted as 112 mm and 100 mm by PSI and SB methods respectively (Figure 5.23c-5.23d). Meanwhile, in Üzülmöz region the deformation was extracted around 100 mm by PSI method, while it was 105 mm in SB results (Figure 5.23e-5.23f). In Üzülmöz the deformation reaches up to 343 mm as maximum in SB result (Figure 5.23h). Furthermore, besides the mining regions the deformation of 270 mm was monitored in SB result within 1 km radius region (Figure 5.23g). Within the cave region a few points showing an uplift displacement was also noticed (Figure 5.21).

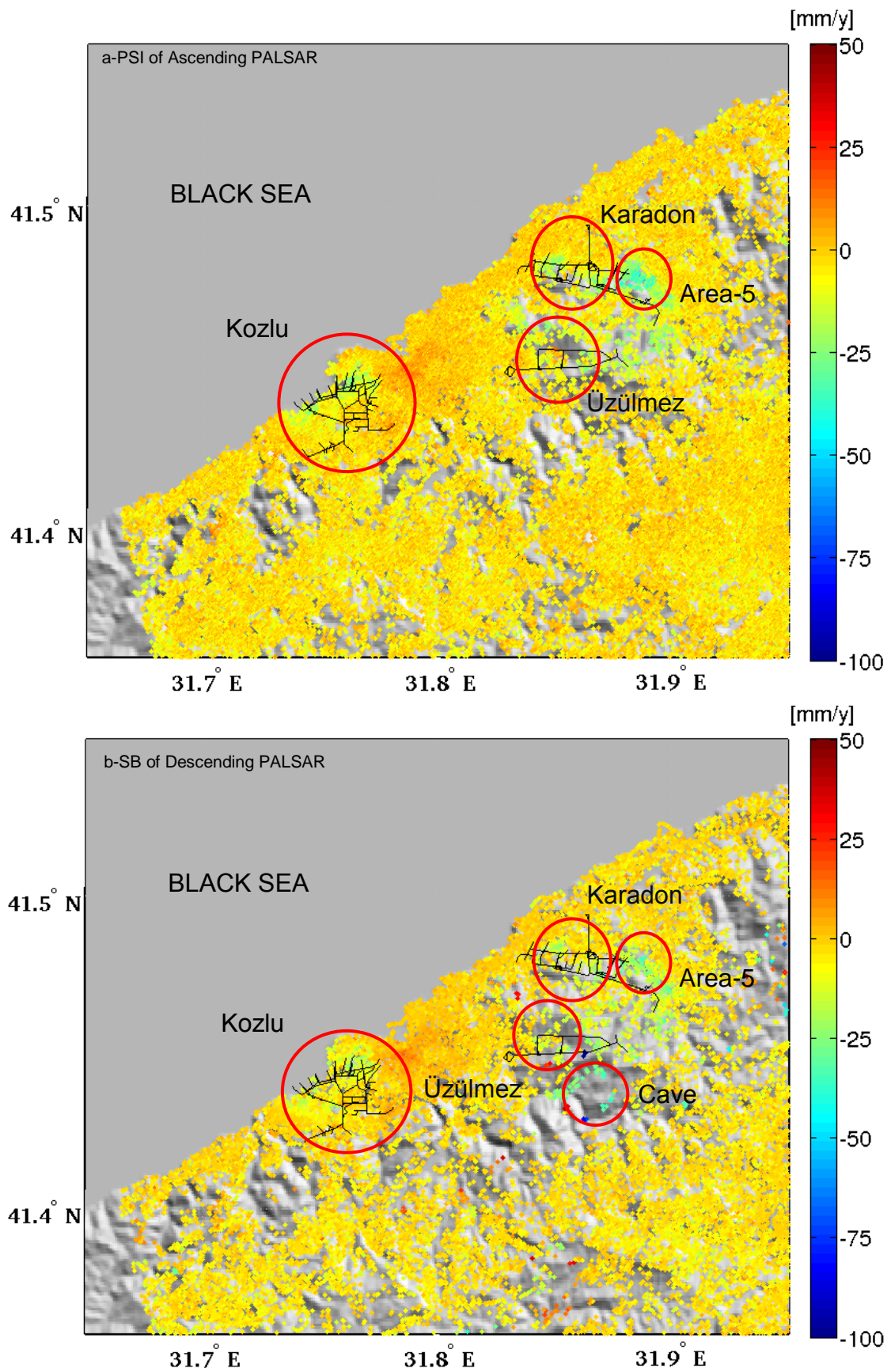


Figure 5. 21 PALSAR ascending track PSI and SB subsidence results along LOS from 2007 to 2010

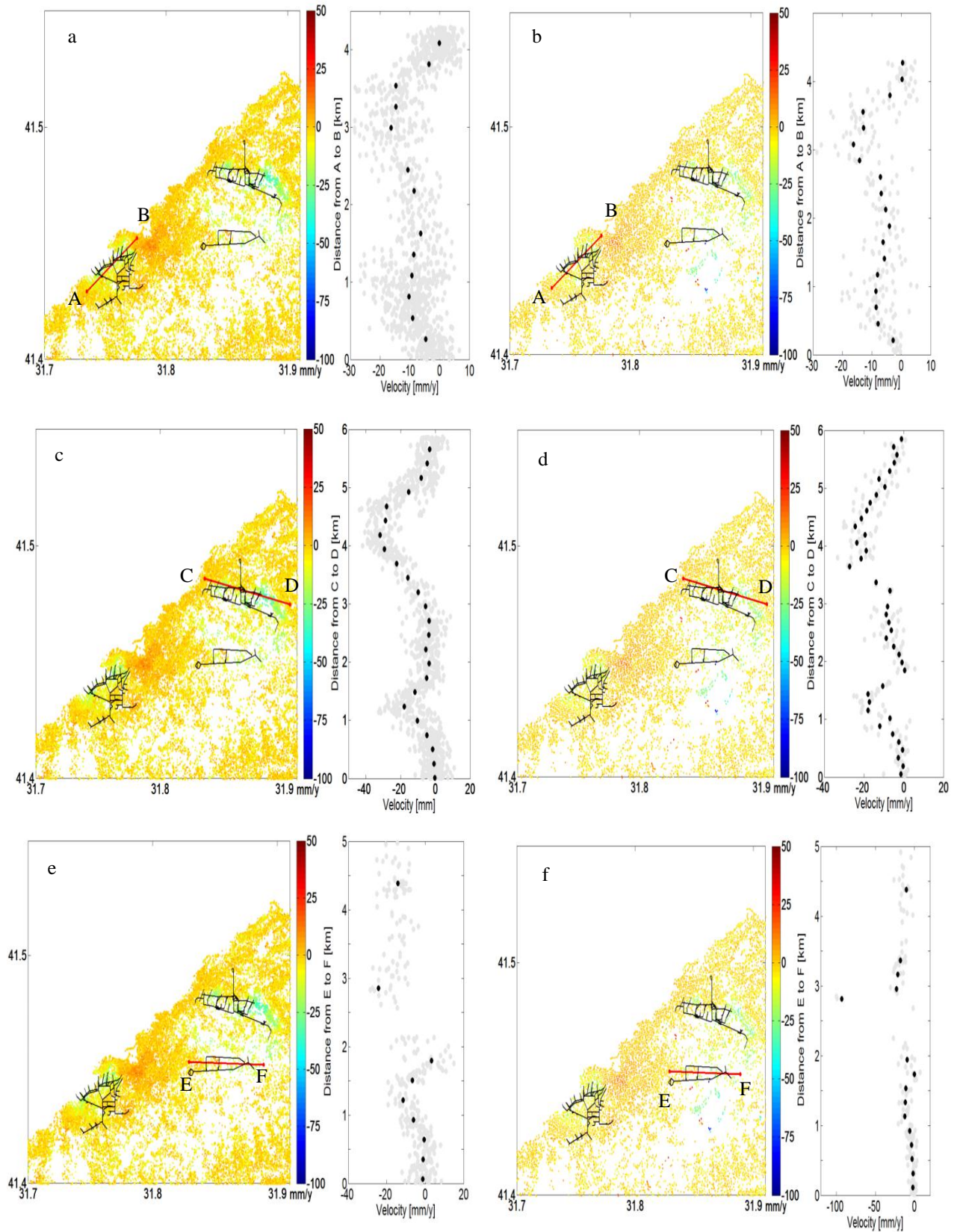


Figure 5. 22 Profile at Kozlu on ascending PALSAR a) PS result, b) SB result; at Karadon c) PS result, d) SB result; at Üzülmöz e) PS result, f) SB result

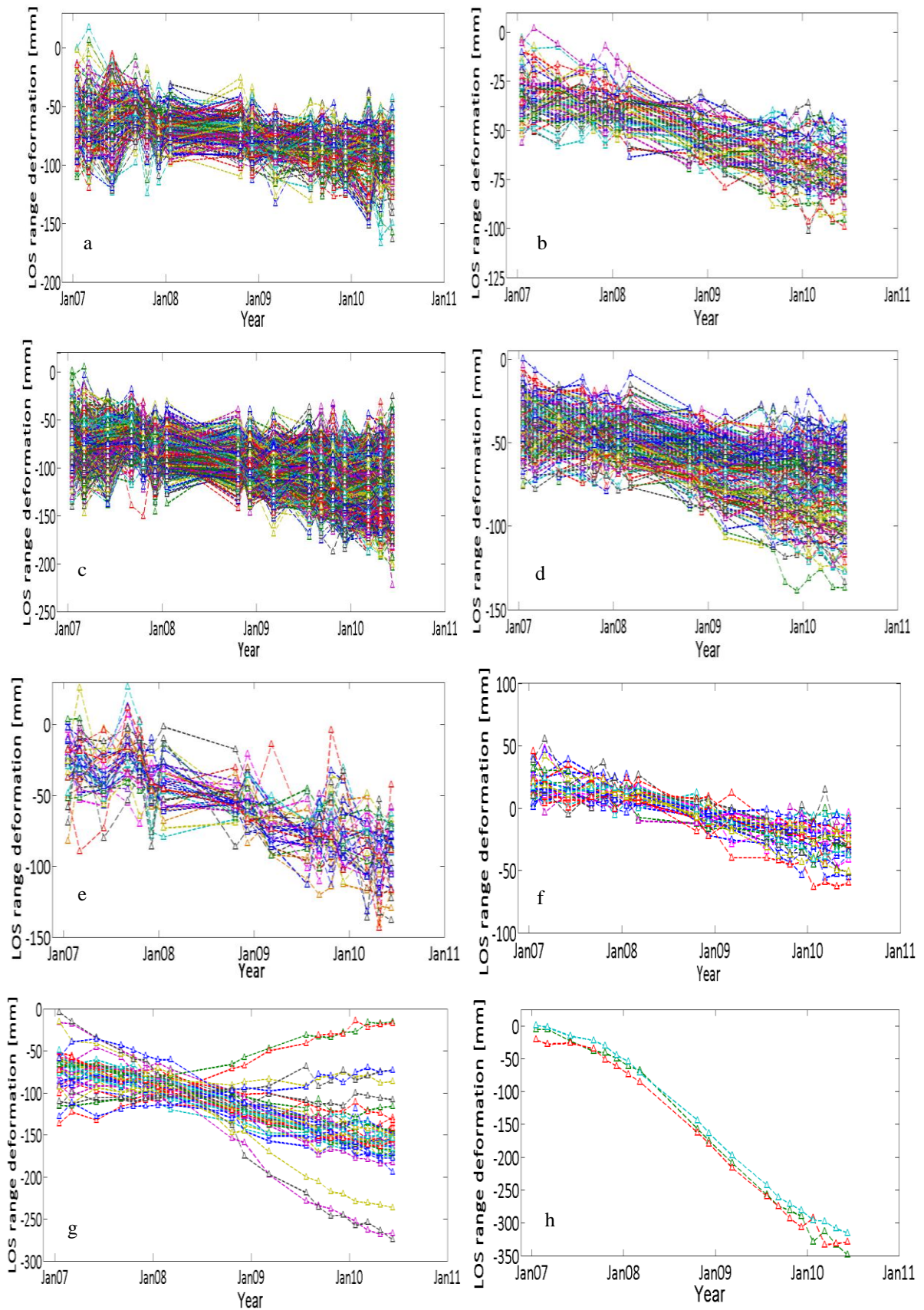


Figure 5. 23 Time series analysis from ascending PALSAR for the regions Kozlu a) PSI results, b) SB results; Karadon c) PSI results, d) SB results; Üzülmöz e) PSI results; f) SB results; g) Cave ; h) Üzülmöz maksimum

5.5 PSI Results Versus SB Results

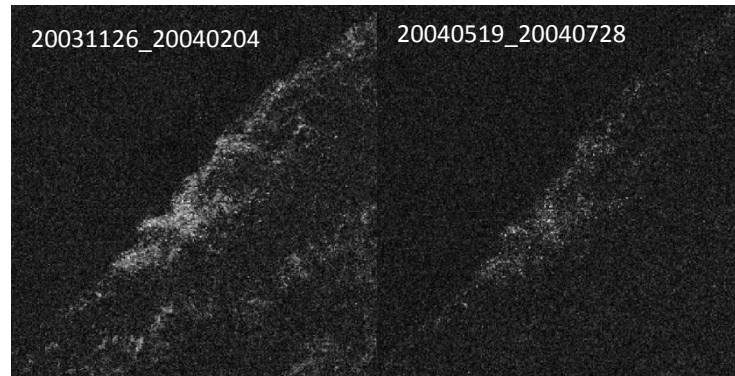
Surface deformation was evaluated in the Province of Zonguldak over the three mining regions. For the comparison of the methods a detailed visual analysis was applied to the Kozlu city, Üzülmöz , Karadon and Çatalağzı. The summary of the counted points for the sensors used and the multi temporal InSAR analyses were figured out in Table 5.8. Comparing to the SB results PSI results contain more scatterer points in all results (Table 5.8). This may change in different studies. For instance, while Hooper [19] concluded SB gets more points, Lazecky [43] and Aobpaet et al [100] computed more points in PSI process.

Table 5. 8 Summary of InSAR results

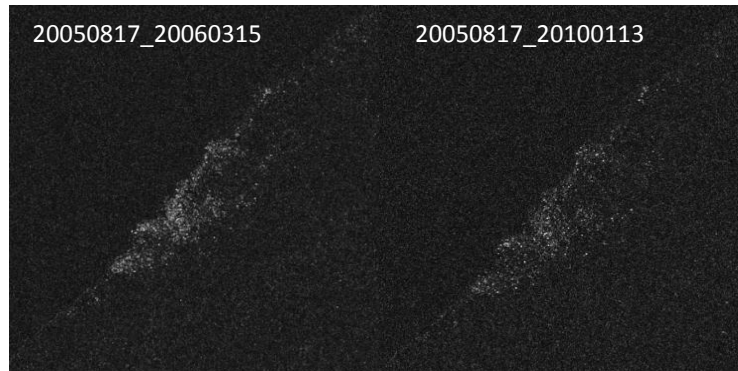
Sensor	Time period	Image no PSI/SB	lfg no PSI/SB	Points Count PSI/SB	Point/km2 PSI/SB
ERS T-21	19930418- 20010110	21/23	20/55	2582/2370	7.6/6.9
ENVISAT T-21	20031126- 20100113	14/17	13/32	3694/3100	10.8/9.1
ENVISAT T-343	20040506- 20100709	26/26	25/73	2249/1315	6.6/3.9
PALSAR T-604	20070118- 20103013	18/20	17/129	70719/15508	207.9/45.6

Coherence also affected to detect coherent points. Coherence of InSAR pairs depends on both temporal and perpendicular baselines. Some examples of extracted coherences of C-band descending ENVISAT (Figure 5.24) and L-band ascending PALSAR (Figure 5.25) are shown below. It is observed that in urbanized region coherence is more stable, however rural areas are lack of high coherence. PALSAR (L-band) pairs have higher coherence in rural area due to having higher penetration on vegetation than ERS and ENVISAT (C-band). This advantage contributed to monitor more stable points in mining area which is located in rural environment.

The velocity values show the small scale deformation (mm/year) on mining areas for the selected time period. In ERS and ENVISAT results SB velocities were higher than PSI velocities. In PALSAR results, SB and PSI velocities were very close to each other, and also SB velocity of descending ENVISAT was reaching to PALSAR velocities. A generalized table of velocities over the study area was created below (Table 5.9).

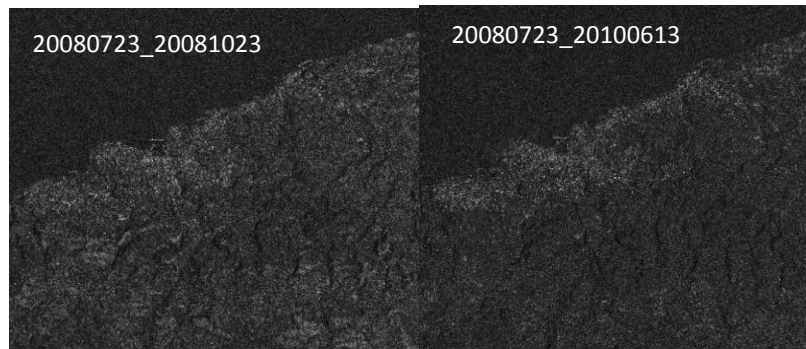


Temp B= 70 days, Perp B= 11 m Temp B= 70 days, Perp B= 235 m

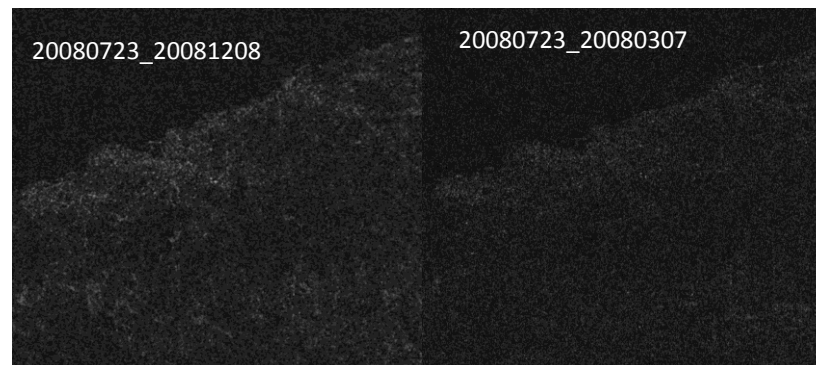


Temp B= 210 days, Perp B= 150 Temp B= 1610 days, Perp B= 149 m

Figure 5. 24 Effects of baselines on descending ENVISAT coherence images



Temp B= 92 days, Perp B= 1961 m Temp B= 690 days, Perp B= 1905 m



Temp B= 138 days, Perp B= 1736 m Temp B= 138 days, Perp B= 2951 m

Figure 5. 25 Effects of baselines on ascending PALSAR coherence images

Table 5. 9 Maximum velocities estimated over study area

Velocity/ Std Dev (mm/year)	ERS 1/2		ENVISAT T-21		ENVISAT T-343		PALSAR	
	PSI	SB	PSI	SB	PSI	SB	PSI	SB
Kozlu	7.5 ±0.8	7.5 ±1.8	7.5 ±0.7	25 ±3.6	5 ±0.5	12 ±4.3	30 ±1.4	28 ±1.8
Karadon	6 ±0.7	19.5 ±2.4	5 ±0.9	23 ±4.0	5 ±1.0	13 ±2.9	31 ±6.5	28.5 ±5.9
Üzülmez	4 ±0.9	5 ±1.1	6 ±0.4	17 ±5.5	1 ±1.4	1.5 ±3.5	28.5 ±6.9	30 ±5.4
Area-1				15 ±3.8				
Area-2				13 ±4.8				
Area-3						6 ±3.9		
Area-4						16 ±5.4		
Area-5							44 ±4.4	35.5 ±13.8
Cave								77 ±11.23

In Table 5.9 maximum velocities over selected areas were shown. A detailed standard deviation of the velocities can be seen at Appendix-C. In the eight of the results over the Kozlu, major deformation features of surface subsidence were detected. The PSI results of C-band showed slightly denser results (Figure 5.26). Only the L-band PALSAR resulted denser deformation in Kozlu with PSI approach. In SB results descending ENVISAT had approximately same deformation with PALSAR in Kozlu (Figure 5.26b-5.26d). In both PSI and SB results Kozlu presented a continuous deformation pattern with both ENVISAT and PALSAR comparing the ERS results. ENVISAT and PALSAR which overlap on time, also had supportive results. Points were extracted mostly in Kozlu town and through the coastline with C-band images. A denser number of points were counted by PALSAR in Kozlu and also in rural region to the south and east of Kozlu (Table 5.10). The highest deformation rate in Kozlu was also extracted with PALSAR results. Maps of underground mining tunnels show that deformations monitored on surface are most probably due to mining activities.

Table 5. 10 Extracted points in Kozlu

Points count	ERS		ENVISAT T-21		ENVISAT T-343		PALSAR	
	PSI	SB	PSI	SB	PSI	SB	PSI	SB
Kozlu	1114	896	1758	1116	777	553	11839	2475
Point/km2	27.8	22.4	43.9	27.9	19.4	13.8	295.9	61.9

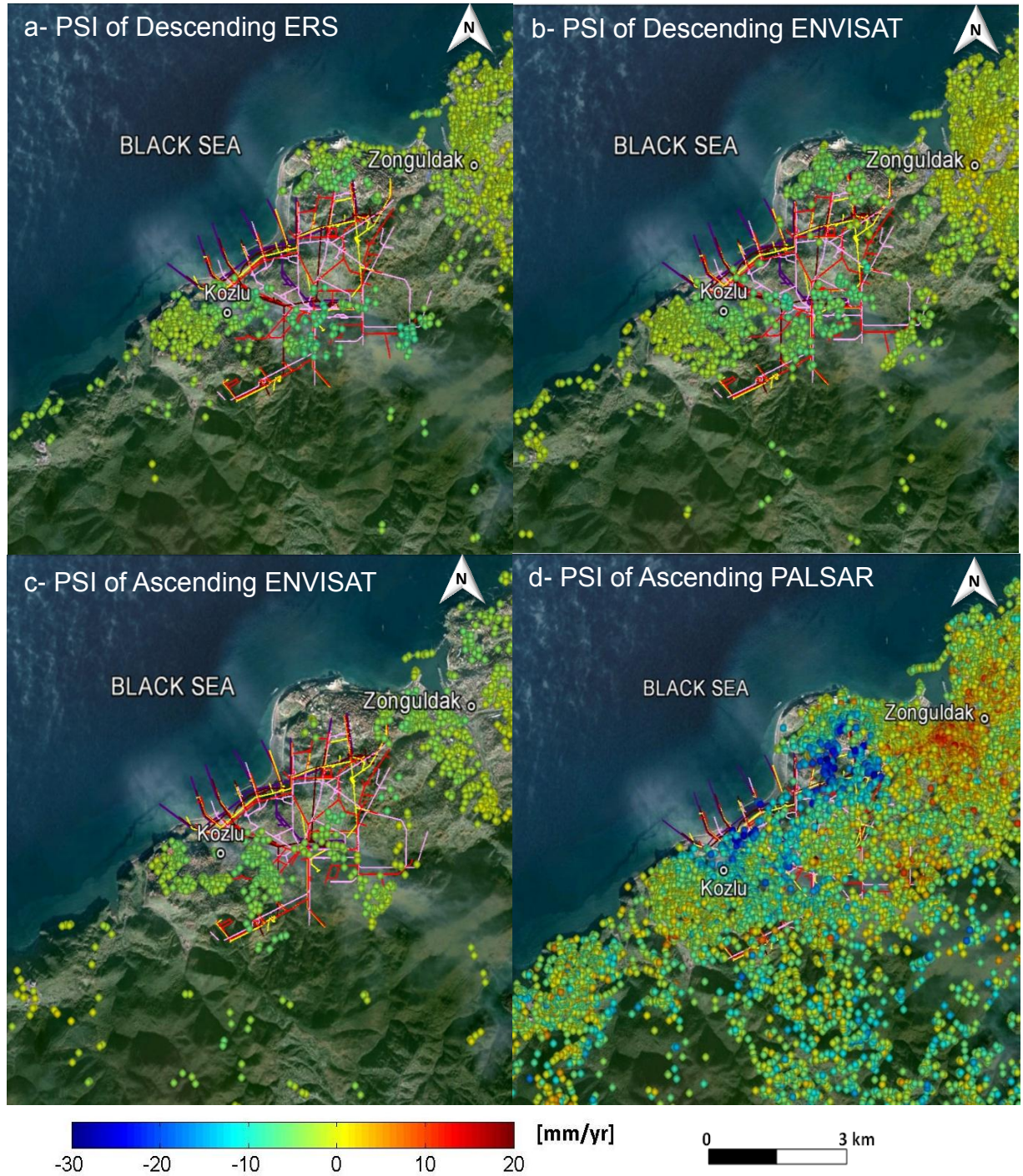


Figure 5. 26 Saturated PSI results shows the velocity along LOS direction with mining galleries on the city of Kozlu: a- Desc. ERS 1-2, b- Desc. ENVISAT, c- Asc. ENVISAT, d- Asc. PALSAR

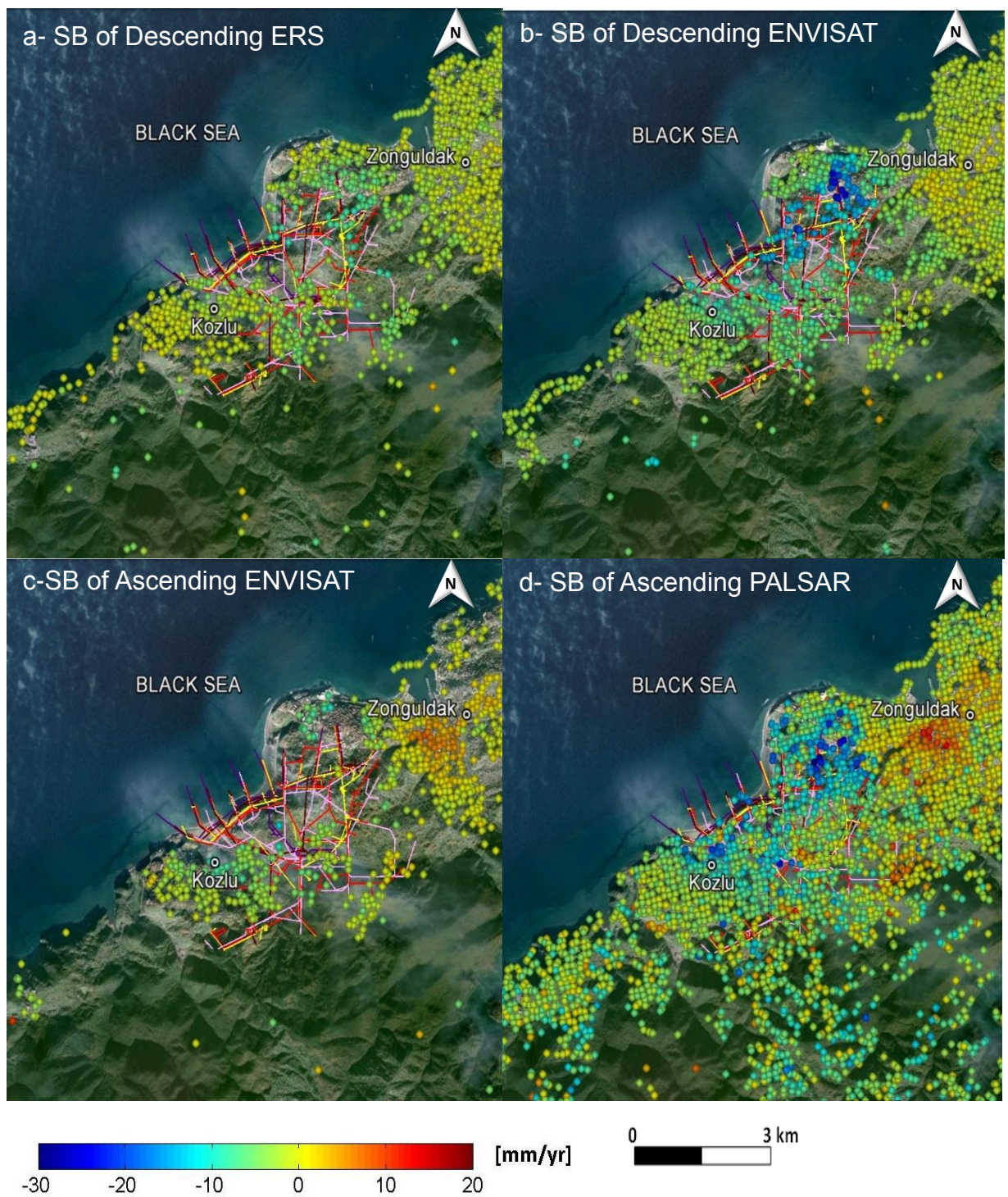


Figure 5. 27 Saturated SB results shows the velocity along LOS direction with mining galleries on the city of Kozlu: a- Desc. ERS 1-2, b- Desc. ENVISAT, c-Asc. ENVISAT, d- Asc. PALSAR

In the second study region Karadon mining is located. It overlaps with the area covering from Kilimli to Gelik towns. Urban area is mostly at the coastline and urbanization decreases through the Gelik. Again in PALSAR results points were denser and also disturbed over the mining tunnels where the velocity reached up to 50 mm/year in PSI results (Figure 5.28a). In this region there is a cave named Kizilelma and located near the Karadon mining. Over this cave the velocity reaches up to ~20 mm/year (Figure 5.28). Maximum deformation was estimated ~18 mm/year from 1993 to 2001 with SB approach (Figure 5.28b). Descending ENVISAT SB result had denser points and higher subsidence rate in C-band (Figure 5.29c-5.29d). Thirdly, another comparison area was determined covering the Üzülmöz mining. This mining is located in the subsidence area which is specified by TTK. In this area a few number of points were counted including the slightly urbanized part of the area (Figure 5.30). This was most probably due to the loss of coherence in this region because of the dense vegetation. In the result of SB with descending ENVISAT data concluded the higher displacement as C-band. L-band indicated points over the vegetated area as expected. In PALSAR results displacement reached up to ~100 mm/year as maximum in SB approach. In addition, in the outside of the subsidence area, a ~77 mm/year subsidence was monitored over the Gökgöl Cave which is located to the south of Üzülmöz (Figure 5.31b).

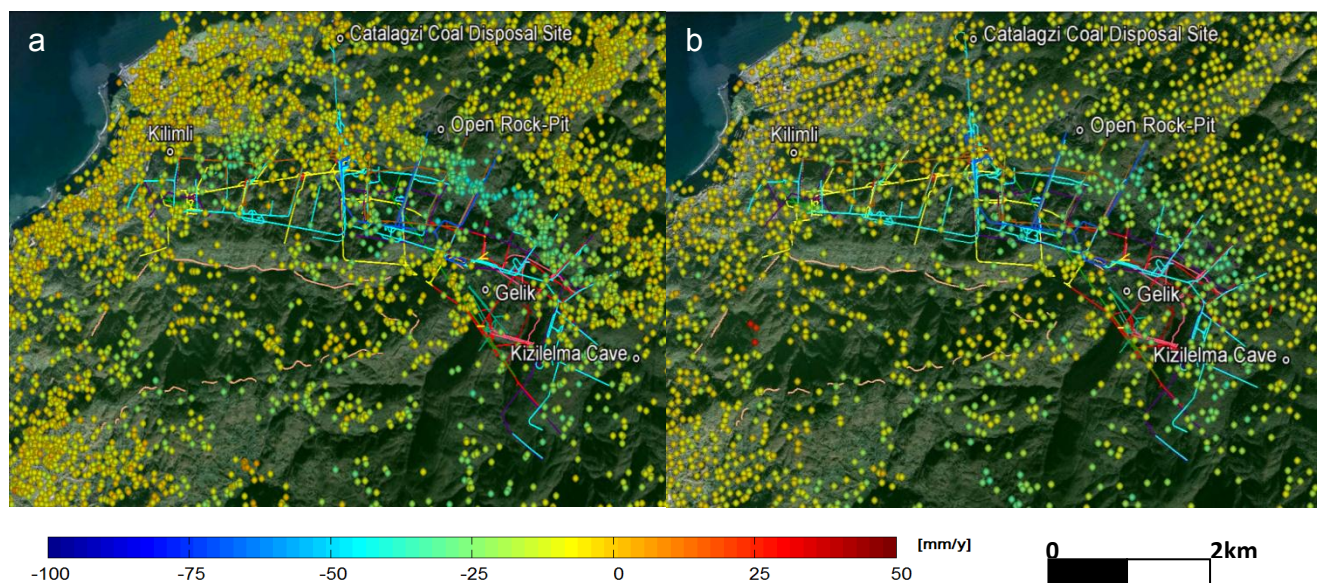


Figure 5. 28 Saturated results shows the velocity along LOS direction with mining galleries on the Karadon: a) PSI of Asc. PALSAR, b) SB of Asc. PALSAR

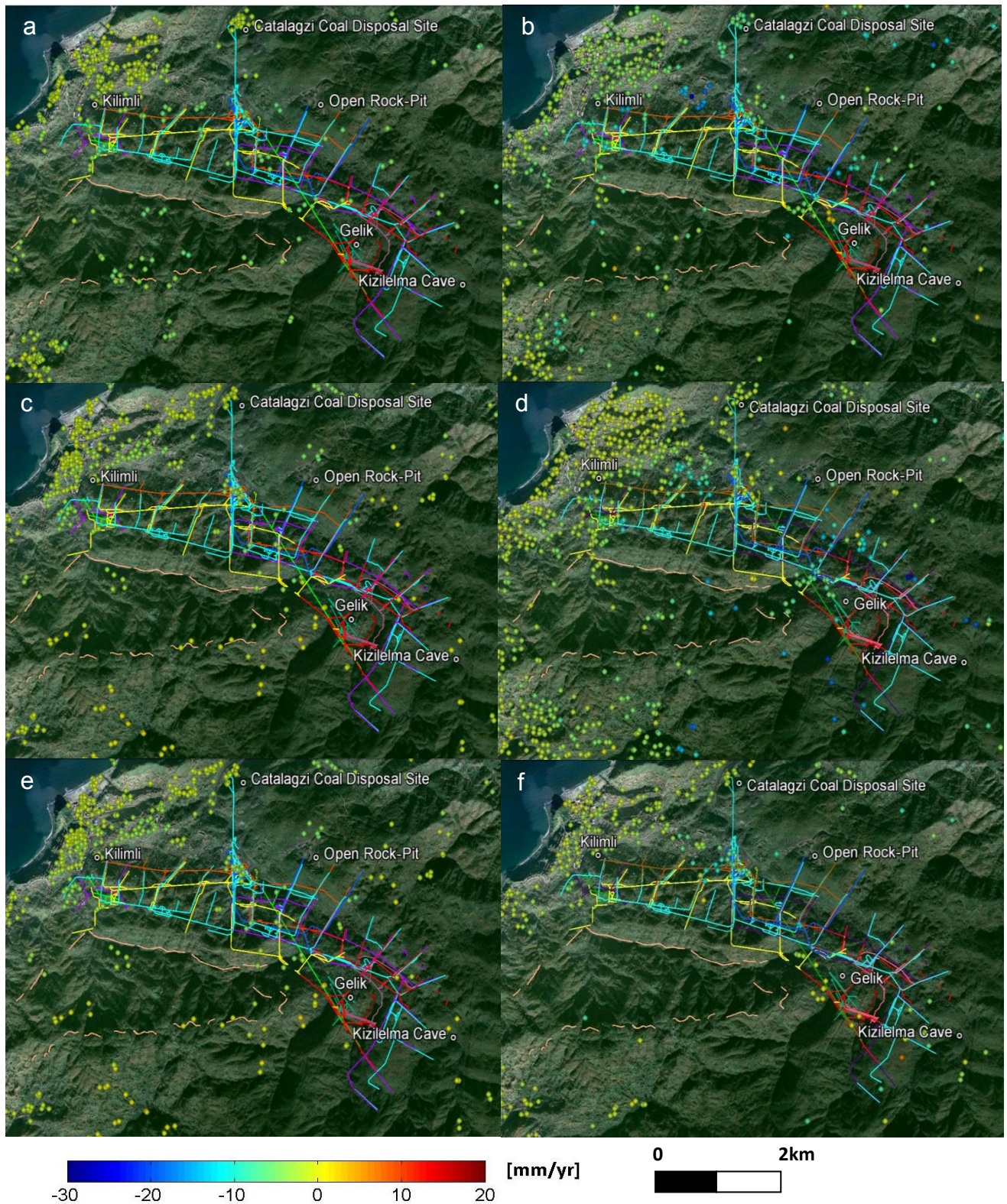


Figure 5. 29 Saturated results shows the velocity along LOS direction with mining galleries on the Karadon: a) PSI of Desc. ERS 1-2, b) SB of Desc. ERS 1-2, c) PSI of Desc. ENVISAT, d) SB of Desc. ENVISAT, e) PSI of Asc. ENVISAT, f) SB of Asc. ENVISAT

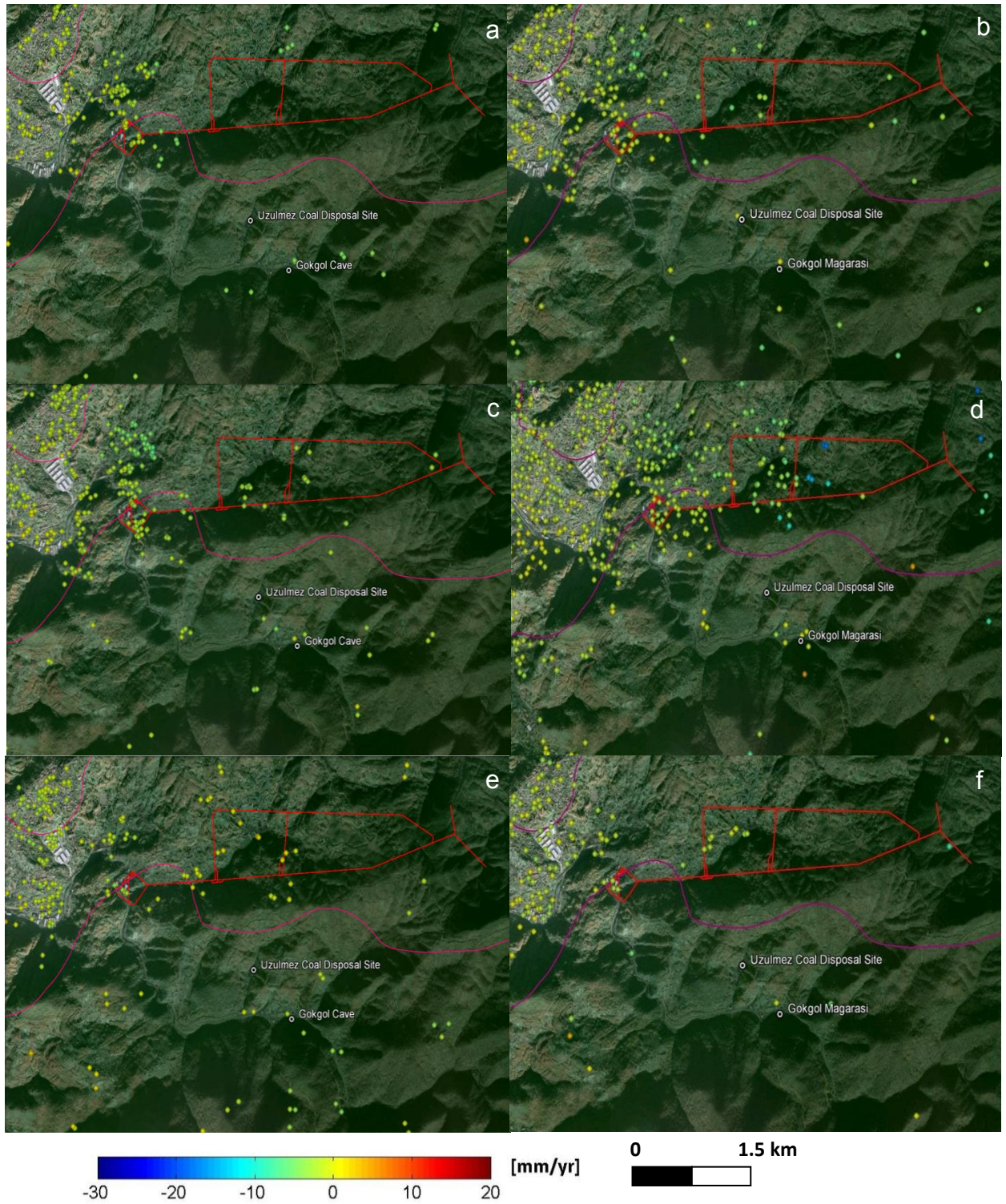


Figure 5. 30 Saturated results shows the velocity along LOS direction with mining galleries on the Üzülmöz : a) PSI of Desc. ERS 1-2, b) SB of Desc. ERS 1-2, c) PSI of Desc. ENVISAT, d) SB of Desc. ENVISAT, e) PSI of Asc. ENVISAT, f) SB of Asc. ENVISAT

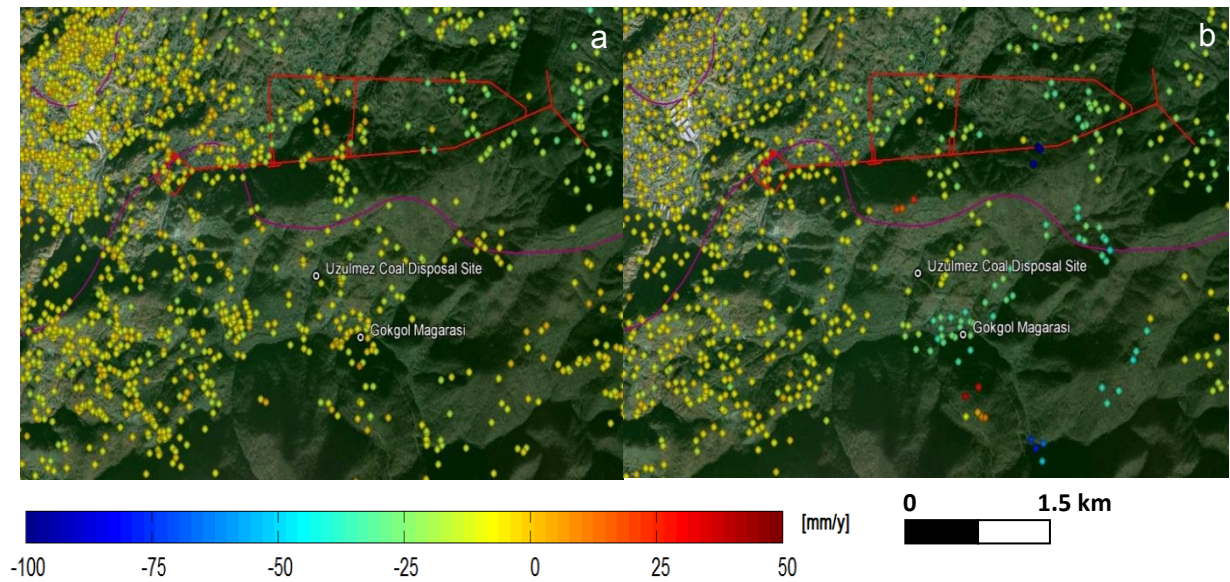


Figure 5. 31 Saturated results show the velocity along LOS direction with mining galleries on the Üzülmöz : a) PSI of Asc. PALSAR, b) SB of Asc. PALSAR

Beside the specification of subsidence area, a potential subsidence area is also specified by TTK. This part is located at east and north-east of Karadon mining, in the city of Çatalağzı. It includes two thermal power plants where energy is produced for industry and daily usage. There are two ports related to these two power plants named Cates and Eren. The second port does not cover any point because it was constructed in 2010. In both ERS and ENVISAT results coherent points were monitored where buildings and old port are located. In this potential subsidence area 3-4 mm/year velocity was detected with both ascending (Figure 5.32e and 5.32f) and descending ENVISAT (Figure 5.32c and 5.32d), where it reached up to 15 mm/year in PALSAR results (Figure 5.33a and 5.33b).

Also in the outside of the potential subsidence area, a small displacement was observed. In descending and ascending ENVISAT results it was reaching up to ~3-5 mm/year and ~2.5 mm/year respectively (Figure 5.32a, 5.32b, 5.32c, 5.32d). PALSAR results showed higher amounts as ~5-7 mm/year. The displacement of ~2-6 mm/year was monitored by ERS results showing that area is subsiding for long time period (Figure 5.33a and 5.33b).

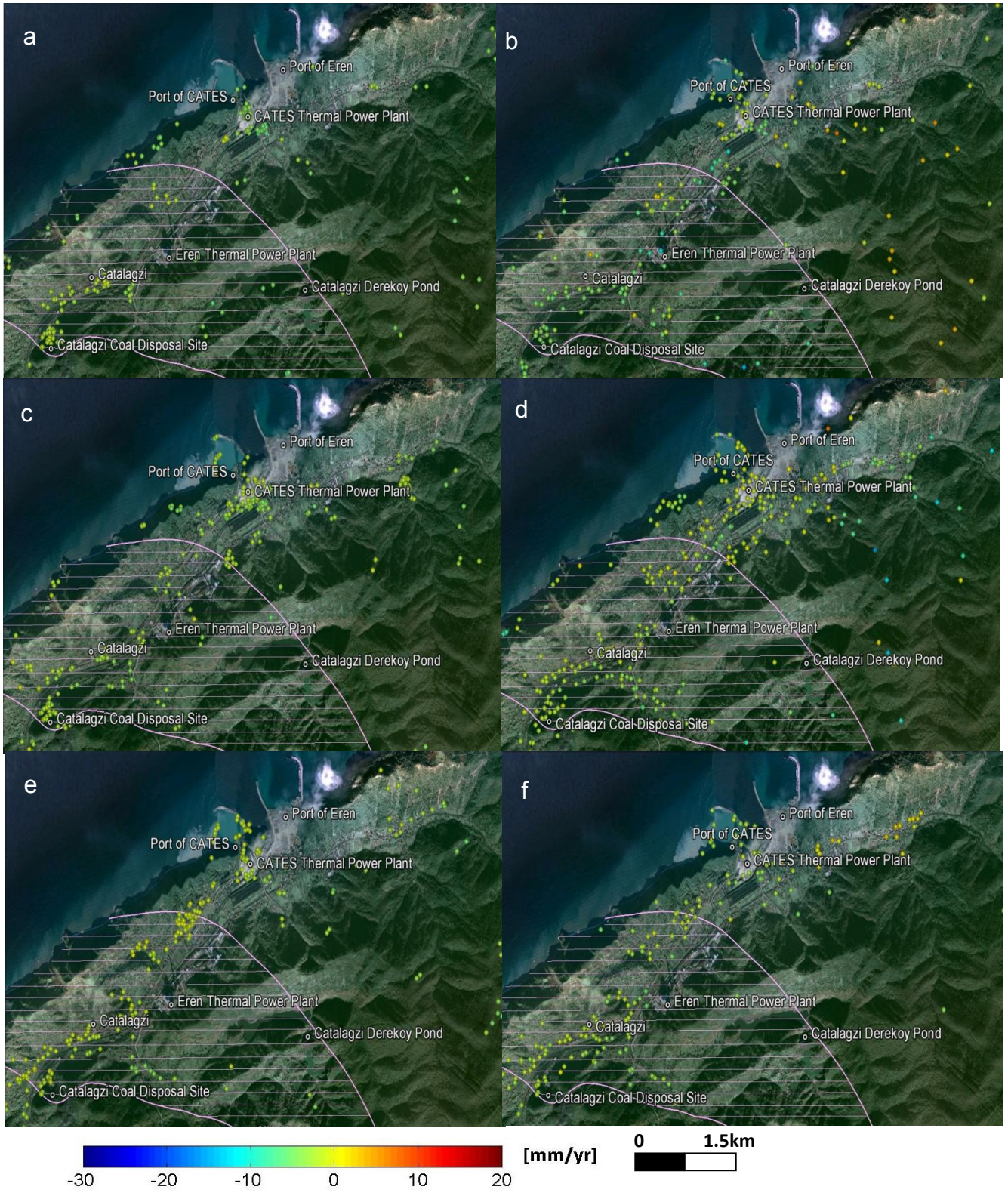


Figure 5. 32 Saturated results shows the velocity along LOS direction on Catalagzi which is located in potential subsidence area: a) PS of Desc ERS, b) SB of Desc. ERS, c) PSI of Desc. ENVISAT, d) SB of Desc. ENVISAT, e) PSI of Asc. ENVISAT, f) SB of Asc. ENVISAT

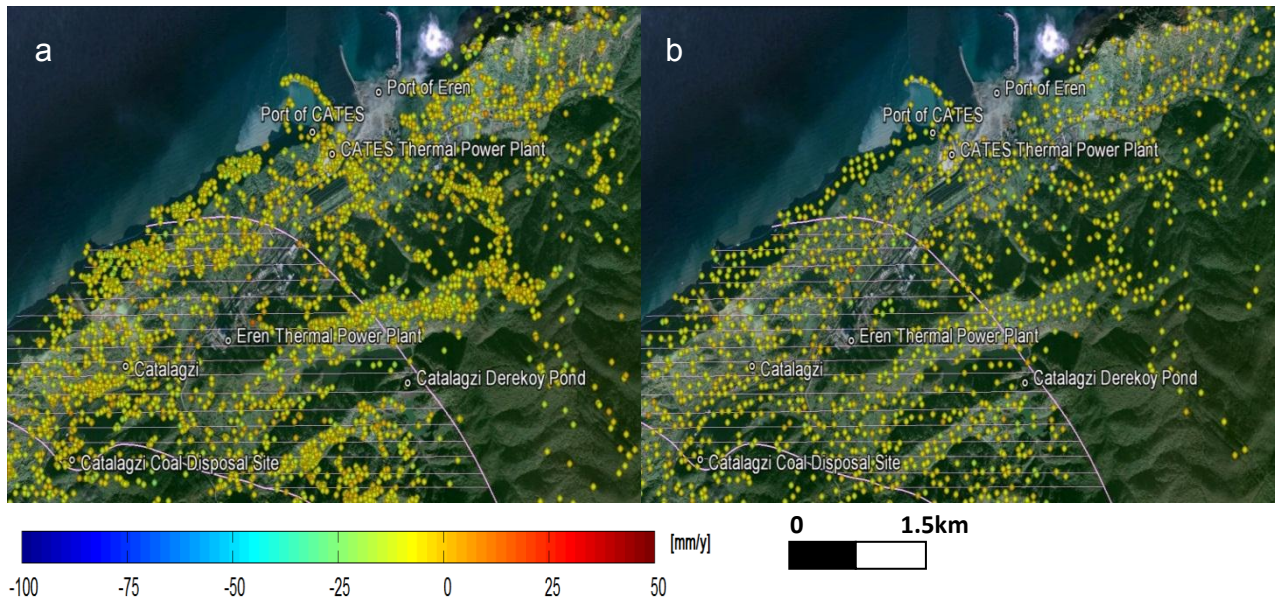


Figure 5.33 Saturated results shows the velocity along LOS direction on Catalagzi which is located in potential subsidence area: a) PSI of Asc. PALSAR, b) SB of Asc. PALSAR

As explained above with the time series and profiles, both PSI and SB results presented the same deformation pattern in Kozlu mine. In Karadon and Üzülmez mines, a small amount of points were gathered with C-band. Higher density of points were identified with L-band results.

After the extraction of points an intersection was applied among the results to find out the common points which were detected in each process. The intersection of the results and the common points were listed in Table 5.11. The first aim was to identify the common points which are located with same coordinates in both PSI and SB results. ERS and both ENVISAT results in ascending and descending tracks gave similar results (Table 5.11). These points were mostly located at urban and coastline (Appendix-D). PALSAR results have the maximum common points as expected (Table 5.11). These points were distributed all over the study area (Appendix-D). Around the Gökgöl Cave where the subsidence was monitored with SB results of PALSAR, the difference of velocity between PSI and SB was extracted as maximum.

Secondly, it was aimed to identify the any points having continuous movement along the 17 years. For this purpose ERS-ENVISAT intersection was applied on both PSI and

SB results. However, just one point was extracted at intersection of PSI ERS-ENVISAT results. Finally, intersection of ascending ENVISAT and descending ENVISAT was applied. These data cover almost the same period but have different LOS which causes to illuminate the different aspect.

Table 5. 11 Common point list in the processes

Intersection of results	Common Points	Intersection of results	Common Points
ERS PSI_ERS SB	51	ENV T-343 PSI_ENV T-343 SB	62
ERS PSI_ENV T-21 PSI	1	ENV T-343 PSI_ENV T-21 PSI	0
ERS SB_ENV T-21 SB	0	ENV T-343 SB_ENV T-21 SB	0
ENV T-21 PSI_ENV T-21 SB	66	PALSAR PSI_ PALSAR SB	1296

As mentioned in chapter 4 the study area is very well known landslide region with high degree of disaster (Turer et al. [78]). It is investigated to figure out landslide movement apart from the mining based subsidence. In Figure 5.26 and Figure 5.27 besides the mining based subsidence a movement can be seen as an uplift. It is located east of Kozlu city and at the center of Zonguldak city center. All results are overlapped with the landslide area which is acquired from MTA. They are described and showed with arrows over city center as new landslide areas in this region (Figure 5.34). The uplift is more dense in both ascending results of ENVISAT and ALOS images. For the ascending ENVISAT results the uplift is more in SB result than PSI result (Figure 5.35).



Figure 5. 34 Landslide regions acquired from MTA

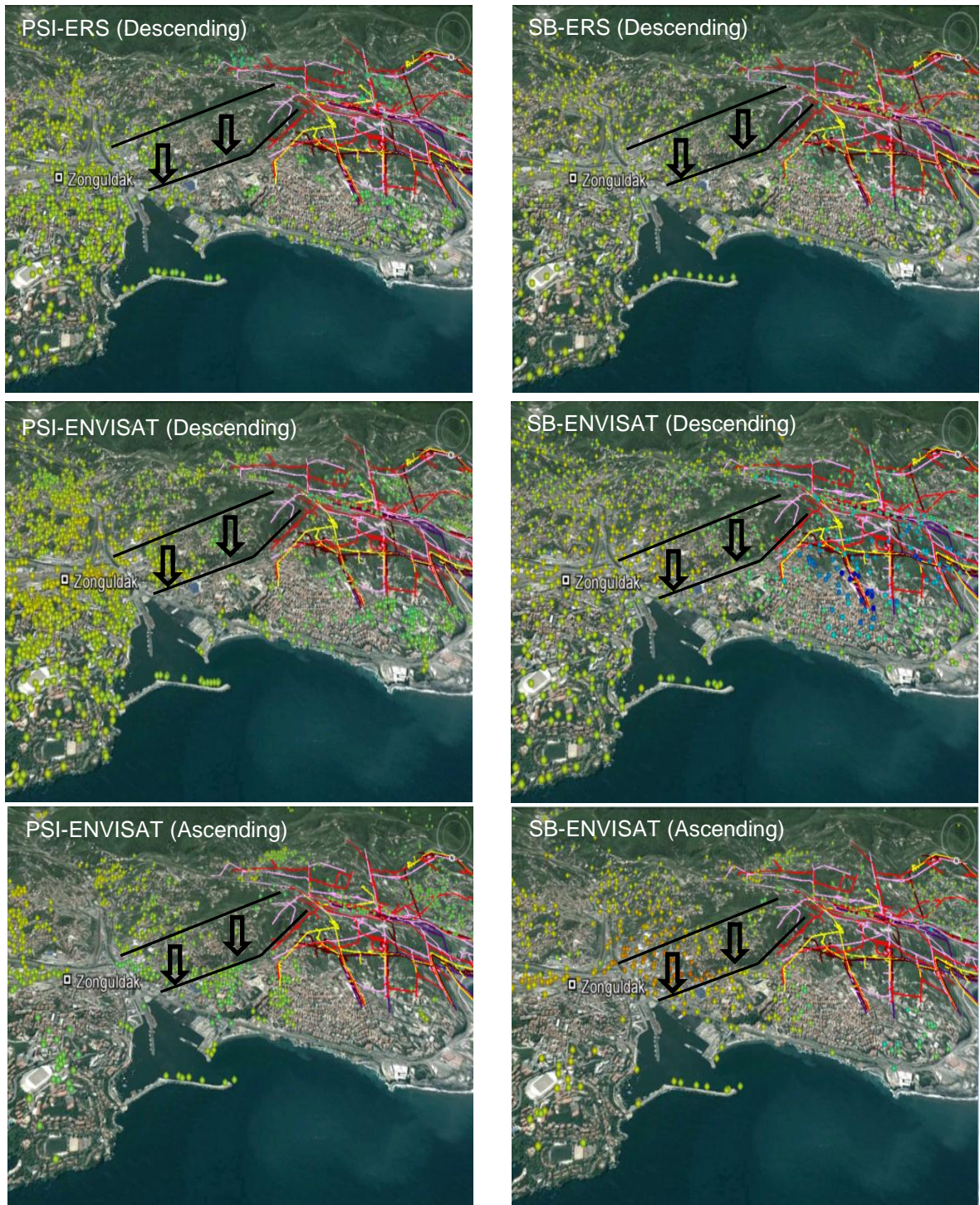


Figure 5. 35 Landslide area at Zonguldak city overlaped with C-band results

In ALOS results the uplift can be seen more clearly in both PSI and SB result. In all results a cross-section profile was taken to describe the spatial distribution of the uplift. A profile which has a 3 km long taken from A to B over landslide area (Figure 5.34). All profiles taken over PSI and SB results are shown in Figure 5.37.

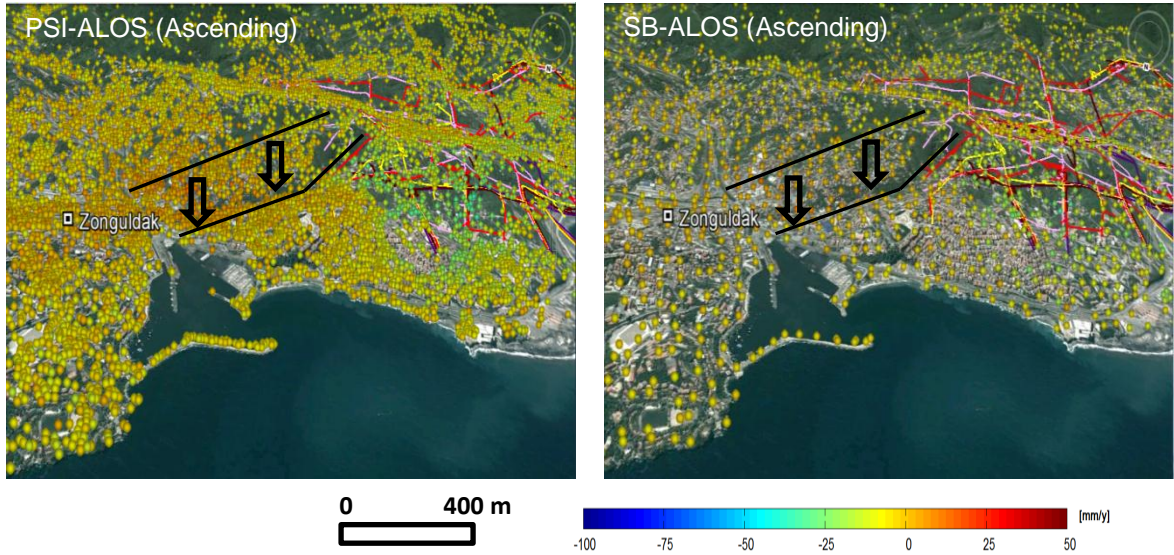


Figure 5. 36 Landslide area at Zonguldak city overlapped with L-band results

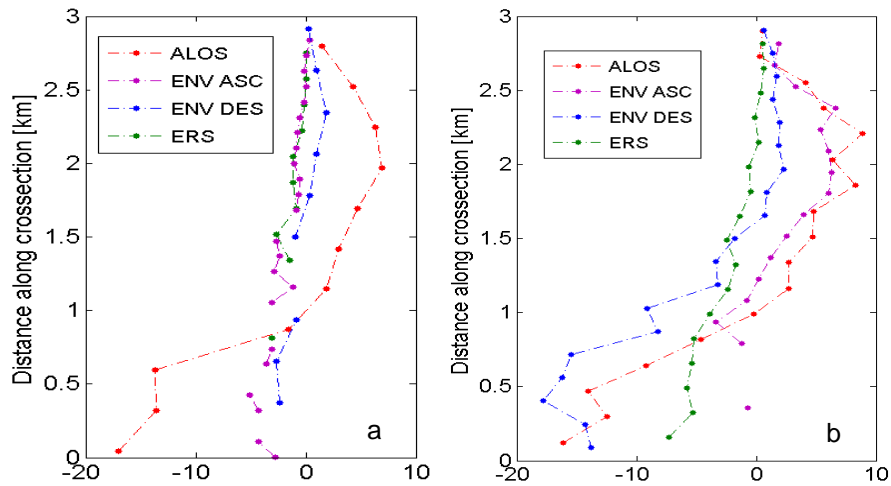


Figure 5. 37 Profiles over landslide area from A to B; a) PSI results, b) SB results

RESULTS AND DISCUSSIONS

In the content of this study, ground surface displacements have been identified for the first time over the underground coal mining in Zonguldak Province for a long term period. InSAR derived surface subsidence has allowed to figure out the spatial and temporal evolution of the deformation. Due to lack of leveling and GPS data multi track and multi temporal SAR data was used for evaluation. Moreover, two techniques are compared over the study area.

Surface deformation was evaluated in the Province of Zonguldak over the three mining regions namely Kozlu, Karadon and Üzülmöz mining areas. As expected, the PSI and SB points were mostly monitored in urban areas where city of Kozlu and the Kozlu mining are located. The most significant output is that a bowl pattern of subsidence was monitored in all SAR data in urbanized Kozlu region. The subsidence rates which were monitored from different sensors (ERS 1/2, ENVISAT and PALSAR), frequency (C-band, L-band), acquisition modes (ascending, descending), and polarization (VV, HH) exposing the same deformation pattern.

Previous studies also indicate the subsidence in this region which endorses the results of this case. In the Zonguldak region, subsidence was monitored by previous conventional DInSAR studies (Akcin et al. [33], Deguchi et al. [35], Kemaldere [36]) which gives information about the deformation in short term time periods. The urban of Zonguldak, which suffered of surface displacement from the beginning of 19th century, has not got long time constant measurements.

First research with InSAR was done with a pair of JERS images (September-May 1995), which have 4.5 months temporal baseline. The study resulted as there was 204 mm

deformation around the Kozlu coalfield. Moreover, about 130 mm deformation was observed at Karadon and Üzülmöz area.

Another InSAR study was done for the period of 2005 and 2006 using 15 Radarsat images. In the urban area of Kozlu, a 44 mm/year of deformation was measured by time series of Radarsat images. DInSAR results of Radarsat were validated with three GPS points which were observed in 4 epochs between October 2005 and October 2006. For the same period an average deformation was obtained as 61 mm/years by three GPS points (Akcin et al. [33]). It is also known that surface deformation are taking place in the Üzülmöz and Karadon mining fields. Both of these fields are covered by forest. Due to the lack of high coherence, deformation could not be detected by the previous DInSAR studies using C-band Radarsat (Akcin et al. [33]).

Meanwhile, 30-40 mm/1.5 months of deformation was extracted using L-band PALSAR data in Üzülmöz and Karadon regions (Deguchi et al. [35]). But no research at Kozlu is mentioned at all.

Kemaldere [36] studied over Zonguldak mining field with DInSAR. In that study, using one pair of PALSAR the deformation of 95 mm/year was calculated from September 2006 to December 2007 in Kozlu. By another pair of PALSAR images the deformations of 88 mm/year and 53 mm/year from December 2007 to March 2010 were monitored in Kozlu and Karadon respectively. The deformation in Üzülmöz was not monitored for the period of 2006 to 2010 with PALSAR data. Moreover, using three pairs of ENVISAT data the deformation was monitored in just Kozlu town. These results were as 50 mm/7months from October 2008 to May 2009, 40 mm/6 months from May 2009 to November 2009, and 50 mm/4.5 months from November 2009 to April 2010. Kemaldere [36] concluded that due to vegetation cover over Karadon and Üzülmöz deformation was not monitored with ENVISAT data.

Additionally, Can et al. [34] obtained 10 to 78 mm/9 months surface displacement using GPS in Kozlu city with two epochs measurements between 2009 August and 2010 May.

In this thesis the results of PSI and SB results are in agreement with the previous DInSAR studies, but it is difficult to compare them precisely because they cover a

shorter time period. In all my processes DEM error, orbit error and atmospheric phase were removed. DEM errors are shown in Appendix-E . The orbit error and atmospheric contributions for each slave images of PALSAR PSI dataset are also shown as an example in Appendix-E.

Although, the results are agreed with the previous study, there are improvements in the following steps:

- 1- ERS data cover 7.5 years and as it is expected mostly the urbanized areas were identified with dense PS points. Main output was in rural Karadon and Üzülmöz regions. PS points were also extracted sparsely over Karadon mining and Kilimli town.
- 2- For the period 2003-2010, ascending and descending acquisition of ENVISAT-ASAR data were gathered, and the results presented that they are concur to each other. However, descending results of PSI and SB have less points, a slight deformation was achieved at Karadon and Üzülmöz mining which could not monitored with the previous studies (Kemaldere [36]). In this thesis, ERS and ENVISAT results clearly monitored subsidence over these areas. Thus, C-band is promising for further studies.
- 3- Moreover, another important output is that the higher subsidence rates were obtained in ENVISAT results than ERS results. After 2001 the amount of mining was decreased, on the contrary the rate of the subsidence has been increased. This occurs due to the new and deeper galleries opened for mining. In Kozlu, at the -560 m and -630 m levels, ~5.5 km progress was made at mining galleries between 2008 and 2010 years. For the same period another ~2.9 km of progress was made at the -425 m and -485 m levels in Kozlu. Additionally in 2009, about ~1.4 km and ~2.3 km progress was made at Üzülmöz and Karadon had respectively (TCE [73], General Union of Mine Workers [101]).
- 4- Furthermore, in both PSI and SB results of C-band ascending and descending processes, other than the deformations in subsidence and the potential subsidence areas, the deformations were monitored in also rural areas.
- 5- PALSAR result contains more number of distributed points both in urban and rural areas mainly due to having L-band and having higher spatial resolution.

Although other data contained gaps in time PALSAR data were collected continuously. In all three regions the subsidence pattern was determined very obviously. L-band was found to be more useful than C-band over Zonguldak region.

- 6- PALSAR results also resulted deformation areas outside of the mining and at the potential mining regions. As a geological structure of the area there are many caves in the study area. A significant deformation was monitored to the south of Üzülmöz over the Gökgöl Cave.
- 7- The results of ENVISAT and PALSAR find out new subsidence phenomena besides the mining. Depending on these results, new subsidences are likely to occur in the future. One source is illegal mining which happens frequently in this region and the other is landslides also happening constantly. Apart from these deformations especially in the results of ascending ENVISAT and PALSAR results landslide movement was monitored at the city center of Zonguldak.
- 8- This study cover a long time period which presents spatial and temporal evolution of the mining subsidence. With this research, PSI and SB teschniques were applied for the first time in Turkey over a mining region. It is proved that multi temporal approaches are suitable to monitor slow deformation rates over long time period in Zonguldak hard coal mining areas.
- 9- As a conclusion, ground surface deformation due to underground coal mining was determined for 17 years from 1993 to 2010 with two periods of SAR data time series analysis.

As a limitation no images are available in 1994 and 1998 for ERS data set and in 2008 for ascending ENVISAT data. Consequently, during these periods probable nonlinear deformations could not be achieved. That may cause the loss of coherence. For some pairs the temporal and perpendicular baselines were higher which were also removed from the process.

For the maintainability of the monitoring system it is suggested to acquire proper satellite images to investigate the further subsidence. Additionally, it could be better to use a conventional measurement techniques and InSAR combination where has not

got any measurements such as Karadon and Üzülmöz (Strozzi et al. [11]). Another alternative for these investigations homogenous distributed corner reflectors could be designed. Corner reflectors, which can be used for validation purpose, have ability to response radar signals (Sousa [48]). L-band ALOS is a common source for subsidence investigation over vegetated areas. If there is not any satellite that provide L-band image it is usefull to set corner reflectors at site to use with C-band images.

According to the results of this study, subsiding area and district of potential subsiding area which are described by TTK should be updated for risk management. Many settlements and governmental buildings are subject to mining based subsidence hazards. It is undoubtedly necessary to monitor these fields continuously for sustainable management. Further studies will be conducted to investigate the landslides in details and subsidence phenomena which are monitored outside of mining regions with geological and geomorphological aspects and to continue subsidence monitoring with new generation SAR missions.

REFERENCES

- [1] Ng, A.H.-M., Ge, L., Yan, Y., Li, X., Chang, H.C., Zhang, K. and Rizos, C., (2010). "Mapping Accumulated Mine Subsidence Using Small Stack of SAR Differential Interferograms in the Southern Coalfield of New South Wales, Australia", *Engineering Geology*, 115: 1-15.
- [2] International Social Security Association, ISSA Mining Ties Relations with Turkish Coal Mining Industry, http://www.issa.int/About-ISSA/node_37009/Section-on-Prevention-in-the-Mining-Industry/Events2/ISSA-Mining-Ties-Relations-with-Turkish-Coal-Mining-Industry , 03 July 2012.
- [3] Gens, R. and van Genderen, J.L., (1996). "SAR Interferometry - Issues, Techniques, Applications", *International Journal of Remote Sensing*, 17: 1803-1835.
- [4] Briole, P., Massonnet, D. and Delacourt, C., (1997). "Post-Eruptive Deformation Associated with the 1986–87 and 1989 Lava Flows of Etna Detected by Radar Interferometry", *Geophysical Research Letters*, 24(1): 37–40.
- [5] Goldstein, R., Engelhardt, H., Kamb, B. and Frolich, R., (1993). "Satellite Radar Interferometry for Monitoring Ice Sheet Motion: Application to an Antarctic Ice Stream", *Science*, 262: 1525–1530.
- [6] Manzo, M., Ricciardi, G.P., Casu, F., Ventura, G., Zeni, G., Borgstrom, S., Berardino, P., Del Gaudio, C. and Lanari, R., (2006). "Surface Deformation Analysis In the Ischia Island (Italy) Based on Spaceborne Radar Interferometry", *Journal of Volcanology and Geothermal Research* 151: 399–416.
- [7] Small, D., (1998). *Generation of Digital Elevation Models Through Spaceborne SAR Interferometry*, PhD Thesis, Remote Sensing Laboratories Department of Geography University of Zurich, Switzerland, Remote Sensing Series 30.
- [8] Massonnet, D., Rossi, M., Carmonia, C., Adragna, F., Peltzer, G., Feigl, K. and Rabaute, T., (1993). "The Displacement of the Landers Earthquake Mapped by Radar Interferometry", *Nature*, 364: 138–142.

- [9] Fruneau, B., Achache, J. and Delacourt,, C., (1996). "Observation and Modelling of the Saint-Etienne De Tinee Landslide Using SAR Interferometry", *Tectonophysics*, 265 (3-4): 181-190.
- [10] Squarzoni, C., Delacourt, C. and Allemand, P., (2003). "Nine Years of Spatial and Temporal Evolution of the La Valette Landslide Observed by SAR Interferometry", *Engineering Geology*, 68: 53–66.
- [11] Strozzi, T., Tosi, L., Wegmuller, U., Werner, C., Teatini, P. and Carbognin L., (2003). "Land Subsidence Monitoring Service in the Lagoon of Venice", *Geoscience and Remote Sensing Symposium, IGARSS '03*, 1:212–214, 21-25 July 2003, Toulouse.
- [12] Ferretti, A., Prati, C. and Rocca, F., (2000). "Nonlinear Subsidence Rate Estimation Using Permanent Scatteres in Differential SAR Interferometry", *IEEE Transactions on Geoscience and Remote Sensing*, 38 (5): 2202-2212.
- [13] Werner, C.L., Wegmuller, U., Strozzi, T. and Wiesman, A., (2003). "Interferometric Point Target Analysis for Deformation Mapping", *Geoscience and Remote Sensing Symposium, IGARSS'03*, 21-25 July 2003, Toulouse.
- [14] Hooper, A., Zebker, H., Segall, P. and Kampes, B., (2004). "A New Method for Measuring Deformation on Volcanoes and Other Non-Urban Areas Using InSAR Persistent Scatterers", *Geophysical Research Letters*, 31(23).
- [15] Kampes, B.M., (2006). *Radar Interferometry-Persistent Scatterer Technique*, Dordrecht, The Netherlands, Springer.
- [16] Hooper, A., Segall, P. and Zebker, H., (2007). "Persistent Scatterer InSAR for Crustal Deformation Analysis, with Application to Volcán Alcedo, Galápagos", *Journal of Geophysical Research*, 112, B07407, doi:10.1029/2006JB004763.
- [17] Berardino, P., Fornaro, G., Lanari, R. and Sansosti, E., (2002). "A New Algorithm for Surface Deformation Monitoring Based on Small Baseline Differential SAR Interferograms", *IEEE Transactions on Geoscience and Remote Sensing*, 40 (11): 2375 – 2383.
- [18] Casu, F., Manzo, M. and Lanari, R., (2006). "A Quantitative Assessment of the SBAS Algorithm Performance for Surface Deformation Retrieval from DInSAR Data", *Remote Sensing of Environment* 102: 195–210.
- [19] Hooper, A., (2008). "A Multi-Temporal InSAR Method Incorporating both Persistent Scatterer and Small Baseline Approaches", *Geophysical Research Letters*, 35, L16302, doi:10.1029/2008GL034654.
- [20] Wright, T.J., Fielding, E.J., Parsons, B.E. and England, P.C., (2001). "Triggered Slip: Observations of the 17 August 1999 Izmit (Turkey) Earthquake Using Radar Interferometry", *Geophysical Research Letters*, 28: 1079-1082.
- [21] Burgmann, R., Ayhan, E., Fielding, E., Wright, T., McClusky, S., Aktug, B., Demir, C., Lenk, O. and Turkezer, A., (2002). "Deformation During the 12 November 1999, Duzce, Turkey Earthquake, from GPS and InSAR Data", *Bulletin of the Seismological Society of America*, 92: 161–171.

- [22] Cakir, Z., Akoglu, A.M., Belabbes, S., Ergintav, S. and Meghraoui, M., (2005). "Creeping Along the Ismetpasa Section of the North Anatolian Fault (Western Turkey): Rate and Extent from InSAR", *Earth and Planetary Science Letters*, 238: 225-234.
- [23] Cakir, Z. and Akoglu, A. M., (2008). "Synthetic Aperture Radar Interferometry Observations of the M = 6.0 Orta Earthquake of 6 June 2000 (NW Turkey): Reactivation of a Listric Fault", *Geochemistry Geophysics Geosystems*, 9, Q08009.
- [24] Motagh, M., Hoffmann, J., Kampes, B., Baes, M. and Zschau, J., (2007). "Strain Accumulation Across the Gazikoy–Saros Segment of the North Anatolian Fault Inferred from Persistent Scatterer Interferometry and GPS Measurements", *Earth and Planetary Science Letters* 255: 432–444.
- [25] Arkan, M., Hooper, A. and Hanssen, R. (2010). "Radar Time Series Analysis over West Anatolia", *FRINGE Workshop*, 30 Nov-4 Dec 2009, Frascati.
- [26] Walters, R.J., Holley, R.J., Parsons, B. and Wright, T.J. (2011). "Interseismic Strain Accumulation Across the North Anatolian Fault from Envisat InSAR Measurements", *Geophysical Research Letters*, 38, L05303.
- [27] Akarvardar, S.E., (2007). *Ground Motion Around Istanbul, Turkey Measured by Satellite Radar Interferometry*, PhD Thesis, Istanbul Technical University, Institute of Science and Technology, Istanbul.
- [28] Chul, J.H. and Min K.D., (2005). "Observing Coal Mining Subsidence from JERS-1 Permanent Scatterer Analysis", *Geoscience and Remote Sensing Symposium, IGARSS 2005*, 7: 4578-4581, 25-29 July 2005, Seoul.
- [29] Mei, S., Poncos, V. and Froese, C. (2008). "Mapping Millimeter-Scale Ground Deformation Over the Underground Coal Mines in the Frank Slide Area, Alberta, Canada, Using Spaceborne Insar Technology", *Canadian Journal of Remote Sensing*, 34 (2): 113-134.
- [30] Guéguen, Y., Deffontaines, B., Fruneau, B., Al Heib, M., de Michele, M., Raucoules, D., Guise, Y. and Planchenault, J. (2009). "Monitoring Residual Mining Subsidence of Nord/Pas-De-Calais Coal Basin from Differential and Persistent Scatterer Interferometry (Northern France)", *Journal of Applied Geophysics*, 69: 24–34.
- [31] Baek, J., Kim, S.W., Park, H.J., Jung, H.S., Kim, K.D. and Kim, J.W., (2008). "Analysis of Ground Subsidence in Coal Mining Area Using SAR Interferometry". *Geosciences Journal*, 12 (3): 277-284.
- [32] Sezer, A.I., Degirmenci, N., Aratoglu, T. and Uzunkavakli, Y., (1992). "Comparison of Measured Values with Influence Function Between 1974 and 1979 in Kozlu Coalfield". 8.th Coal Congress of Turkey, 99-112 (In Turkish).
- [33] Akçın, H., Kutoğlu, H.S., Kemaldere, H., Deguchi, T. and Köksal, E., (2010). "Monitoring Subsidence Effects in The Urban Area Of Zonguldak Hardcoal Basin of Turkey by Insar-GIS Integration". *Natural Hazards and Earth System Sciences*, 10: 1807-1814.

- [34] Can, E., Kuşçu, S. and Mekik, C., (2011). "Determination of Underground Mining Induced Displacements Using GPS Observations in Zonguldak-Kozlu Hard Coal Basin", *International Journal of Coal Geology*, doi:10.1016/j.coal.2011.08.006.
- [35] Deguchi, T., Kato, M., Akçın, H. And Kutoğlu, S., (2007). "Monitoring of Mining Induced Land Subsidence Using L and C Band SAR Interferometry", *Geoscience and Remote Sensing Symposium, IGARSS 2007*, 2122-2125, 23-27 July, Barcelona.
- [36] Kemaldere, H., (2011). *Monitoring of Undercity Mining and Subsidence Effect by Differential InSAR Technique in Zonguldak Metropolitan Area*, PhD Thesis, Bülent Ecevit University, Institute of Science and Technology, Zonguldak (In Turkish).
- [37] Herrera, G., Tomas, R., Lope-Sanchez, J.M., Delgado, J., Mallorqui, J.J., Duque, D. and Mulas, J., (2007). "Advanced DInSAR Analysis on Mining Areas: La Union Case Study (Murcia, SE Spain)", *Engineering Geology*, 90:148–159.
- [38] Buyurgan, S., (1980). "Subsidence Deformations at Zonguldak Coal Basin and Future of Zonguldak Province", *2th Coal Congress of Turkey*, 251-267, 12-16 May 1980, Zonguldak, (In Turkish).
- [39] ESA, Radar Course III, Electromagnetic spectrum, [http://earth.esa.int/applications/data_util/SARDOCS/spaceborne/Radar Courses/Radar Course III/electromagnetic.htm](http://earth.esa.int/applications/data_util/SARDOCS/spaceborne/Radar_Courses/Radar_Course_III/electromagnetic.htm), 03 July 2012.
- [40] Cakir, Z., (2003). *Analysis of the crustal deformation caused by the 1999 Marmara earthquake sequence using synthetic aperture radar interferometry*, PhD Thesis, ITU Institute of Science and Technology, Istanbul & Institut de Physique du Globe de Paris.
- [41] Wright, J.T., (2000). *Crustal Deformation in Turkey from Synthetic Aperture Radar Interferometry*, PhD Thesis, Wolfson College, Faculty of Physical Sciences, Oxford, England.
- [42] Graham, L.C., (1974). "Synthetic Interferometer Radar for Topographic Mapping," *Proc. of the IEEE*, 62(2): 763-768.
- [43] Lazecký, M., (2011). *Monitoring of Terrain Relief Changes using Synthetic Aperture Radar Interferometry*, PhD Thesis, Technical University of Ostrava, Institute of Geoinformatics Ostrava-Poruba, Czech Republic.
- [44] Hanssen, R.F., 2001. *Radar Interferometry: Data interpretation and error analysis*, Kluwer Academic Publishers, Dordrecht.
- [45] ESA, TIGER initiative principles of remote sensing, basic radar course, http://www.tiger.esa.int/TrainingCds/cd_01/content_2/sez_2_2/pg2_2_04.htm#Microwaves, 03 July 2012.
- [46] Abdikan, S., (2007). *Quality Sssessment of DEMs Generated from Interferometric SAR and Stereo SAR*, Yıldız Technical University, Institute of Science and Technology, Istanbul.

- [47] Freitas, C.C., Soler, L.S., Sant'Anna, S.J.S., Dutra, L.V., Santos, J.R., Mura, J.C. and Correia, A.H., (2008). "Land Use and Land Cover Mapping in the Brazilian Amazon Using Polarimetric Airborne P-Band SAR Data", *IEEE Transactions on Geoscience and Remote Sensing*, 46 (10): 2956-2970.
- [48] Sousa, J.J.M., (2009). Potential of integrating PSI methodologies in the detection of surface deformation, PhD thesis, University of Porto, Department of Applied Mathematics of the Faculty of Sciences, Porto, Portugal.
- [49] Massom, R. and Lubin, D., (2006). *Polar Remote Sensing Volume II, Ice Sheets*, Praxis Publishing Ltd, Chichester, UK.
- [50] ESA, CEOS Earth Observation handbook-catalogue of satellite missions, <http://database.eohandbook.com/database/missiontable.aspx>, 03 July 2012.
- [51] NASA Jet Propulsion Laboratory, Imaging Radar, <http://southport.jpl.nasa.gov/>, 03 July 2012.
- [52] MacDonald, Dettwiler and Associates (MDA), Satellite data, <http://gs.mdacorporation.com/SatelliteData/SatelliteData.aspx>, 03 July 2012.
- [53] The Japan Aerospace Exploration Agency, ALOS overview and objectives, http://www.eorc.jaxa.jp/ALOS/en/about/about_index.htm, 03 July 2012.
- [54] Zisk, S.H., (1972). "A new, Earth-based Radar Technique for the Measurement of Lunar Topography Moon", 4(3/4): 296 – 306.
- [55] Zebker, H. and Goldstein, R., (1986). "Topographic Mapping from Interferometric SAR Observations", *Journal of Geophysical Research*, 91: 4993–5001.
- [56] Goldstein, R.M. and Zebker, H.A., (1987). "Interferometric Radar Measurement of Ocean Surface Currents", *Nature*, 328: 707–709.
- [57] Gabriel, A.K., Goldstein, R.M. and Zebker, H.A., (1989). "Mapping Small Elevation Changes over Large Areas: Differential Radar Interferometry", *Journal of Geophysical Research*, 94: 9183-9191.
- [58] Madsen, S.N., Zebker, H.A. and Martin, J., (1993). "Topographic Mapping Using Radar Interferometry: Processing Techniques", *IEEE Transactions on Geoscience and Remote Sensing*, 31: 246–256.
- [59] Massonnet, D. and Feigl, K.L., (1998). "Radar Interferometry and Its Application to Changes in the Earth Surface", *Reviews of Geophysics* 36(4): 441–500.
- [60] Bamler, R. and Hartl, P., (1998). "Synthetic Aperture Radar Interferometry", *Inverse Problems*, 14(4),R1-R54.
- [61] Rosen, P.A., Hensley, S., Joughin, I.R., Li, F.K., Madsen, S.N., Rodriguez, E. and Goldstein, R.M., (2000). "Synthetic Aperture Radar Interferometry", *Proceedings of IEEE*, 88(3): 333–382.
- [62] Schmidt, D.A. and Burgmann, R., (2003). "Time-Dependent Land Uplift and Subsidence in the Santa Clara Valley, California, from a Large Interferometric

- Synthetic Aperture Radar Data Set”, *Journal of Geophysical Research*, 108 (B9): 2416–2428.
- [63] Rosen, P.A., Hensley, S., Peltzer, G. and Simons, M., (2004). “Updated Repeat Orbit Interferometry Package Released”, *EOS Transactions - American Geophysical Union*, 85 (5).
- [64] Kampes, B.M., Hanssen, R. and Perski, Z., (2003). “Radar Interferometry with Public Domain Tools”, *FRINGE Workshop*, 1-5 Dec 2003, Frascati, Italy.
- [65] Hooper, A. (2006). *Persistent Scatterer Radar Interferometry for Crustal Deformation Studies and Modeling of Volcanic Deformation*. PhD Thesis, Stanford University, Department of Geophysics, California, USA.
- [66] Hooper, A., 2009. *StaMPS/MTI Manual Version 3.0*. Department of Earth Observation and Space Systems, Delft University of Technology, The Netherlands.
- [67] Ferretti A., Prati C. and Rocca F., (2001). “Permanent Scatterers in SAR Interferometry”, *IEEE Transactions on Geoscience and Remote Sensing*, 39 (1): 8-20.
- [68] Crosetto, M., Arnaud, A., Duro, J., Biescas, E. and Agudo, M., (2003). “Deformation monitoring using remotely sensed radar interferometric data”, *11th FIG Symposium on Deformation Measurements*, 25-28 May, Santorini.
- [69] Hooper, A., Bekaert, D., Spaans, K. and Arkan M., (2012). “Recent Advances in SAR Interferometry Time Series Analysis for Measuring Crustal Deformation”, *Tectonophysics*, 514-517:1-13.
- [70] van der Kooij, M., Hughes, W., Sato, S. and Poncos, V., (2006). “Coherent Target Monitoring at High Spatial Density: Examples of Validation Results”, *F FRINGE Workshop*, 28 Nov-02 Dec 2005, Frascati, Italy.
- [71] Lanari, R., Mora, O., Manunta, M., Mallorqui, J.J., Berardino, P. And Sansosti, E., (2004). “A Small-Baseline Approach for Investigating Deformations on Full-Resolution Differential SAR Interferograms”, *IEEE Transactions on Geoscience and Remote Sensing* 42 (7): 1377–1386.
- [72] Turkish Statistical Institute, Population database in 2011, http://rapor.tuik.gov.tr/reports/rwervlet?adnksdb2&ENVID=adnksdb2Env&report=wa_turkiye_il_koy_sehir.RDF&p_kod=1&p_yil=2011&p_dil=1&desformat=html, 04 July 2012, (in Turkish).
- [73] Turkish Coal Enterprises, TTK Annual Report, 2011 <http://www.taskomuru.gov.tr/file/2010.pdf>, 04 July 2012, (in Turkish).
- [74] Governorship of Zonguldak, Environment report of Zonguldak Province, 2010, <http://www.cedgm.gov.tr/CED/Files/icdr/zonguldak/zonguldakicd2010.pdf>, (in Turkish), 04 July 2012, (in Turkish).
- [75] Turkish State Meteorological Service, Statistic data of the province and districts, <http://www.dmi.gov.tr/veridegerlendirme/il-ve-ilceler-istatistik.aspx?m=ZONGULDAK>, 04 July 2012, (in Turkish).

- [76] Turkish Statistical Institute, Population Statistics
http://www.tuik.gov.tr/PreTablo.do?alt_id=39, 04 July 2012.
- [77] Düzgün, H.S.B., (2005). "Analysis of Roof Fall Hazards and Risk Assessment for Zonguldak Coal Basin Underground Mines", International Journal of Coal Geology, 64: 104-115.
- [78] Turer D., Nefeslioglu H.A., Zorlu K. and Gokceoglu C., (2008). "Assessment of Geo Environmental Problems of the Zonguldak Province (NW Turkey)", Environmental Geology, 55(5): 1001-1014.
- [79] Yilmaz, M., (2008). Hydrogeology of Ereğli Zonguldak Hardcoal Basin, Master Thesis, Dokuz Eylül University, Graduate School of Natural and Applied Sciences, Izmir (In Turkish).
- [80] Hatir, V. (2006). The Geotechnical Investigation of Land Using Features Around Zonguldak City Center, Master Thesis, Bülent Ecevit University, Institute of Science and Technology, Zonguldak (In Turkish).
- [81] Citiroglu H.K. and Baysal, G. (2011). "Effects of Geological and Hydrological Factors on the Creation of Flooding in Kozlu, Zonguldak, NW Turkey", International Journal of the Physical Sciences 6(6): 1360-1373.
- [82] Hosgormez, H., (2007). "Origion and Secondary Alteration of Coalbed and Adjacent Rock Gases in the Zonguldak Basin, Western Black Sea Turkey", Geochemical Journal, 41: 207-211.
- [83] Bülent Ecevit University, Cave research club,
<http://magara.karaelmas.edu.tr/english/COZ.HTM>, 04 July 2012.
- [84] Güney, M., (1967). "Underground Mining Operations in Zonguldak Coal Mines", Bulletin of The Mineral Research and Exploration Institute of Turkey, 68: 89-124.
- [85] Turkish Coal Enterprises (TTK), Annual production report,
http://www.taskomuru.gov.tr/file/Is_Zekasi_Raporlari/Muessese_Bazinda_Yillik_Uretimler.mht , 15 January 2012, (in Turkish).
- [86] Turkish Coal Enterprises (TTK), Annual reports of accidents, 15 Jan 2012 (in Turkish),
http://www.taskomuru.gov.tr/file/Is_Zekasi_Raporlari/mue_gore_yillik_kazalar.mht
- [87] Akçın, H., Karakış, S., Büyüksalih, G. and Oruç, M., (2004). "GIS Based Analysis of Landcover Changes Arising from Coal Production Wastes in Zonguldak Metropolitan Area-Turkey", XX. ISPRS Congress Geo-imagery Bridging the Continents, 12-23 July 2004, Istanbul, Türkiye.
- [88] Akçın, H. and Çakır, A. (2011). "Temporal Analise of Mining Environmental Effects by Internet-Based GIS", TMMOB GIS Congress, 31 Oct-04 Nov 2011, Antalya (In Turkish).
- [89] Duman T.Y., Çan, T., Emre O., Keçer, M., Doğan, A., Ateş, Ş. and Durmaz, S., (2005). "Landslide inventory of northwestern Anatolia, Turkey", Engineering Geology, 77: 99– 114.

- [90] Newspaper, [http://www.posta.com.tr/turkiye/HaberDetay/Zonguldak ta obruk korkusu .htm?ArticleID=103644](http://www.posta.com.tr/turkiye/HaberDetay/Zonguldak%20ta%20obruk%20korkusu.htm?ArticleID=103644), 04 July 2012 (in Turkish).
- [91] Kutođlu, H., Akçın, H., Kemaldere, H., Deguchi, T. and Kato, M. (2010). "Detecting Illegal Mining Activities Using Dinsar", Bulletin of Chamber of Survey and Cadastre Engineers of Turkey, 101-12.THBTk Special Issue (in Turkish).
- [92] akır, A. and Barıř, K. (2009). "Assessment of an Underground Coal Mine Fire: A Case Study From Zonguldak, Turkey", Coal 2009: Coal Operators' Conference, University of Wollongong & the Australasian Institute of Mining and Metallurgy, 259-270, 12-13 February 2009.
- [93] Bauer, R., (2008). Planned coal mine subsidence in Illinois: A public information booklet, Illinois State geological survey, Circular 573.
- [94] Can, E., Kuřcu, ř. And Kartal, M.E., (2011). "Effects of Mining Subsidence on Masonry Buildings in Zonguldak Hard Coal Region in Turkey", Environmental Earth Sciences, DOI: 10.1007/s12665-011-1473-2.
- [95] Düzgün H.S. and Demirel, N. (2011). Remote Sensing of the Mine Environment, CRC Press, ISBN 9780415878791, London, UK.
- [96] Can, E., Mekik, C., Kuřcu, ř. and Akçın, H., (2011). "Subsidence occurring in mining regions and a case study of Zonguldak–Kozlu Basin", Science Research Essays 6(6): 1317–1327.
- [97] Miranda, N., Duesmann, B., Pinol, M., Giudici, D. and D'Aria, D., (2010). Impact of the Envisat Mission Extension on SAR data-1.0, ESA.
- [98] ESA, ASAR product handbook, (2007). 04 July 2012. http://envisat.esa.int/pub/ESA_DOC/ENVISAT/ASAR/asar.ProductHandbook.2_2.pdf,
- [99] Sandwell D.T., Myer, D., Mellors, R., Shimada, M., Brooks, B. and Foster, J., (2008). "Accuracy and Resolution of ALOS Interferometry: Vector Deformation Maps of the Father's Day", IEEE Transactions on Geoscience and Remote Sensing, 46(11): 3524-3534.
- [100] Aobpaet, A., Cuenca M.C., Hooper, A. and Trisirisatayawong, I., (2009). "Land Subsidence Evaluation Using InSAR Time Series Analysis in Bangkok Metropolitan Area", FRINGE Workshop, 30 Nov-4 Dec 2009, Frascati, Italy.
- [101] General Union of Mine Workers (Genel Maden İřçileri Sendikası), TTK report 2011, Zonguldak, 04 July 2012 (in Turkish). <http://www.genelmadenis.org.tr/Depo/File/TTK%20Raporu%202011.pdf>,

FLOWCHART OF RESEARCH STUDY

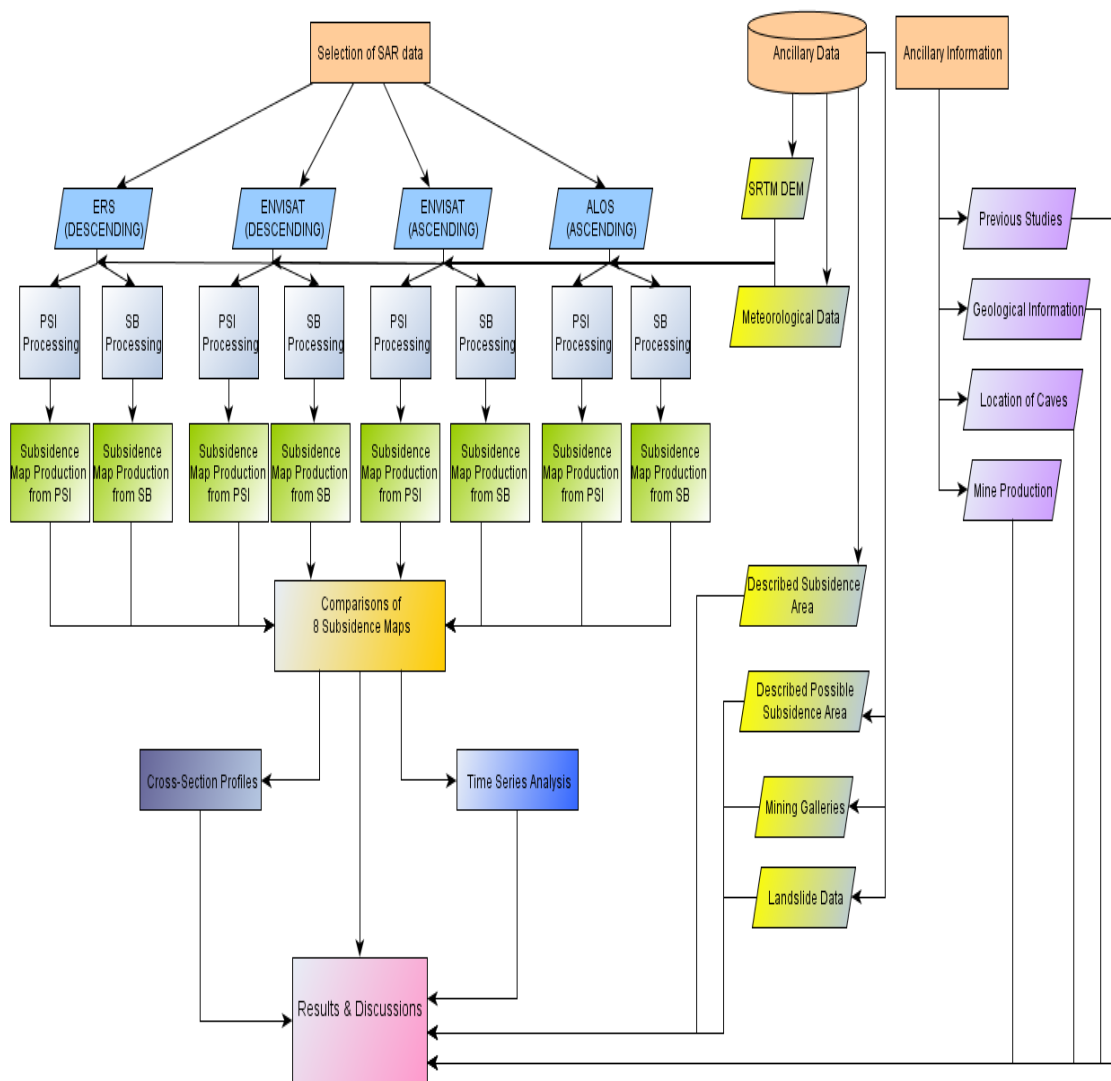


Figure A.1 Flowchart of research study

INSAR PAIRS GENERATED WITH SB APPROACH

Table A.1 ERS Pairs used in SB approach

No	Master	Slave	Temp B (day)	Perp B (m)	$\sigma_{\text{Noise}}(^{\circ})$
1	27-Jun-93	11-Apr-95	653	-1	56.932
2	27-Jun-93	20-Jun-95	723	-144	60.030
3	27-Jun-93	30-Aug-95	794	19	57.518
4	5-Sep-93	14-Nov-93	70	-103	54.680
5	5-Sep-93	25-Jul-95	688	-85	55.895
6	5-Sep-93	26-Jul-95	689	-124	56.864
7	5-Sep-93	3-Oct-95	758	93	58.104
8	14-Nov-93	25-Jul-95	618	18	51.925
9	14-Nov-93	26-Jul-95	619	-21	52.661
10	14-Nov-93	3-Oct-95	688	196	61.295
11	19-Dec-93	4-Oct-95	654	-151	60.311
12	11-Apr-95	20-Jun-95	70	-143	55.263
13	11-Apr-95	30-Aug-95	141	20	51.783
14	11-Apr-95	1-Jan-97	631	161	55.889
15	11-Apr-95	21-May-97	771	115	57.453
16	16-May-95	20-Jun-95	35	141	57.471
17	20-Jun-95	30-Aug-95	71	163	56.960
18	25-Jul-95	26-Jul-95	1	-39	41.082
19	25-Jul-95	3-Oct-95	70	178	52.03
20	25-Jul-95	1-Jan-97	526	-219	59.638
21	26-Jul-95	30-Aug-95	35	-322	66.025
22	26-Jul-95	3-Oct-95	69	217	54.388
23	26-Jul-95	1-Jan-97	525	-181	54.140
24	26-Jul-95	21-May-97	665	-227	62.000
25	26-Jul-95	30-Jul-97	735	-159	56.780
26	30-Aug-95	1-Jan-97	490	141	53.117
27	30-Aug-95	21-May-97	630	95	54.239
28	30-Aug-95	30-Jul-97	700	164	57.691
29	3-Oct-95	23-Oct-96	386	329	74.340
30	4-Oct-95	23-Oct-96	385	-117	56.985
31	1-Jan-97	21-May-97	140	-47	49.253
32	1-Jan-97	30-Jul-97	210	22	49.289

Table A.1 continuing

No	Master	Slave	Temp B (day)	Perp B (m)	$\bar{\sigma}_{\text{Noise}}(^{\circ})$
33	1-Jan-97	17-Mar-99	805	116	56.701
34	21-May-97	30-Jul-97	70	69	51.335
35	21-May-97	17-Mar-99	665	163	56.988
36	21-May-97	4-Aug-99	805	9	54.999
37	30-Jul-97	17-Mar-99	595	94	54.108
38	30-Jul-97	4-Aug-99	735	-59	55.384
39	17-Mar-99	4-Aug-99	140	-154	53.010
40	17-Mar-99	17-Nov-99	245	-264	59.329
41	17-Mar-99	1-Nov-00	595	-77	54.967
41	17-Mar-99	10-Jan-01	665	-19	56.341
43	4-Aug-99	17-Nov-99	105	-111	52.018
44	4-Aug-99	22-Dec-99	140	-272	67.010
45	4-Aug-99	14-Jun-00	315	-129	59.523
46	4-Aug-99	1-Nov-00	455	76	55.639
47	4-Aug-99	10-Jan-01	525	135	56.309
48	17-Nov-99	22-Dec-99	35	-162	53.615
49	17-Nov-99	14-Jun-00	210	-19	54.734
50	17-Nov-99	1-Nov-00	350	187	57.604
51	17-Nov-99	10-Jan-01	420	246	60.932
52	22-Dec-99	14-Jun-00	175	143	59.491
53	14-Jun-00	1-Nov-00	140	206	60.641
54	14-Jun-00	10-Jan-01	210	264	65.957
55	1-Nov-00	10-Jan-01	70	59	49.729

Table A.2 ENVISAT descending pairs used in SB approach

No	Master	Slave	Temp B (day)	Perp B (m)	6Noise(°)
1	26-Nov-2003	04-Feb-2004	70	11	45.761
2	26-Nov-2003	19-May-2004	175	218	54.093
3	26-Nov-2003	23-Jun-2004	210	2	48.117
4	26-Nov-2003	06-Oct-2004	315	229	60.21
5	26-Nov-2003	15-Dec-2004	385	110	51.799
6	26-Nov-2003	19-Jan-2005	420	-83	52.744
7	04-Feb-2004	19-May-2004	105	206	53.145
8	04-Feb-2004	23-Jun-2004	140	-10	47.852
9	04-Feb-2004	06-Oct-2004	245	218	59.001
10	04-Feb-2004	15-Dec-2004	315	99	49.852
11	04-Feb-2004	19-Jan-2005	350	-94	50.174
12	04-Feb-2004	30-Nov-2005	665	-51	51.811
13	10-Mar-2004	28-Jul-2004	140	-191	60.118
14	10-Mar-2004	01-Sep-2004	175	-58	54.669
15	10-Mar-2004	04-May-2005	420	124	57.742
16	19-May-2004	23-Jun-2004	35	-216	51.182
17	19-May-2004	28-Jul-2004	70	235	58.735
18	19-May-2004	06-Oct-2004	140	12	45.055
19	19-May-2004	15-Dec-2004	210	-107	49.857
20	19-May-2004	17-Aug-2005	455	55	51.366
21	23-Jun-2004	06-Oct-2004	105	228	54.65
22	23-Jun-2004	15-Dec-2004	175	109	48.309
23	23-Jun-2004	19-Jan-2005	210	-85	49.455
24	23-Jun-2004	17-Aug-2005	420	271	61.105
25	23-Jun-2004	30-Nov-2005	525	-41	51.103
26	28-Jul-2004	01-Sep-2004	35	133	52.893
27	28-Jul-2004	06-Oct-2004	70	-223	52.875
28	28-Jul-2004	17-Aug-2005	385	-180	52.488
29	28-Jul-2004	15-Mar-2006	595	-30	54.254
30	01-Sep-2004	04-May-2005	245	182	57.862
31	01-Sep-2004	15-Mar-2006	560	-162	57.707
32	06-Oct-2004	15-Dec-2004	70	-119	48.932
33	06-Oct-2004	17-Aug-2005	315	43	45.851
34	06-Oct-2004	30-Nov-2005	420	-269	63.52
35	06-Oct-2004	15-Mar-2006	525	194	55.595
36	15-Dec-2004	19-Jan-2005	35	-193	49.318
37	15-Dec-2004	17-Aug-2005	245	162	53.643
38	15-Dec-2004	30-Nov-2005	350	-150	49.788
39	19-Jan-2005	17-Aug-2005	210	355	72.279
40	17-Aug-2005	30-Nov-2005	105	-312	65.533
41	17-Aug-2005	20-Dec-2006	490	89	51.57
42	17-Aug-2005	28-Feb-2007	560	64	51.861
43	30-Nov-2005	09-May-2007	525	151	55.564
44	30-Nov-2005	18-Jul-2007	595	111	56.477
45	15-Mar-2006	20-Dec-2006	280	-61	50.177
46	15-Mar-2006	28-Feb-2007	350	-86	49.396
47	15-Mar-2006	09-May-2007	420	-311	66.264
48	20-Dec-2006	28-Feb-2007	70	-25	42.145

Table A.2 continuing

49	20-Dec-2006	09-May-2007	140	-250	53.938
50	20-Dec-2006	18-Jul-2007	210	-290	61.256
51	20-Dec-2006	31-Oct-2007	315	-21	50.158
52	28-Feb-2007	09-May-2007	70	-225	51.261
53	28-Feb-2007	18-Jul-2007	140	-265	58.95
54	28-Feb-2007	31-Oct-2007	245	4	50.064
55	09-May-2007	18-Jul-2007	70	-40	46.322
56	09-May-2007	31-Oct-2007	175	229	58.463
57	18-Jul-2007	31-Oct-2007	105	269	62.907
58	18-Jul-2007	19-Nov-2008	490	-234	64.711
59	31-Oct-2007	13-May-2009	560	-135	59.434
60	31-Oct-2007	17-Jun-2009	595	142	61.467
61	31-Oct-2007	26-Aug-2009	665	85	51.811
62	19-Nov-2008	22-Jul-2009	245	206	60.118
63	19-Nov-2008	30-Sep-2009	315	99	54.669
64	19-Nov-2008	13-Jan-2010	420	285	57.742
65	13-May-2009	17-Jun-2009	35	278	51.182
66	13-May-2009	22-Jul-2009	70	-162	58.735
67	13-May-2009	26-Aug-2009	105	220	45.055
68	13-May-2009	30-Sep-2009	140	-269	49.857
69	13-May-2009	13-Jan-2010	245	-83	51.366
70	17-Jun-2009	26-Aug-2009	70	-57	54.65
71	22-Jul-2009	30-Sep-2009	70	-107	48.309
72	22-Jul-2009	13-Jan-2010	175	79	49.455
73	30-Sep-2009	13-Jan-2010	105	186	61.105

Table A.3 ENVISAT ascending pairs used in SB approach

No	Master	Slave	Temp B (day)	Perp B (m)	$\sigma_{\text{Noise}}(^{\circ})$
1	6-May-04	19-Aug-04	105	347	43.218
2	6-May-04	6-Jan-05	245	129	32.219
3	6-May-04	10-Feb-05	280	-246	39.267
4	6-May-04	4-Aug-05	455	-29	37.192
5	6-May-04	2-Mar-06	665	123	38.236
6	10-Jun-04	15-Jul-04	35	309	48.691
7	10-Jun-04	28-Oct-04	140	-271	48.088
8	15-Jul-04	28-Oct-04	105	-581	64.864
9	15-Jul-04	10-Feb-05	210	451	62.581
10	15-Jul-04	15-Jun-06	700	27	44.655
11	19-Aug-04	6-Jan-05	140	-218	35.530
12	19-Aug-04	4-Aug-05	350	-376	50.863
13	19-Aug-04	2-Mar-06	560	-224	39.388
14	28-Oct-04	8-Sep-05	315	-359	53.219
15	28-Oct-04	20-Jul-06	630	-207	54.309
16	6-Jan-05	10-Feb-05	35	-375	43.611
17	6-Jan-05	4-Aug-05	210	-158	35.239
18	6-Jan-05	2-Mar-06	420	-6	31.868
19	10-Feb-05	4-Aug-05	175	218	38.622
20	10-Feb-05	2-Mar-06	385	369	44.598
21	10-Feb-05	15-Jun-06	490	-424	58.489
22	4-Aug-05	2-Mar-06	210	152	32.770
23	8-Sep-05	20-Jul-06	315	152	51.327
24	2-Mar-06	22-Nov-07	630	-331	50.205
25	22-Nov-07	17-Sep-09	665	21	43.013
26	22-Nov-07	26-Nov-09	735	-97	44.094
27	17-Sep-09	26-Nov-09	70	-118	36.418
28	17-Sep-09	15-Apr-10	210	203	40.207
29	17-Sep-09	29-Jul-10	315	-324	49.774
30	26-Nov-09	15-Apr-10	140	320	43.168
31	26-Nov-09	29-Jul-10	245	-206	44.406
32	15-Apr-10	29-Jul-10	105	-526	64.713

Table A.4 PALSAR pairs used in SB approach

No	Master	Slave	Temp B (day)	Perp B (m)	6Noise(°)
1	18-Jan-2007	05-Mar-2007	-46	1790	56.586
2	18-Jan-2007	05-Jun-2007	-138	1924	56.984
3	18-Jan-2007	05-Sep-2007	-230	2708	67.181
4	18-Jan-2007	21-Oct-2007	-276	3009	69.607
5	18-Jan-2007	06-Dec-2007	-688	3199	65.752
6	18-Jan-2007	21-Jan-2008	-368	3669	71.195
7	18-Jan-2007	23-Jul-2008	-552	1407	57.628
8	18-Jan-2007	23-Oct-2008	-644	-554	56.189
9	18-Jan-2007	08-Dec-2008	-690	-329	61.274
10	05-Mar-2007	05-Jun-2007	-92	135	51.902
11	05-Mar-2007	05-Sep-2007	-184	918	54.322
12	05-Mar-2007	21-Oct-2007	-230	1219	52.813
13	05-Mar-2007	06-Dec-2007	-276	1410	57.186
14	05-Mar-2007	21-Jan-2008	-322	1879	60.361
15	05-Mar-2007	07-Mar-2008	-368	2568	62.546
16	05-Mar-2007	23-Jul-2008	-506	-383	54.727
17	05-Mar-2007	23-Oct-2008	-598	-2344	68.624
18	05-Mar-2007	10-Mar-2009	-736	-1099	57.170
19	05-Jun-2007	05-Sep-2007	-92	783	44.032
20	05-Jun-2007	21-Oct-2007	-138	1085	44.853
21	05-Jun-2007	06-Dec-2007	-184	1275	50.611
22	05-Jun-2007	21-Jan-2008	-230	1744	53.479
23	05-Jun-2007	07-Mar-2008	2433	-276	68.435
24	05-Jun-2007	23-Jul-2008	-518	-414	46.632
25	05-Jun-2007	23-Oct-2008	-2479	-506	65.191
26	05-Jun-2007	08-Dec-2008	-2254	-552	67.242
27	05-Jun-2007	10-Mar-2009	-1233	-644	52.975
28	05-Sep-2007	21-Oct-2007	301	-46	33.122
29	05-Sep-2007	06-Dec-2007	491	-92	43.304
30	05-Sep-2007	21-Jan-2008	961	-138	47.725
31	05-Sep-2007	07-Mar-2008	1650	-184	58.538
32	05-Sep-2007	23-Jul-2008	-1301	-322	41.728
33	05-Sep-2007	23-Oct-2008	-3262	-414	71.497
34	05-Sep-2007	08-Dec-2008	-3037	-460	71.260
35	05-Sep-2007	10-Mar-2009	-2017	-552	56.740
36	21-Oct-2007	06-Dec-2007	190	-46	37.411
37	21-Oct-2007	06-Dec-2007	660	-46	43.298
38	21-Oct-2007	07-Mar-2008	1349	-138	54.171
39	21-Oct-2007	23-Jul-2008	-1602	-276	40.347
40	21-Oct-2007	23-Oct-2008	-3563	-368	63.673
41	21-Oct-2007	08-Dec-2008	-3338	-414	63.050
42	21-Oct-2007	10-Mar-2009	-2318	-506	55.963
43	21-Oct-2007	26-Jul-2009	-2051	-644	48.372
44	21-Oct-2007	10-Sep-2009	-1513	-690	44.521
45	06-Dec-2007	21-Jan-2008	469	-46	40.168
46	06-Dec-2007	07-Mar-2008	1159	-92	62.303

Table A.4 continuing

No	Master	Slave	Temp B (day)	Perp B (m)	6Noise(°)
47	06-Dec-2007	23-Jul-2008	-1793	-230	46.357
48	06-Dec-2007	23-Oct-2008	-3754	-322	69.612
49	06-Dec-2007	08-Dec-2008	-3529	-368	67.048
50	06-Dec-2007	10-Mar-2009	-2508	-460	55.740
51	06-Dec-2007	26-Jul-2009	-2241	-598	52.221
52	06-Dec-2007	10-Sep-2009	-1703	-644	47.304
53	06-Dec-2007	26-Oct-2009	-1397	-690	46.112
54	06-Dec-2007	11-Dec-2009	-1161	-736	47.560
55	06-Dec-2007	26-Jan-2010	-532	-782	62.781
56	21-Jan-2008	07-Mar-2008	689	-46	63.050
57	21-Jan-2008	23-Jul-2008	-2262	-184	52.581
58	21-Jan-2008	23-Oct-2008	-4223	-276	65.942
59	21-Jan-2008	08-Dec-2008	-3998	-322	64.514
60	21-Jan-2008	10-Mar-2009	-2977	-414	64.714
61	21-Jan-2008	26-Jul-2009	-2711	-552	59.344
62	21-Jan-2008	10-Sep-2009	-2173	-598	51.049
63	21-Jan-2008	26-Oct-2009	-1867	-644	47.968
64	21-Jan-2008	11-Dec-2009	-1630	-690	49.446
65	21-Jan-2008	26-Jan-2010	-1001	-736	63.251
66	21-Jan-2008	13-Mar-2010	-420	-782	48.637
67	07-Mar-2008	23-Jul-2008	-2951	-138	70.803
68	07-Mar-2008	10-Mar-2009	-3667	-368	67.022
69	07-Mar-2008	10-Sep-2009	-2862	-552	77.541
70	07-Mar-2008	13-Mar-2010	-1109	-736	67.772
71	23-Jul-2008	23-Oct-2008	-1961	-92	46.364
72	23-Jul-2008	08-Dec-2008	-1736	-138	49.679
73	23-Jul-2008	10-Mar-2009	-716	-230	43.209
74	23-Jul-2008	26-Jul-2009	-449	-368	35.775
75	23-Jul-2008	10-Sep-2009	89	-414	35.007
76	23-Jul-2008	26-Oct-2009	395	-460	35.934
77	23-Jul-2008	11-Dec-2009	632	-506	41.703
78	23-Jul-2008	26-Jan-2010	1261	-552	63.371
79	23-Jul-2008	13-Mar-2010	1842	-598	50.731
80	23-Jul-2008	28-Apr-2010	1895	-644	51.968
81	23-Oct-2008	08-Dec-2008	225	-46	39.717
82	23-Oct-2008	26-Jul-2009	1246	-276	46.837
83	23-Oct-2008	26-Jul-2009	1512	-276	45.662
84	23-Oct-2008	10-Sep-2009	2050	-322	49.120
85	23-Oct-2008	26-Oct-2009	2356	-368	50.303
86	23-Oct-2008	11-Dec-2009	2593	-414	58.478
87	23-Oct-2008	26-Jan-2010	3222	-460	62.348
88	08-Dec-2008	10-Mar-2009	1021	-92	45.365
89	08-Dec-2008	26-Jul-2009	1287	-230	49.710
90	08-Dec-2008	10-Sep-2009	1825	-276	52.274
91	08-Dec-2008	26-Oct-2009	2131	-322	53.302
92	08-Dec-2008	11-Dec-2009	2368	-368	60.243

Table A.4 continuing

No	Master	Slave	Temp B (day)	Perp B (m)	6Noise(°)
93	08-Dec-2008	26-Jan-2010	2997	-414	71.783
94	10-Mar-2009	26-Jul-2009	267	-138	39.503
95	10-Mar-2009	10-Sep-2009	805	-184	39.708
96	10-Mar-2009	26-Oct-2009	1111	-230	39.586
97	10-Mar-2009	11-Dec-2009	1348	-276	41.718
98	10-Mar-2009	26-Jan-2010	1976	-322	65.622
99	10-Mar-2009	13-Mar-2010	2557	-368	55.933
100	10-Mar-2009	28-Apr-2010	2611	-414	63.552
101	10-Mar-2009	13-Jun-2010	2621	-460	68.228
102	26-Jul-2009	10-Sep-2009	538	-46	30.959
103	26-Jul-2009	26-Oct-2009	844	-92	32.276
104	26-Jul-2009	11-Dec-2009	1081	-138	38.998
105	26-Jul-2009	26-Jan-2010	1710	-184	62.775
106	26-Jul-2009	13-Mar-2010	2291	-230	50.631
107	26-Jul-2009	28-Apr-2010	2344	-276	51.877
108	26-Jul-2009	13-Jun-2010	2354	-322	56.561
109	10-Sep-2009	26-Oct-2009	306	-46	27.923
110	10-Sep-2009	11-Dec-2009	543	-92	34.937
111	10-Sep-2009	26-Jan-2010	1172	-138	58.758
112	10-Sep-2009	13-Mar-2010	1753	-184	44.171
113	10-Sep-2009	28-Apr-2010	1806	-230	45.732
114	10-Sep-2009	13-Jun-2010	1816	-276	50.078
115	26-Oct-2009	11-Dec-2009	237	-46	31.537
116	26-Oct-2009	26-Jan-2010	866	-92	57.983
117	26-Oct-2009	13-Mar-2010	1447	-138	40.970
118	26-Oct-2009	28-Apr-2010	1500	-184	41.985
119	26-Oct-2009	13-Jun-2010	1510	-230	48.117
120	11-Dec-2009	26-Jan-2010	629	-46	57.255
121	11-Dec-2009	13-Mar-2010	1210	-92	40.178
122	11-Dec-2009	28-Apr-2010	1263	-138	48.217
123	11-Dec-2009	13-Jun-2010	1273	-184	51.411
124	26-Jan-2010	13-Mar-2010	581	-46	58.049
125	26-Jan-2010	28-Apr-2010	634	-92	61.751
126	26-Jan-2010	13-Jun-2010	644	-138	63.553
127	13-Mar-2010	28-Apr-2010	53	-46	40.876
128	13-Mar-2010	13-Jun-2010	63	-92	47.414
129	28-Apr-2010	13-Jun-2010	10	-46	46.074

STANDARD DEVIATIONS OF RESULTS

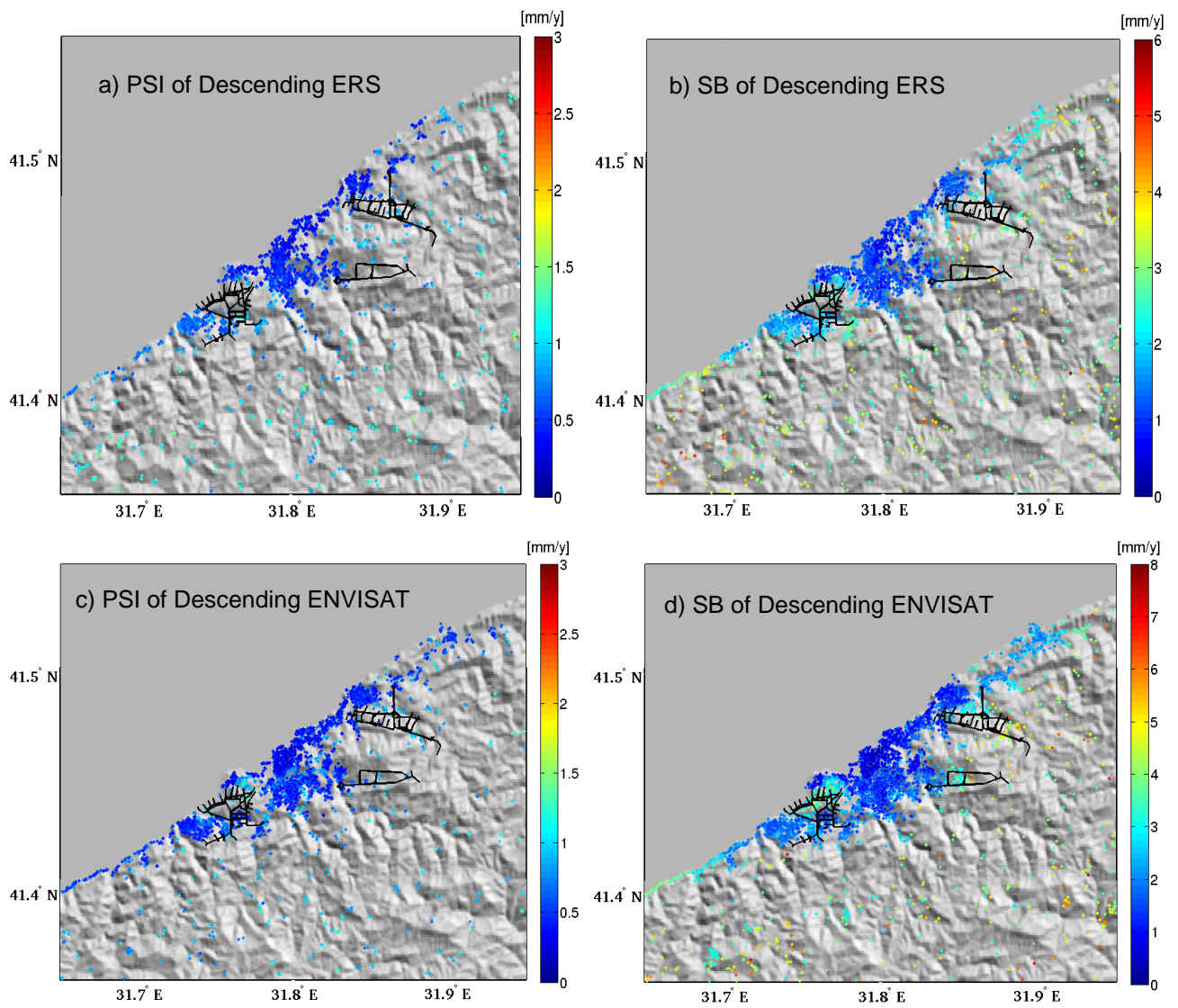


Figure A.2 Standard deviations; a)ERS PSI result, b) ERS SB result, c) Desc. ENVISAT PSI result, d) Desc. ENVISAT SB result

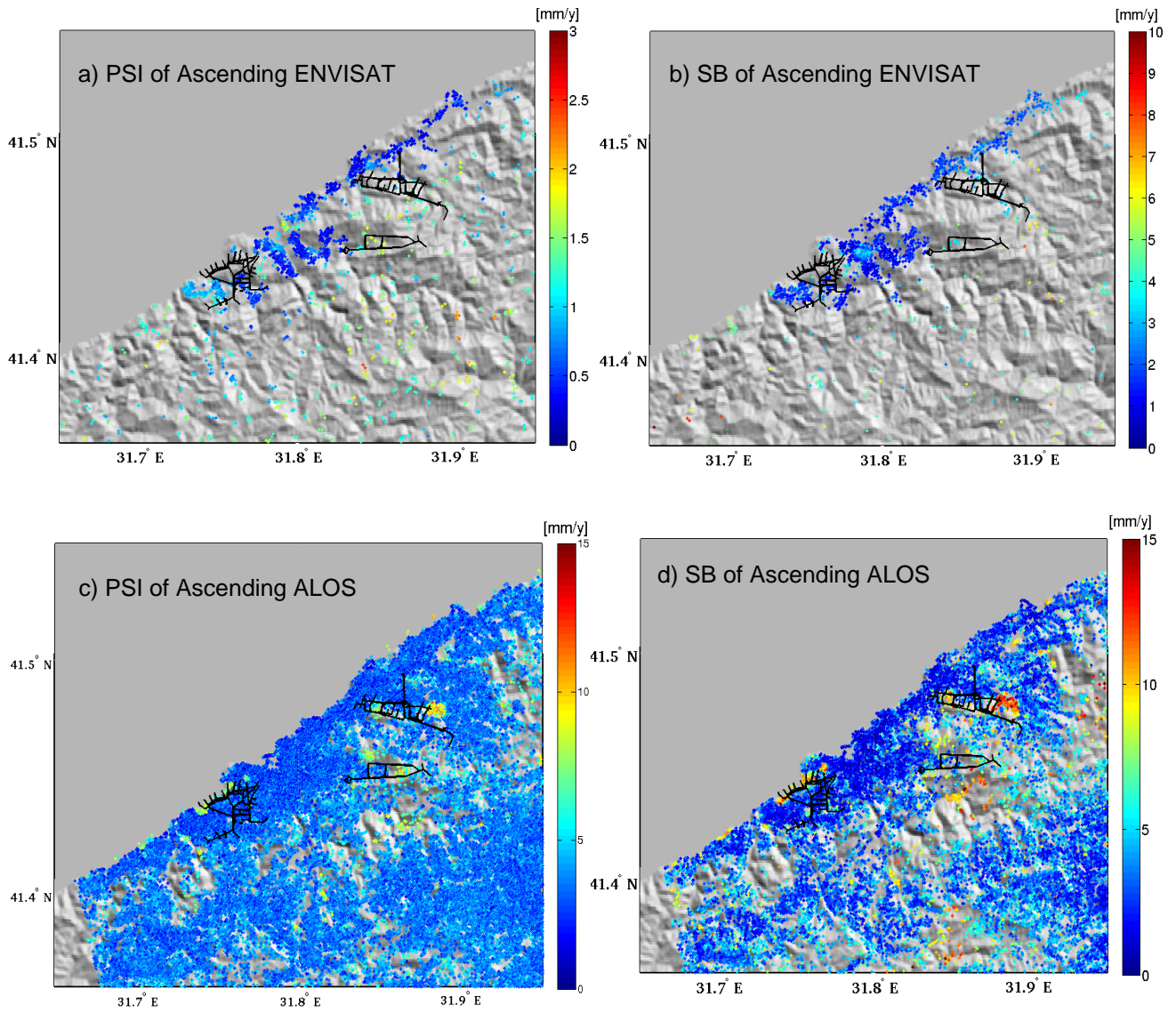


Figure A.3 Standard deviations; a)Asc. ENVISAT PSI result, b) Asc. ENVISAT SB result, c) PALSAR PSI result, d) PALSAR SB result

INTERSECTION OF RESULTS

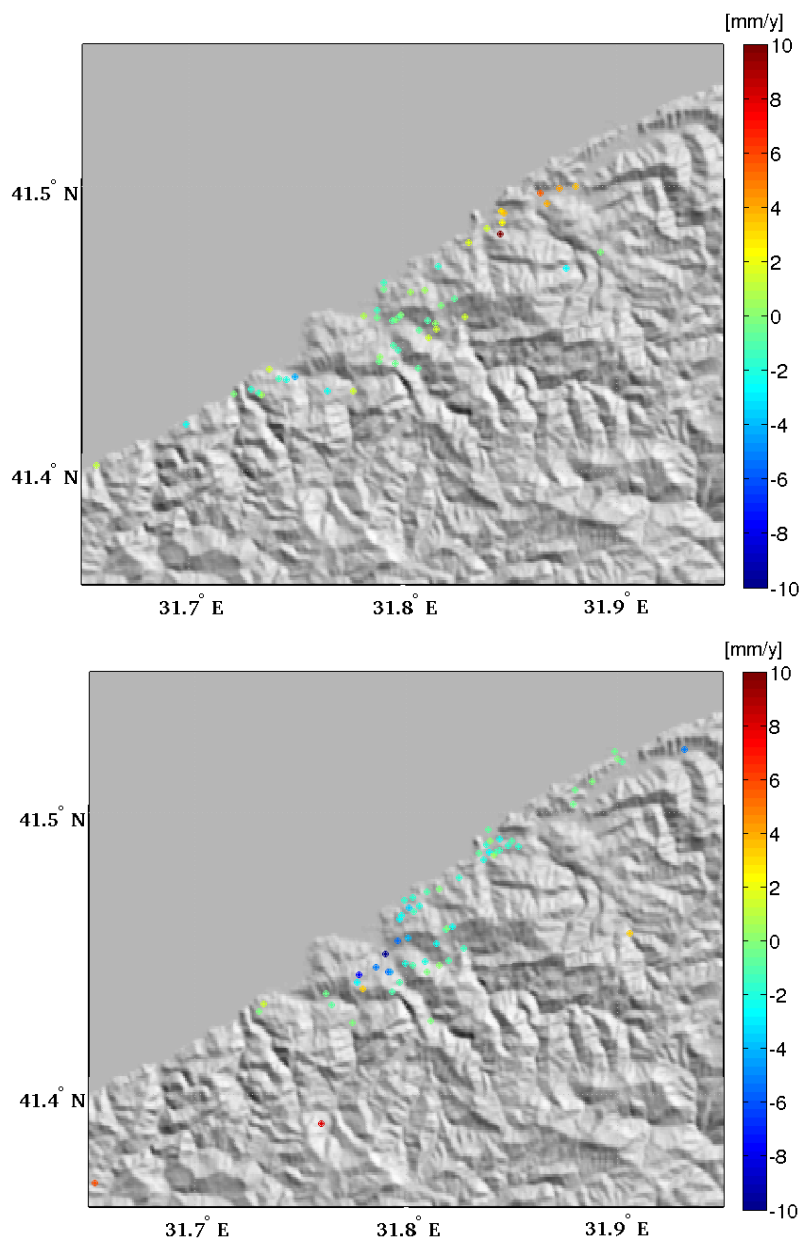


Figure A.4 Common points of PSI and SB results: a) ERS, b) ENVISAT t-343

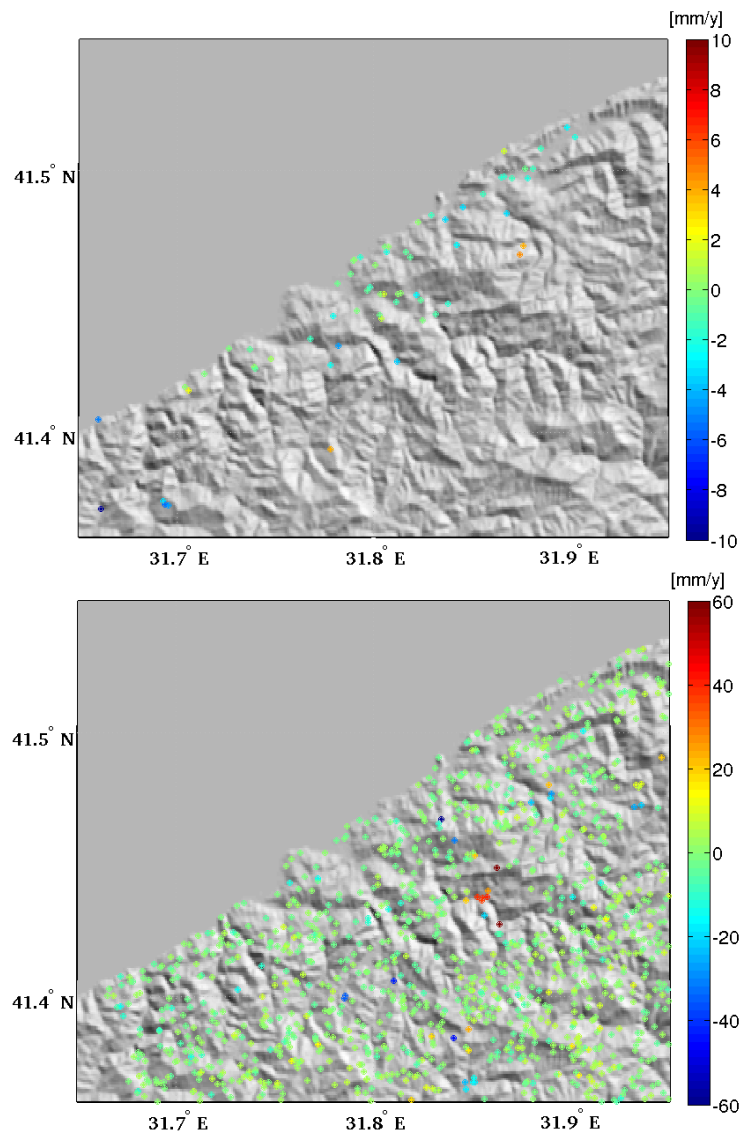


Figure A.5 Common points of PSI and SB results: a) ENVISAT t- 21, b) PALSAR

CONTRIBUTION PHASES

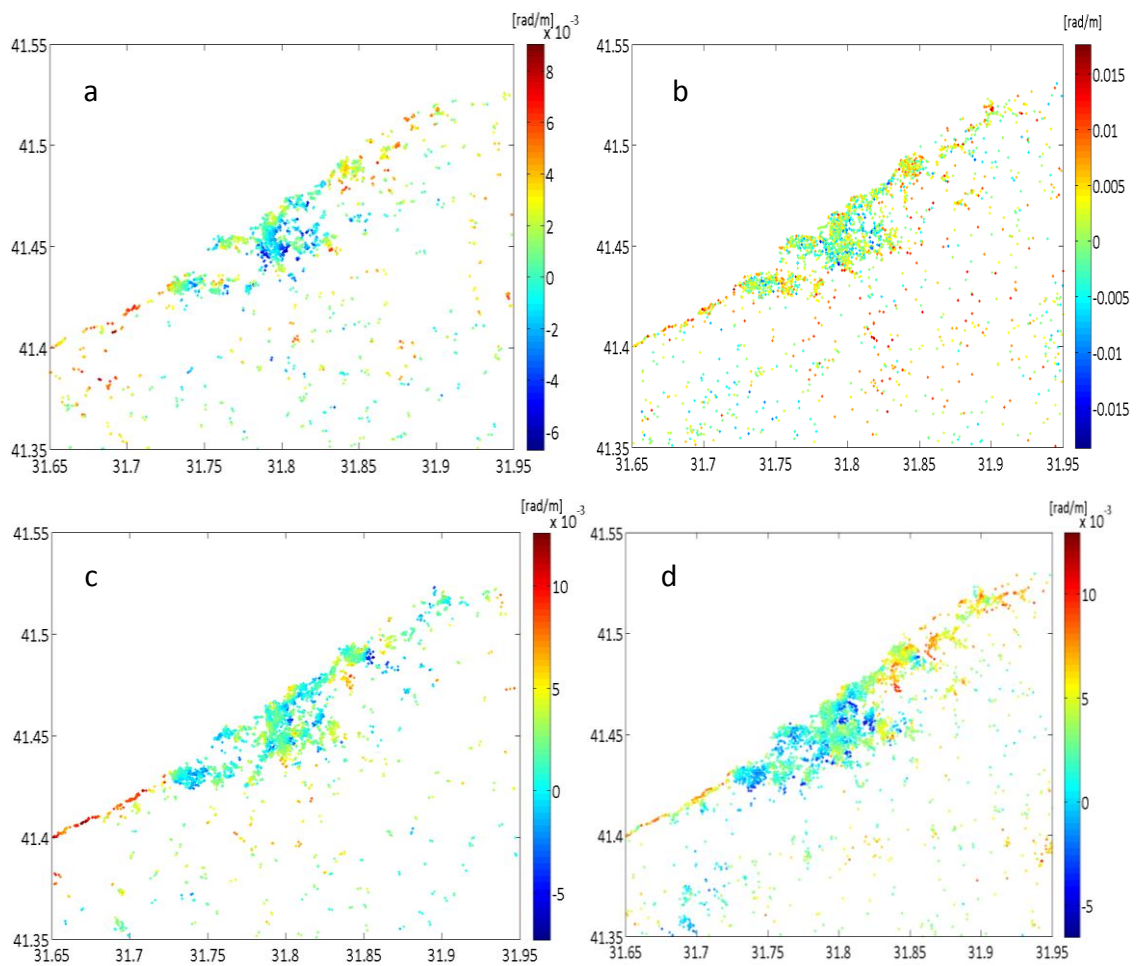


Figure A.6 DEM error removed from phase; a) ERS PSI result, b) ERS SB result, c) Desc. ENVISAT PSI result, d) Desc. ENVISAT SB result

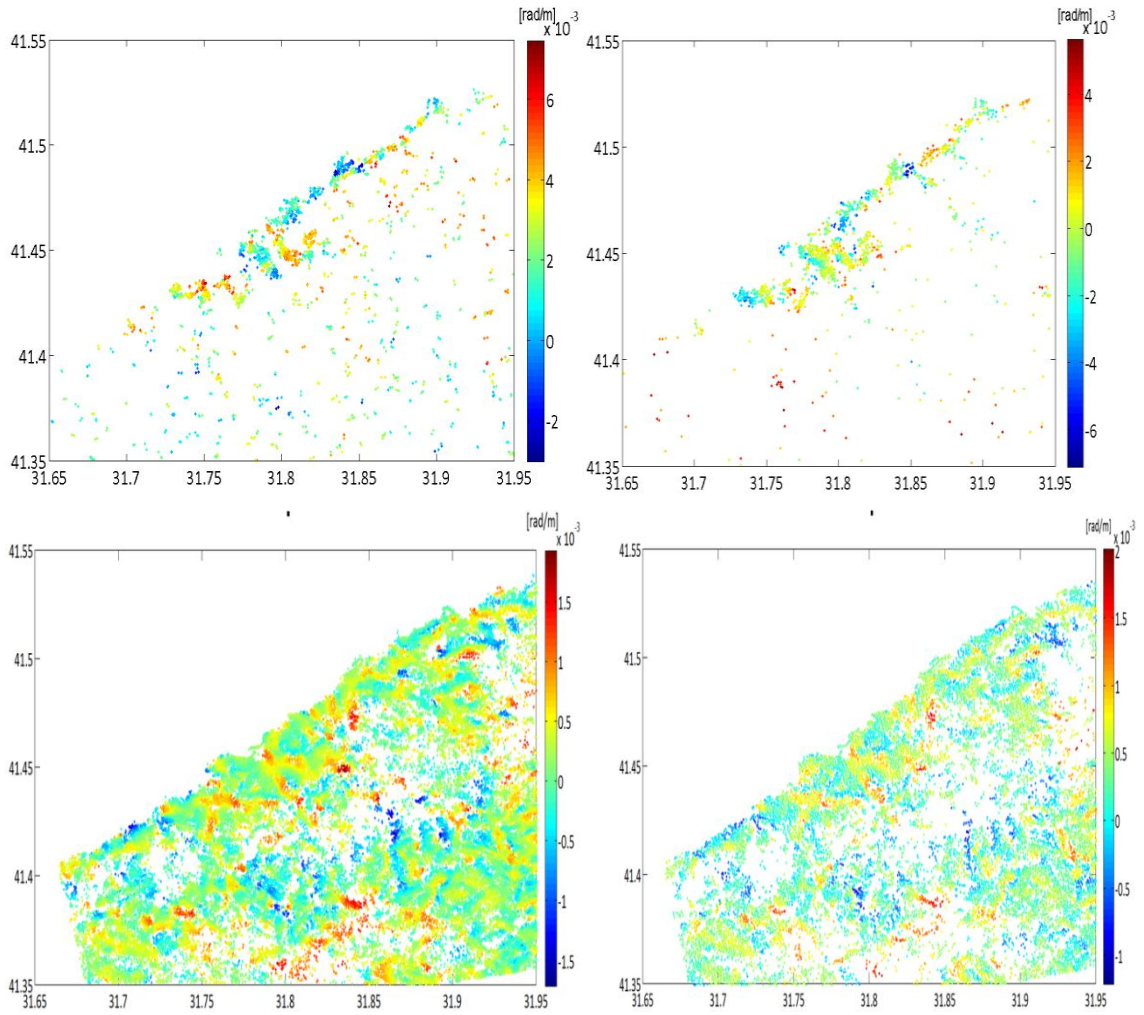


Figure A.7 DEM error removed from phase; a) Asc. ENVISAT PSI result, b) Asc. ENVISAT SB result, c) PALSAR PSI result, d) PALSAR SB result

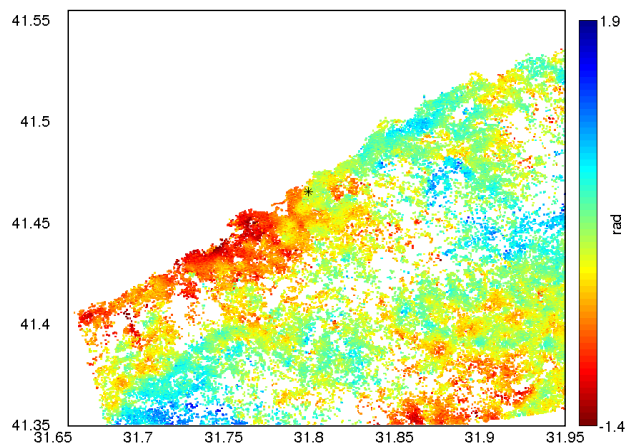


Figure A.8 Atmosphere and orbital error of master image (20080723) which is included in all interferograms in PSI process

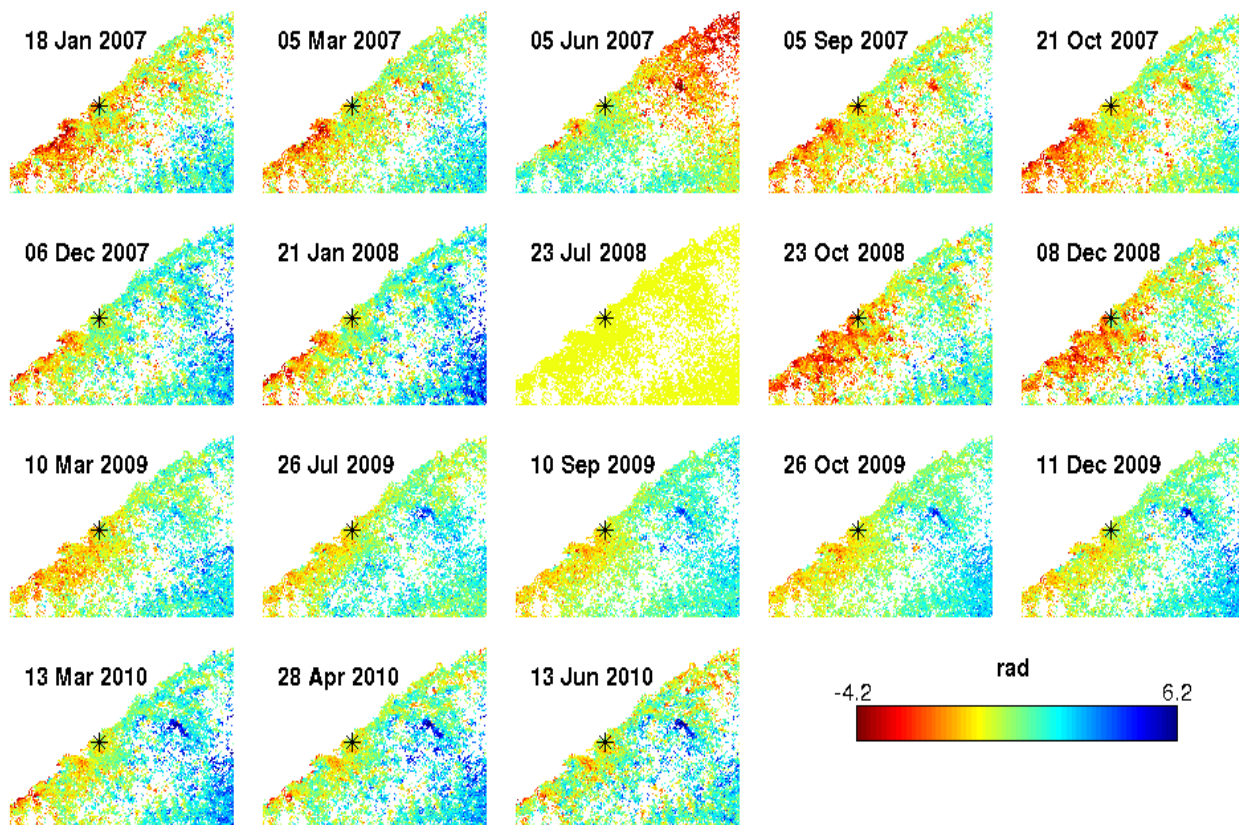


Figure A.9 Unwrapped phase of PALSAR images in PSI application

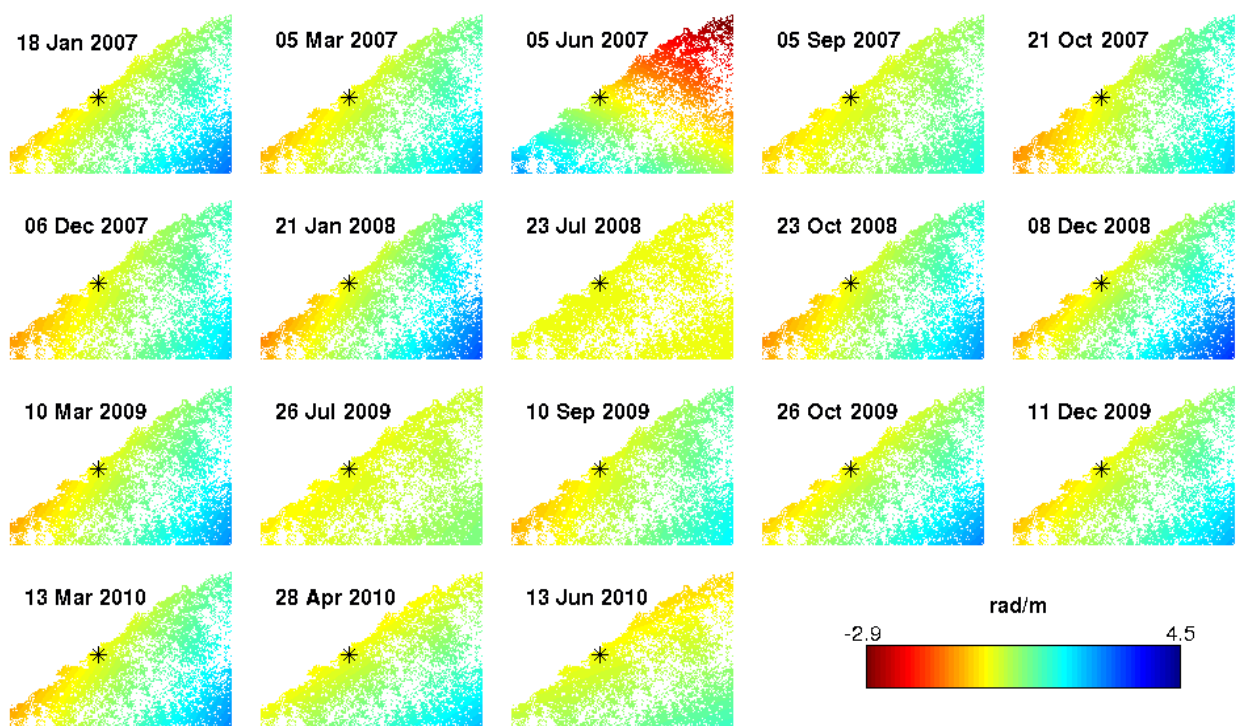


Figure A.10 Orbit errors of PALSAR images in PSI application

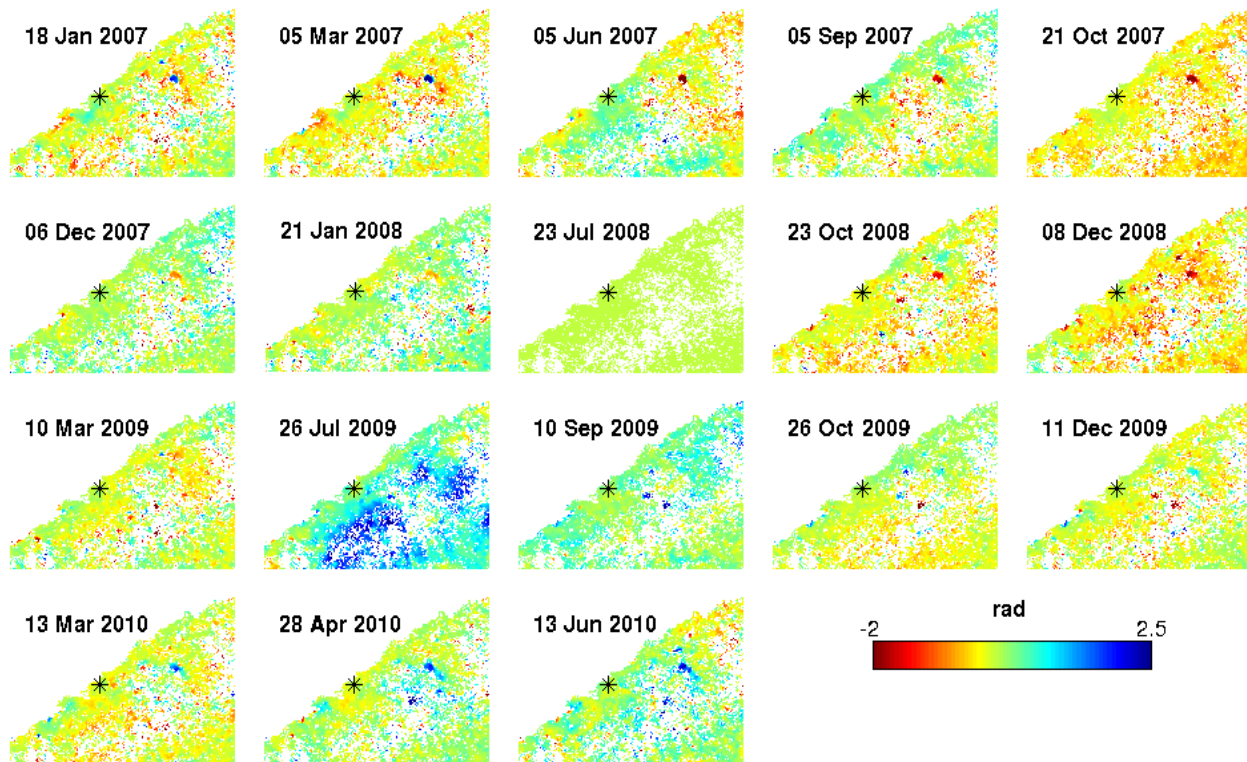


Figure A.11 Atmospheric phase of PALSAR images in PSI application

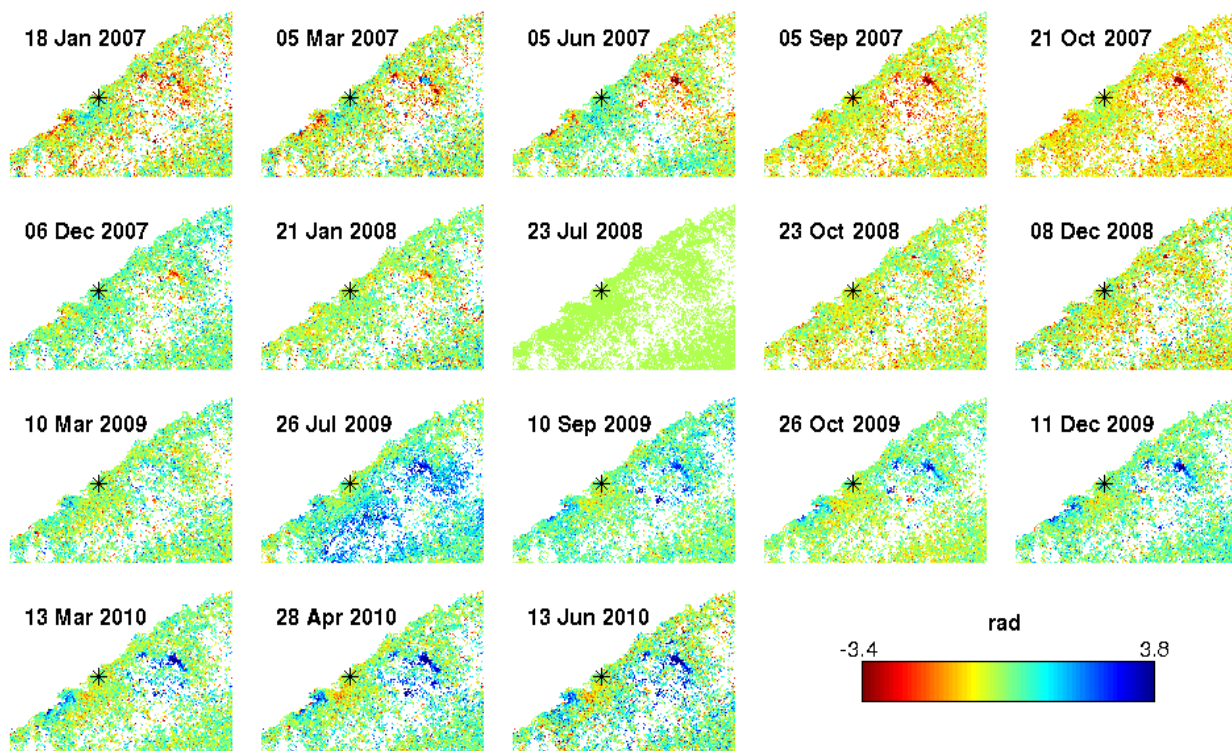


Figure A.12 DEM error and orbit phase removed unwrapped phase of PALSAR images in PSI application

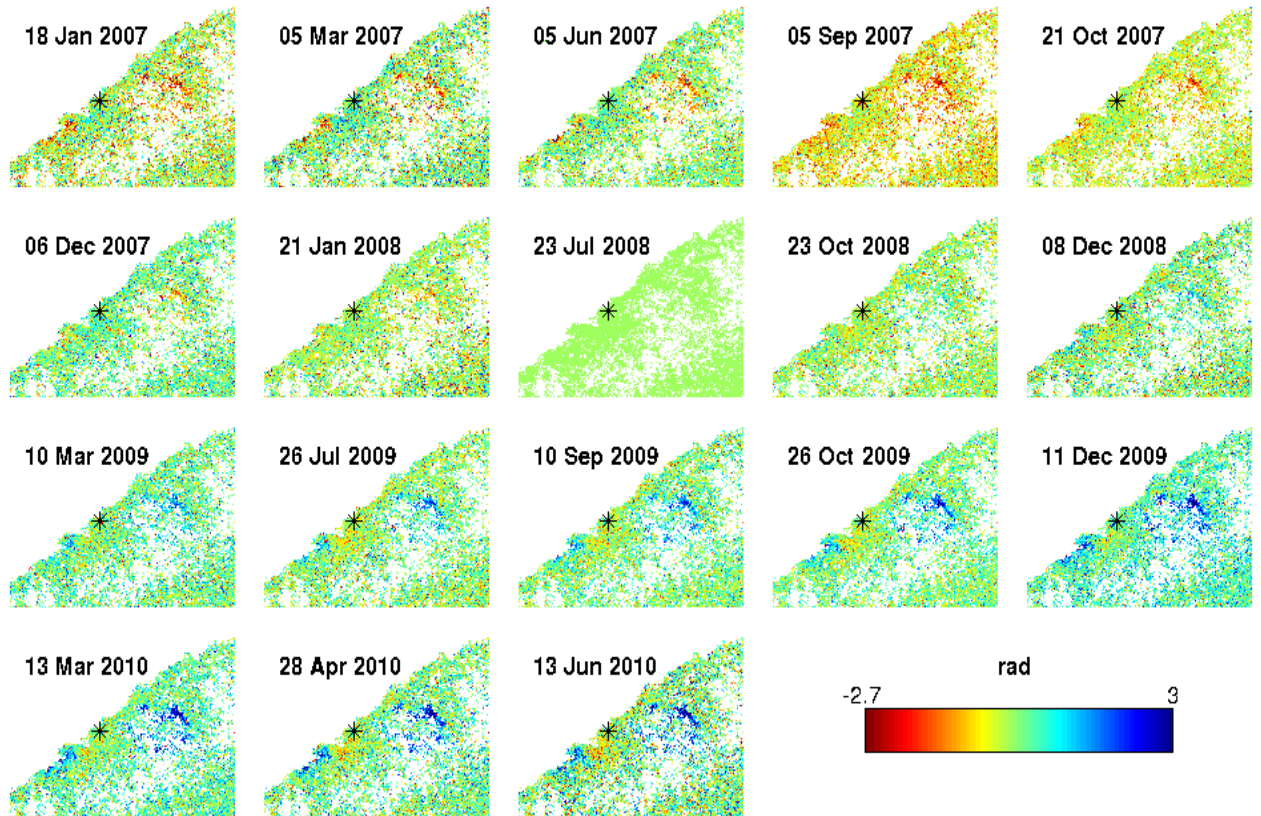


Figure A.13 DEM error, atmospheric and orbit phase of slave images and master image removed unwrapped phase of PALSAR images in PSI application

As noticed in Figure A.5 after the removal of errors, evaluation of deformation phase can be seen clearly at Kozlu, Karadon and Üzülmez regions in time period.

CURRICULUM VITA

PERSONAL INFORMATION

Name Surname : Saygın ABDIKAN
Place and Date of Birth : Turhal and 02.07.1981
Foreign Language : English
E-posta : sayginabdikan@gmail.com

EDUCATIONAL

Degree	Department	University	Date of Graduation
Master	Remote Sensing and GIS	YTU	2007
Bachelor	Geomatics Engineering	YTU	2004
High School	Science	Milas Anatolian High School	1999

WORK EXPERIENCE

Year	Corporation/Institute	Enrollment
2012	TU Delft	Researcher
2009	YTU	Researcher
2005	IkiNokta Information Technologies	Engineer

PUBLISHERMENTS

Papers

- 1 **Abdikan, S.**, Balik Sanli, F., (2012). "Comparison of Different Fusion Algorithms in Urban and Agricultural Areas Using SAR (PALSAR and RADARSAT) and Optical (SPOT) Images", Geodetic Sciences Bulletin Vol 18 - N° 4, 509-531.
- 2 **Abdikan, S.**, Balik Sanli, F., Sunar, F., Ehlers, M., (2012)." A Comparative Data-Fusion Analysis of Multi-Sensor Satellite Images", International Journal of Digital Earth, DOI:10.1080/17538947.2012.748846, in press.

Proceedings

International Proceedings

- 1 Acar, U., Bayram, B., Balik Sanli, F., **Abdikan, S.**, Sunar, F., Cetin, D., (2012). "An Algorithm for Coastline Detection Using SAR Images", XXII. Congress of the ISPRS, Int. Arch. Photogramm. Remote Sens. Spatial Inf. Sci., XXXIX-B3, 457-460, doi: 10.5194/isprsarchives-XXXIX-B3-457-2012, 2012 25 Aug - 01 Sept 2012, Melbourne, Australia.
- 2 Bektas Balcik, F., Balik Sanli, F., **Abdikan, S.**, Esetlili, Goksel, C., M.T., Kurucu, Y., (2012). "Mapping Crop Types Using Support Vector Machine Classifiers from Rapideye data in Menemen Plain, İzmir", 8th International Soil Science Congress, 15-17 May 2012, Cesme-Izmir, Turkey.
- 3 **Abdikan, S.**, Hooper A., Arikan, M., Balik, Sanli F., Cakir., Z., Kemaldere, H., (2011). "InSAR Time Series Analysis of Coal Mining in Zonguldak City NW Turkey", FRINGE 2011 Workshop, 19-23 September 2011, Frascati-Rome, Italy.
- 4 Balik Sanli, F., Esetlili, M.T., Kurucu, Y., **Abdikan, S.**, (2008). "Soil Moisture **Abdikan, S.**, Balik Sanli, F., Bektas Balcik, F., Goksel, C., (2008). "Fusion of SAR Images (PALSAR and RADARSAT-1) With Multispectral Spot Image: a Comparative Analysis of Resulting Images", XXI. Congress of the ISPRS Silk Road: For Information from Imagery, 03-11 July 2008, Beijing China. ISSN 1682-1750, Vol: XXXVII Part B7 TC VII pp: 1197-1202.
- 5 Estimation from Radarsat -1, ASAR and PALSAR Data in Agricultural Fields of Menemen Plane of Western Turkey", XXI. Congress of the ISPRS Silk Road: For Information from Imagery, 03-11 July 2008 Beijing China, ISSN 1682-1750, Vol: XXXVII Part B7 TC VII pp: 75-82.
- 6 **Abdikan, S.**, Esetlili, M.T., Sanli Balik, F., Kurucu, Y., (2008). "Land use/cover mapping using multisensor image fusion technique", 28. EARSel Symposium, "Remote Sensing for a Changing Europe, 2-5 June 2008, Istanbul Turkey, ISBN 978-1-58603-986-8, pp: 157-164.

- 7 Balik Sanli, F., Esetlili, M.T., Kurucu, Y., **Abdikan, S.**, Goksel, C., Hussin, Y., (2007). "Comparison of soil moisture estimation from RADARSAT and ASAR data using image fusion technique", Conference on Information Extraction from SAR and Optical Data, with Emphasis on Developing Countries, Istanbul, 16-18 May 2007. VolXXXVI-7 (C46) ISBN no: 1682-1750.
- 8 Balik Sanli, F. and **Abdikan, S.**, (2006). "Comparing a stereoscopic DEM with an interferometric DEM using the same Radarsat data pair", ISPRS Mid-term Symposium 2006 Remote Sensing: From Pixels to Processes Symposium, Vol. XXXVI part7 pp: 69-75, 8-11 May 2006, Enschede, the Netherlands.

National Proceedings

- 1 Balik Sanli, F., **Abdikan, S.**, Arıkan, M., Cakir, Z., Kemaldere, H., (2012). "InSAR Zaman Serileri ile Yer Yüzeyi Hareketlerinin İzlenmesi: Zonguldak Kozlu Maden Alanı Örneği", IV. UZAL-CBS Sempozyumu, 16-18 Ekim 2012, Zonguldak.
- 2 Acar, U., Bayram, B., Balik Sanli, F., **Abdikan, S.**, Ustuner, M., Maktav, D., Sunar, F., (2012). "SAR Görüntülerinden Kıyı Şeridi Belirleme Algoritması", IV. UZAL-CBS Sempozyumu, 16-18 Ekim 2012, Zonguldak.
- 3 Balik, Sanli, F., **Abdikan, S.**, Bayram, B., Esetlili, M.T., Kurucu, Y., (2010). "SAR ve Optik Uydu Görüntülerinden Nesne Tabanlı Sınıflandırma Tekniği Kullanılarak Arazi Örtüsünün Belirlenmesi", 3. UZAL-CBS Sempozyumu, 11-13 Ekim 2010, Gebze.
- 4 **Abdikan, S.**, Balik, Sanli, F., (2008). "Sar Görüntülerinin (Palsar ve Radarsat-1) Multispektral Spot Görüntüsü ile Birleştirilmesi: Sonuç Görüntülerin Karşılaştırmalı Analizi", UZALCBS Uzaktan Algılama ve Coğrafi Bilgi Sistemleri Sempozyumu, Kayseri, 13-15 Ekim 2008.
- 5 **Abdikan, S.**, Alkış, Z., Alkış, A., (2007). "İnterferometrik Radarsat Verileri İle Üretilen Sayısal Yükseklik Modelinin Değerlendirilmesi", TUFUAB IV. Sempozyumu, İTÜ, İstanbul, 5-7 Haziran 2007.
- 6 **Abdikan, S.**, Balik, Sanli, F., Alkış, Z., Alkış, A., (2007). "SAR Görüntülerinden Üretilen İnterferometrik ve Stereo Sayısal Yükseklik Modellerinin Kalitesinin İncelenmesi", 11. Türkiye Harita Bilimsel ve Teknik Kurultayı, ODTU Ankara, 2-6 Nisan 2007.

Projects

- 1 Researcher, DLR TerraSAR-X Science Service System Project: Monitoring of landslides on east part of North Antolia Fault Zone (Kelkit Valley) using PS-InSAR method with TerraSAR-X data, ID: GEO1232, 2012-2015.
- 2 Researcher, ESA Project: Monitoring of Koyulhisar landslides using PS-InSAR method, ID: 10956, 2012-2014.
- 3 Principal Investigator, ESA Project: Sinkhole subsidence monitoring in Konya Basin with Interferometric SAR time series analysis, ID: 10050, 2011-2014

- 4 Researcher, ESA Project: Monitoring Subsidence Using PS-InSAR: A Case Study for Zonguldak Mining Area, ID: 6543. 2009-2012.
- 5 Researcher, ESA Project: Investigating the Mechanism of the Subsidence in Town of Guzelburc (Amik Basin, Hatay), Southern Turkey, and Using Hydrologic and Tectonic Methods with the Aid of GPS-InSAR-Levelling Techniques, ID: 4907, 2009-2012.
- 6 Researcher, Monitoring Subsidence Using PS-InSAR: A Case Study for Zonguldak Mining Area – Yıldız Technical University, BAPK Project No: 28-05-03-02, 30 000 YTL., 2008-2011.

AWARDS

- 1 IV. National Remote Sensing & GIS Symposium, II. Best Presentation Award, 16-18 October 2012, Zonguldak, Turkey.
- 2 The Huygens Scholarship for the period 2009-2011, from Nuffic - Netherlands organization for international cooperation in higher education.
- 3 XXI. ISPRS Congress Best Poster Paper Award, XXI. Congress of the ISPRS Silk Road: For Information from Imagery, 03-11 July 2008, Beijing China.